NASA TECHNICAL MEMORANDUM

NASA TM X - 53315

August 6, 1965

NASA TM X - 53315

N66-10676

(ACCESSION NUMBER)

111

(PAGES)

(NASA CR OR TMX OR AD NUMBER)

(THRU)

1

(CODE)

32

(CATEGORY)

FACILITY FORM 602

COMPRESSION TESTS ON INTEGRALLY STIFFENED CYLINDERS

by LESTER KATZ
Propulsion and Vehicle Engineering Laboratory

GPO PRICE $ ______

CFSTI PRICE(S) $ ______

Hard copy (HC) 4.00

Microfiche (MF) .75

ff 653 July 65

NASA

George C. Marshall Space Flight Center,
Huntsville, Alabama

NASA - GEORGE C. MARSHALL SPACE FLIGHT CENTER

TECHNICAL MEMORANDUM X - 53315

August 6, 1965

COMPRESSION TESTS ON INTEGRALLY STIFFENED CYLINDERS

By

Lester Katz

PROPULSION AND VEHICLE ENGINEERING LABORATORY
RESEARCH AND DEVELOPMENT OPERATIONS

TECHNICAL MEMORANDUM X - 53315

COMPRESSION TESTS ON INTEGRALLY STIFFENED CYLINDERS

By

Lester Katz

George C. Marshall Space Flight Center
Huntsville, Alabama

ABSTRACT

10676

Uniform axial compressive loads were applied to 23 unpressurized circular cylinders until failure by buckling occurred. Twenty-one of the cylinders were integrally stiffened, with stringer and frame patterns that may be described as: 0°-90° waffle, 45° waffle, and stringer-only configurations. Experimentally determined buckling loads for general and local instability were compared with analytical predictions. Relative structural efficiencies were obtained for the various patterns tested and experimental stress distribution data were determined for all the test cylinders.

Author

TABLE OF CONTENTS

		Page
SUMMARY		1
SECTION I.	INTRODUCTION	1
SECTION II.	TEST SPECIMENS AND TEST PROCEDURE	2
	A. Test Specimens	2
	B. Test Procedure	4
SECTION III.	RESULTS AND DISCUSSION	5
SECTION IV.	ANALYSIS OF DATA	7
	A. General Instability	7
	B. Local Buckling	9
	1. Zero-Ninety Cylinders	9
	2. Skew-Stiffened Cylinders	9
SECTION V.	CONCLUSIONS AND RECOMMENDATIONS	10
APPENDIX		97
	A. General Instability Methods	97
	B. Local Instability Methods	99
	C. Conversion of U. S. Customary Units to SI Units	100
REFERENCES		101

LIST OF ILLUSTRATIONS

Figure	Title	Page
1.	Typical Dimensional Nomenclature	12
2.	Nominal Cylinder Geometry	13
3.	View of Compressive Loading Machine	19
4.	Strain Gage Locations	20
5.	View of Buckled Cylinders	25
6.	End Moment Due to Eccentricity	29
7.	Polar Plots of Stress Distributions	30
8.	Stress versus Load	42
9.	Test Results	86
10.	Monocoque Results	87
11.	Comparison of Test Data with Method of Ref. 5	88
12a.	Local Buckling Stresses for Group 2 (0° - 90°) Cylinders	89
12b.	Local Buckling Stresses for Group 3 (0° - 90°) Cylinders	90
13.	Local Buckling Stresses for Group 4 (45°) Cylinders	91

LIST OF TABLES

Table	Title	Page
I.	Nominal Cylinder Geometry	93
II.	Cylinder Dimensions in General Instability Region [a]	94
III,	Load Summary	95
IV.	General Instability Predictions, P_{cr} (kips) for Integrally Stiffened Cylinders	96

LIST OF SYMBOLS

Figure 1 illustrates many of the symbols used in this report. In consonance with generally accepted flight-structure terminology the following terms are employed: stringers and frames are designated as stiffeners which run in the axial and circumferential directions, respectively; skew stiffeners are helix-like stiffeners oriented at 45° to the cylinder axis. All symbols used in the report are shown below except for a few introduced in the Appendix which are defined there, as used.

Although the system of units employed in the report are U.S. Customary Units, conversion to the International System of Units (SI) may easily be made by use of the conversion factors presented in the Appendix, section C.

Symbol	Definition
A	area, in.^{2} (cm^2)
a	width of skin between adjacent frames, in. (cm)
b	width of skin between adjacent stringers, in. (cm)
b_f	width of flange on tee-shaped stringers, in. (cm)
b_s	distance between centerlines of adjacent skew stiffeners, in. (cm)
b_x	distance between centerlines of adjacent frames, in. (cm)
b_y	distance between centerlines of adjacent stringers, in. (cm)
C	coefficient in buckling equation $P_{cr} = 2\pi CEt^2$
c	coefficient of end fixity
E	Young's Modulus (compression), psi (N/cm^2)
H	height of stiffener plus skin, in. (cm)

LIST OF SYMBOLS (Continued)

Symbol	Definition
I_x	principal moment of inertia per unit length of circumference (includes stringers), in.^{3} (cm^3)
I_y	principal moment of inertia per unit length in the axial direction (includes frames), in.^{3} (cm^3)
L	total length of patterns in axial direction (distance between heavy end-rings for monocoque cylinders), in. (cm)
N	load per inch of circumference, kips/in. (kN/cm)
n_s	number of individually milled repeating skewed patterns on Group 4 cylinders
n_{sx}, n_{sy}	number of partial patterns on Group 4 cylinders, see Figure 2.
n_x, n_y	number of individually milled repeating 0°-90° patterns in the axial and circumferential directions, respectively
P_{cr}	load at which general instability occurs, kips (kN)
R	radius to mid-thickness of skin, in. (cm)
R_c	corner radius at intersection of two stiffeners, in. (cm)
R_f	fillet radius at skin-stiffener juncture, in. (cm)
t	thickness of skin, in. (cm)
$\bar{t}$	thickness of an equivalent monocoque cylinder with same <u>weight</u>, length, and radius as the given integrally stiffened cylinder, in. (cm)
t^*	thickness of an equivalent monocoque cylinder with same <u>strength</u>, length, and radius as the given integrally stiffened cylinder, in. (cm)
t_f	flange height of tee-shaped stringers, in. (cm)

Symbol	Definition
t_h	stiffener height, in. (cm)
t_s	width of skew stiffeners, in. (cm)
t_x	width of frames, in. (cm)
t_y	width of stringers, in. (cm)
ν	Poisson's ratio
σ^o, σ^i	stresses on outside, inside surfaces of shell, ksi (MN/m^2)
θ^o, θ^i	direction of principal stress on outside, inside surfaces of shell, degrees

Subscripts

1, 2	direction of maximum, minimum principal stresses
cr	corresponds to buckling load

TECHNICAL MEMORANDUM X - 53315

COMPRESSION TESTS ON INTEGRALLY STIFFENED CYLINDERS

SUMMARY

Uniform axial compressive loads were applied to 23 unpressurized circular cylinders until failure by buckling occurred. Twenty-one of the cylinders were integrally stiffened, with stringer and frame patterns that may be described as: 0°-90° waffle, 45° waffle, and stringer-only configurations. Experimentally determined buckling loads for general and local instability were compared with analytical predictions. Relative structural efficiencies were obtained for the various patterns tested and experimental stress distribution data were determined for all the test cylinders.

SECTION I. INTRODUCTION

A group of integrally stiffened cylinders were individually subjected to uniform axial compressive loads until failure by buckling occurred. Within the limitations of specimen geometry and loading the purposes of the investigation were to:

(a) Compare experimentally attained buckling loads with the predictions of some analytical methods;

(b) Determine the relative structural efficiencies of the various configurations; and

(c) Obtain experimental stress distribution data.

The methods used for making the comparisons mentioned in part (a) above were meant to serve as a sampling rather than an endorsement of these particular methods.

The cylindrical specimens were originally conceived in terms of four groups based upon stiffener orientation: monocoque, 0°-90° waffle, 45° waffle, and stringer-only; all specimens were fabricated by longitudinally butt-welding adjacent panels into a complete cylinder. Later a particular circumferential weld design was introduced into the 0°-90° waffle configuration, making a total of five groups.

The geometric and material property values for the test specimens (Young's modulus, yield stress, cylinder diameter, stiffener height, etc.) were chosen so that the instability mode of failure would occur at stresses in the elastic range of the material. A further restraint upon the choice of cylinder geometry was imposed by the capacity of available loading fixtures. These factors resulted in cylinders with nominal dimensions as follows: 52-inch diameter; 60-inch length; skin thickness of 0.0375 inch; stringer heights of 0.2125 inch; stringer widths of 0.106 inch; and with nominal dimensionless parameters of $R/t=680$, $\frac{L}{R} = 2$, and $\frac{t}{H} = 0.15$. Because of the fairly low ratio of stringer area to skin area (about 0.25), the cylinders may be considered as moderately stiffened cylinders; that is, they fall in a strength transition region between monocoque and "heavily" stiffened orthotropic cylinders.

SECTION II. TEST SPECIMENS AND TEST PROCEDURE

A. TEST SPECIMENS

The test specimens consisted of 23 right circular cylinders fabricated from 6061-T6 aluminum sheet. Two were monocoque, while the remainder were integrally stiffened. The cylinders may be divided into five groups (see Fig. 1):

Group 1. Monocoque;
Group 2. 0°-90° waffle stiffeners (with circumferential and axial welds);
Group 3. 0°-90° waffle stiffeners (with welds in the axial direction only);
Group 4. Skew or 45° waffle stiffeners;
Group 5. Stringer-only stiffeners.

Figure 2 depicts the nominal dimensions of each cylinder tested; that is, the dimensions specified on the fabrication blue-prints. These dimensions are summarized in Table I. (For purposes of buckling predictions which appear in Table IV, the measured dimensions given in Table II were used). An idea of the geometry range of the integrally stiffened cylinders that were tested can be obtained from the following approximate structural ratios: $R/t = 680$; $L/R = 2.0$; and $t/H = 0.15$. The specific ratios for each cylinder are also shown in Table I.

All the cylinders were the same in the following respects. Their overall length was 60.25 inches (however the total length of stringers, L, varied from specimen to specimen). The cylinders were fabricated with two heavy rings on each end as detailed in Figure 2; one inside and the other outside, attached to the skin by Huckbolts. After attachment of these rings to the skin, their bearing surfaces were milled perpendicular to the cylinder centerline. The grain of 6061-T6 aluminum was oriented in the circumferential direction. All seams on each cylinder were hand-welded using the helium arc process. The stiffener patterns were all on the outside of the cylinders as shown in Figure 2. A minimum of 2.5 inches (10H) of unmilled skin existed in the axial direction between the end frames and the patterns.

Samples cut from each lot of material used in fabricating the cylinders were tested in compression to obtain an average value of Poisson's ratio and Young's modulus in the with-grain and transverse-grain directions. The average values obtained from 105 compression specimens tested and their maximum variation from the mean in the transverse-grain direction were: $E = 10.48 \times 10^6$ psi $\pm$ 2.2 percent variation, $\nu = 0.325 \pm 3.2$ percent; in the with-grain direction: $E = 10.44 \times 10^6$ psi $\pm$ 1.5 percent, $\nu = 0.320 \pm 2.2$ percent. Since the cylinders were all fabricated with the grain running in the circumferential direction, the applied principal compressive stress acted in the transverse grain direction. Therefore the average material properties chosen for purposes of calculation were those of the transverse direction: $E = 10.5 \times 10^6$ psi, $\nu = 0.325$.

Each cylinder consisted of panels welded together as shown in Figure 2. The monocoque cylinders, Group 1, were fabricated from sheet in the as rolled condition. Groups 2, 3, and 4 were first chemically milled to the desired skin thickness, then mechanically milled to obtain the other final geometry such as stiffener thicknesses, corner radii (R_c), and fillet radii (R_f). Mechanical milling alone was used on Group 5 to attain the final dimensions. In Groups 2, 3, 4 and 5 the sheets were milled as panels in the flat condition, then welded together and rolled to the cylindrical shape. After the end rings were installed, the final operation was to true up the bearing surfaces. A detailed quality control schedule was maintained to provide the large number of thickness, diameter, and stiffener-width measurements necessary for the test program calculations.

B. TEST PROCEDURE

The test apparatus used to apply the compressive load is shown in Figure 3, and was operated as follows: The test specimen was centrally positioned on the lower platen. A hydraulic ram raised the lower platen off the stops compressing the specimen against the upper platen. This in turn reacted the load through a hardened ball and socket against the frame. A double output load-cell was interposed between the ram and lower platen to monitor the applied load. Because of the flexible cruciform between the ram and lower platen, and the universal-joint action of the ball-and-socket, the fabrication quality of the specimen rather than lead screws or sliding constraints as in conventional test machines, was influential in obtaining uniform compression. To monitor the stress distribution in each cylinder, strain gage rosettes were placed at every 30° as shown in Figure 4. These locations were numbered 1 through 12, counting counter-clockwise from weld 1. At each location, four strain-gage rosettes were used. Two rosettes were attached to the inside and outside surfaces of the skin, and two rosettes were attached to the inside and outside surfaces of the right-hand adjacent stringer.

Prior to each test, the specimen was centered in the loading machine with location 8 pointing due north so that every cylinder was oriented with respect to the testing machine in the same way. Then compressive load was applied, and readings were taken at each 10 percent increment of the predicted overall buckling load until 50 percent of P_{cr} was reached. During this time axial stress distributions were plotted to ascertain whether the compressive stresses were uniform. Usually they were not, and the load was released to zero so that shim stock (to the nearest mil) could be slipped under the ends of the cylinder as required. Then compressive load was again applied to the cylinder and the stress distribution checked once more. This process was repeated until the compressive stresses were within ±5 percent of the mean value. The mechanics of attaining uniform load on any given cylinder took approximately one day. At any load increment, the strain data was acquired, reduced to principal stress values, and printed out on-line in its final digital form within two minutes. The format showed percent load, strain gage location, maximum and minimum principal stresses, shear stress, and principal direction.

The emphasis in the test program was upon determining the loads and stresses associated with instability. However, radial deflection and end-shortening measurements were also made.

SECTION III. RESULTS AND DISCUSSION

Load was applied to each cylinder until general instability occurred. This condition was reached, in some cases, after local instability had occurred. As will be seen, for some cylinders local instability was limited to isolated locations, while for others it was rather widespread. In this report, local instability means buckling of the skin in the pocket between adjacent stringers and adjacent frames. Two types of general instability were observed; one in which relatively small diamond-shaped buckle patterns appeared (Groups 1, 2, 3, and 4), and another (wide-column mode) in which the buckle wavelength extended over the entire length of the cylinder (Group 5).

Figure 5 depicts the buckled cylinders arranged by groups. The photographs of Group 5 (stringer-only) and Cylinder 1B were taken with those cylinders under load, because their general instability buckle patterns vanished upon load release. With the reapplication of load on these seven cylinders, only 70 percent as much load was necessary to cause general instability as had been applied initially, indicating the formation of plastic hinges in the shell. The third and succeeding applications of load reduced P_{cr} to approximately 60 percent of the initial value. However, it appears possible, by careful restraint of the buckle deformations [16] to obtain repeatability of the initial buckling loads. Figure 5 gives some idea of the uniformity of the buckle formation around each cylinder. It also shows that Cylinder 3A buckled so close to its end that a premature failure is indicated; that is, local end moments were instrumental in causing this failure. As shown in Figure 6, this moment is directed toward the center of the cylinder. Because the cylinder wall also fails by buckling toward the center, this moment could contribute to a premature buckling failure near the end of the cylinder. The characteristic length for decaying 95 percent of the local end moment was approximately 4 inches for the shells tested. Cylinder 3A was the only specimen exhibiting this type of premature buckling failure. Figure 5 illustrates that Groups 1, 2, 3, and 4 failed with a diamond-shaped buckle; Group 5 failed in a wide-column or panel mode. Notice the local buckling that is evident in the Group 4 failure photographs as horizontal lines in the waffle patterns. The skew stiffeners appeared to act as toggle mechanisms, and as the applied loads increased, the skin between them was snapped from a uniformly curved surface to almost a plane. The load corresponding to this snap-through is their local buckling load.

The compressive membrane stress distribution in each cylinder is shown in the polar plots of Figure 7. The stresses are plotted at 30° intervals around the cylinder as detailed in Figure 4, on both the skin and the adjacent stringers, when present. Group 4 has 45° waffle stiffener patterns, and the principal stresses on the outside of these stringers are also oriented at 45° to the axis of the cylinder. Therefore only the skin stresses, whose principal directions are longitudinal, are plotted in Figure 7. The stresses shown for each cylinder are the arithmetical average of inside and outside values (axial membrane stress). There are two plots per cylinder. The plot on the left corresponds to the stress distribution at approximately 50 percent of the general instability load; the right-hand plot indicates the stress distribution very close to P_{cr}. Primarily, because of the occurrence of local instability, there are shifts in the compressive membrane stress distribution, from essentially uniform in the 50 percent of P_{cr} range (plots on the left), to non-uniform in the general instability plots (on the right).

Figure 8 is a compilation of the stress data for each cylinder, from zero load to P_{cr}. There are 12 strain gage locations around the circumference at midlength[(a)] of the cylinder for which the stresses have been plotted. Each page of Figure 8 gives the stresses at locations 1 through 12 for a particular cylinder for both skin and stringers. The inside and outside circumferential and longitudinal stresses[(b)] are shown. In addition, principal directions are shown as a function of load for most cases. Zero degrees refers to the axial (x) direction. An exception is Group 4, the skew stiffened cylinders. For these, an angle of 0° means a direction in-line with the stringer (45° to the cylinder axis), while an angle of 45° coincides with the axial direction. In this case, the outside surface stresses of the skew stringers which are called "longitudinal" on Figure 8, have an actual direction which can be interpreted from their accompanying principal direction plots. End-shortening deflection measurements as a function of applied load, which are not included in the report, reflect the modulus of elasticity for the cylinders. In the case of Group 4 (45°) cylinders, the large amount of local buckling was indicated by a change in slope of the end shortening curves.

(a) An exception is Group 2, which has a circumferential weld at midlength (see Figure 4 for strain gage location details).

(b) The inside stress on the stringer is taken to be that stress measured on the inside skin surface directly beneath the stringer.

SECTION IV. ANALYSIS OF DATA

A. GENERAL INSTABILITY

The critical buckling loads for the stiffened test cylinders were computed by the methods shown in Table IV. The Appendix indicates the assumptions made in using these methods. The dimensions used in the calculations were measured in the regions where general instability buckling occurred, and are listed in Table II. Test cylinder buckling loads, wavelengths, and comments are shown in Table III. The "comments" indicate that the circumferential weld reduced the critical load capability of all of the cylinders in Group 2. In addition P_{cr} for cylinder 3A was low due to premature failure near the cylinder's upper end. Therefore the predicted values for 3A and Group 2 should be higher than the test values. Only method [8] [a] predicts lower values. This implies that the use of [8] for 0°-90° waffle configurations may lead to structures which are overdesigned.

Cylinders 3B-1, 3B-2, 3C, and 3D of Group 3 (0°-90° waffle) were tested to failure with no unusual phenomena noted. Only [5] and [6] predict P_{cr} close to these test values, while [1], [3], [12], and [13] are off by a factor of about two.

P_{cr} for the 45° waffle stiffened cylinders (Group 4) was predicted closely by [8]. Method [13] was off by a factor of about 1.5 to 2. The fact that [8] showed good correlation is surprising because local buckling was widespread for the Group 4 cylinders (as shown by Figs. 5 and 8) often at values as low as 50 percent of P_{cr}.

The predictions for cylinders 5A-1 and 2, 5B-1 and 2 of Group 5 (external stringer-only) were most accurately made using method [4]. This method, however, is known to yield accurate results for internally stringer-stiffened cylinders, and nonconservative results for externally stringer-stiffened cylinders, see [4] and [17]. From this evidence, it appears that for the moderate amount of stiffening of the above test cylinders, location of stringers on either the outside or inside surfaces should have little effect on buckling strength. The test values from 5B-1 and 2, while close to each other, appear to be lower than they should be. Since their $\bar{t}$ is greater than that of 5A-1 and 2, one would have expected a higher value for P_{cr}. Method [4] yielded P_{cr} predictions on the low

---

(a) Numbers in brackets refer to references located at the rear of the report.

side for cylinders 5C-1 and especially 5C-2; these were externally tee-stiffened. The eccentricity of these stringers (as measured by the distance from stringer-skin centroid to skin median surface), and the ratio of stringer to skin area was greater than the 5A and 5B cylinders. Therefore, the relatively heavier stiffeners of the 5C cylinders were sufficient to increase their average buckling strength above the wide-column predictions of method [4], and reflect the effects of external stiffener eccentricity on strength. The other methods shown in Table IV gave predictions that varied from the test results by large amounts. Since only [4] used a mode shape that was representative of Group 5 failures (a buckle pattern having an axial half-wavelength equal to the cylinder length) the lack of correlation is not altogether unexpected.

Figure 9 is a plot of the test critical buckling loads, P_{cr} versus $\bar{t}$. Since all the cylinders had essentially the same mean radius, this graph represents a weight-strength plot of the test results. For comparison purposes, if a structural index or efficiency is defined as $\eta = \frac{\text{strength}}{\text{weight}} \times$ (enclosed fluid volume), then as this ratio increases the cylinder design becomes more optimum from a tankage point of view. Using the monocoque cylinders as a datum, the stringer-only cylinders (Group 5) were slightly more efficient; approximately 20 percent. Groups 3 and 4, however, had an efficiency of some 250 percent above monocoque. Cylinder 3A is not plotted in Figure 9 because of its premature end-failure. The performance of Group 2 cylinders, which have the same stiffener patterns as Group 3, lies below the Group 3 data. This degradation was caused by their circumferential welds, which were of a particular design believed amenable to flight hardware.

The skew-stiffened configuration of Group 4 always showed extensive local skin buckling well below P_{cr}, which available methods [13] did not predict. In the analysis of the Group 4 cylinders for P_{cr}, method [8] specified that monocoque cylinder results be used to supply an empirical coefficient. This empirical coefficient is supplied by the same author in a later paper, [11]. A comparison between the monocoque cylinders and [11] shows good correlation (Fig. 10). The Kanemitsu-Nojima equation [18] is also plotted in Figure 10.

The predictions of method [5], which yielded good accuracy for Group 3 (0°-90° waffle), are plotted in Figure 11. N_{cr} and $\bar{t}$ are used as the coordinates, with $\bar{t}$ as the third parameter. It was found through a plot of the strain gage data of Figure 8 that there were usually four high values of N_{cr} in sequence around the cylinder whose average value corresponded to the measured P_{cr}/A stress, while an average of all 12 gage measurements produced somewhat lower values.

B. LOCAL BUCKLING

Local buckling (the instability mode which is characterized by skin buckling in the pocket formed by adjacent stringers and adjacent frames) was observed on 0°-90° cylinders and skew stiffened cylinders. The local buckling stress was determined by averaging the measured outside and inside longitudinal compressive stresses, and plotting this membrane stress as a function of applied load. The load corresponding to $\frac{d\sigma}{dP} = 0$ was taken as the local buckling load. Once attained, this slope remained zero until general instability failure. Figure 8 graphically illustrates the on-set of local buckling.

1. Zero-Ninety Cylinders

Of the cylinders tested no local buckling was observed in the Group 1 and Group 5 cylinders. The 0°-90° waffle cylinders of Groups 2 and 3, however, evidenced some local skin buckling as applied load approached the general instability load. Figure 12 is a plot of local buckling stress versus skin thickness for the cylinders that had local buckling: 2B-1, 2B-2, 2C, 3B-1, 3B-2, 3C, and 3D. The stress was determined by strain gages, and the skin thicknesses were measured in the local buckling region. Predictions for local buckling by six methods (outlined in the Appendix, Section B) are shown in Figure 12. It was found that the best upper and lower bounds were given by Redshaw's method (Appendix, Section B, paragraph 3) and modified Redshaw method (Appendix, Section B, paragraph 4), respectively, for an aspect ratio a/b of 1 to 3. For the aspect of a/b $\doteq$ 0.5 (Cylinders 2A and 3A) local buckling was not observed. Yet the methods plotted in Figure 12 predict local buckling. Local buckling did not occur in the Group 5 cylinders that had an aspect ratio a/b > 20 (infinite in effect). Since the methods shown in the Appendix, Section B, paragraphs 1, 2, 3, 4, and 5 are independent of aspect ratio, these methods erroneously predict local buckling. Although the method shown in paragraph 6 of this section considers aspect ratio, it too would have erroneously predicted local buckling.

2. Skew-Stiffened Cylinders

All of the skew-stiffened (45° waffle pattern) cylinders gave indications of local skin buckling, which may be seen in some of the post-buckling photographs of Figure 5, and in the stress plots of Figure 8. Using the method [13] described in the Appendix, Section B, paragraph 5, the graph of Figure 13 was constructed. Although the suggested coefficient of 7.0 gave average buckling predictions, a figure of 4.4 appears to be better for design purposes.

SECTION V. CONCLUSIONS AND RECOMMENDATIONS

The remarks that follow are valid within the limitations of the specimen geometry tested; that is, for moderately stiffened cylinders with a ratio of stringer area to skin area on the order of 0.25. Although there is some empirical evidence that more heavily stiffened cylinders would yield results closer to orthotropic classical predictions (which include the effects of stiffener eccentricity and adequate boundary conditions), the strength effects of stringer eccentricity on the cylinders tested were small. The cylinders appeared to be affected by the same major item that tends to lower monocoque test values from classical values—imperfections.

The weight-strength comparison, using a structural index of $\frac{\text{strength}}{\text{weight}} \times$ (enclosed volume), referred to a monocoque datum, showed that 0°-90° and skew (45°) stiffened cylinders performed with essentially the same efficiency (about 250 percent above monocoque) while stringer-only stiffened cylinders were much less efficient (about 20 percent monocoque).

The general instability loads for the test cylinders were predicted most accurately by the following referenced methods:

(a)	Monocoque ----	[11]	- Seide, Weingarten, and Morgan;
		[14]	- Kanemitsu and Nojima
(b)	0°-90° waffle --	[5]	- Almroth
(c)	45° waffle ----	[8]	- Seide
(d)	Stringer-only --	[4]	- Peterson and Dow.

Application of a coefficient of 0.5 to referenced methods [1] and [12], and of 0.61 to [3] and [13] would bring them into good agreement for the 0°-90° waffle stiffened cylinders.

Local skin buckling loads for panel aspect ratios a/b of 1 to 3, for 0°-90° waffle-stiffened cylinders, were predicted by:

(a)	Upper bound ---	[18]	- Redshaw
(b)	Lower bound ---	[18]	- Modified Redshaw by Sechler and Dunn.

Good average local skin buckling predictions for the 45° waffle configurations were obtained by using [13] - Schneider, although a coefficient of K=4.4 yields better local buckling estimations for design purposes.

The stress distributions for the monocoque, 0°-90° waffle and stringer-only cylinders indicated that principal stringer and skin stresses were very nearly the same in the axial direction, and essentially zero in the circumferential direction. The skew stiffened cylinder's skin had P/A membrane stresses in the axial direction and essentially zero circumferential stresses; the 45° stringer outside principal stresses were at 45° to the cylinder axis, while the inside stringer stresses were axially and circumferentially disposed.

Because heavy stiffening will diminish the effects of initial imperfections and contribute to substantial strength increases (if stiffener eccentricity is properly located), it is recommended that a test program be initiated to evaluate these effects. The cylinders should be sufficiently large so that normal machining tolerance errors will not affect nominal desired geometries. End or boundary conditions should be carefully controlled to distribute load uniformly and to preclude premature buckling at the ends.

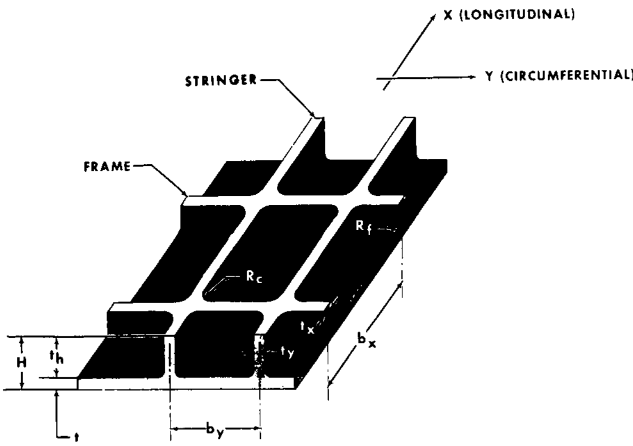

GROUPS 2 AND 3

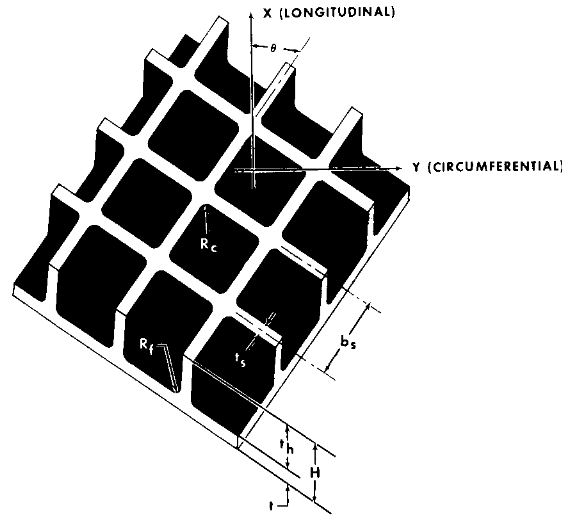

GROUP 4

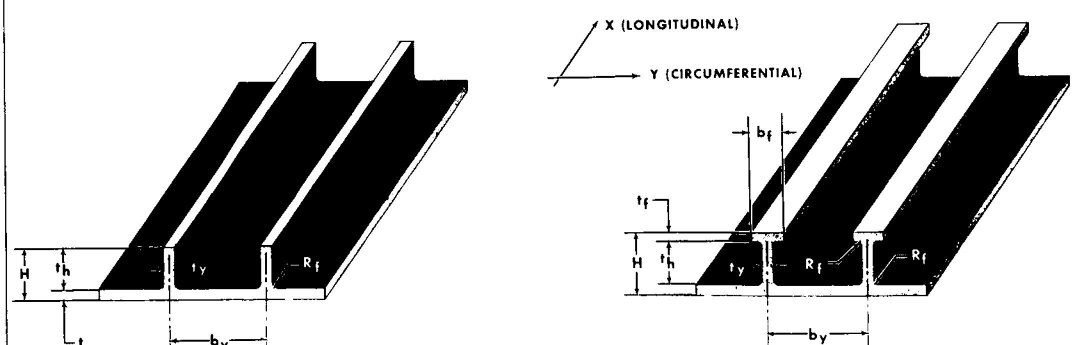

GROUP 5

TYPICAL DIMENSIONAL NOMENCLATURE

FIG. 1

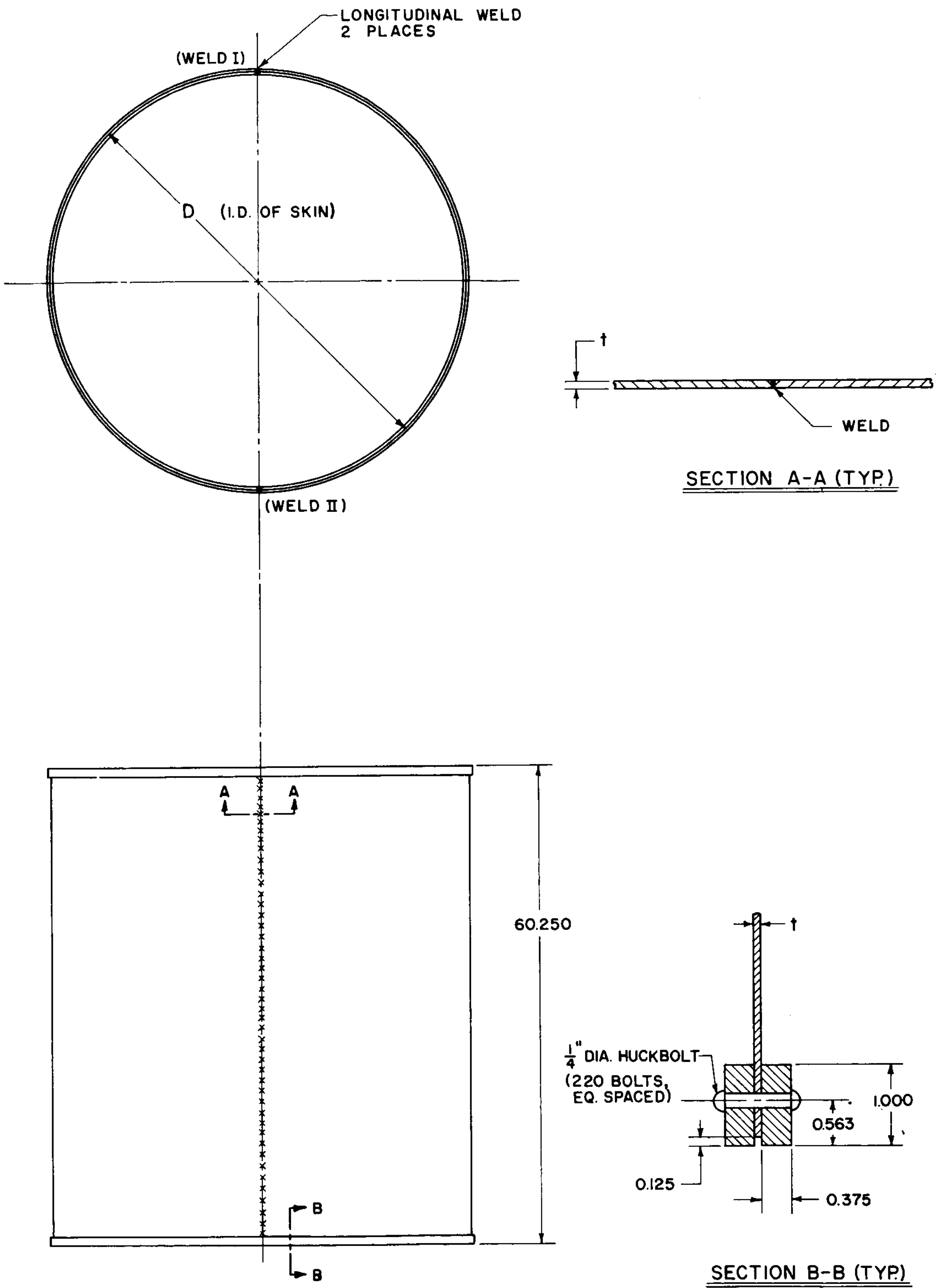

GROUP I		
CYLINDER NO.	D	t
1A	52.320	0.0400
1B	52.124	0.0936

NOMINAL CYLINDER GEOMETRY

FIG. 2

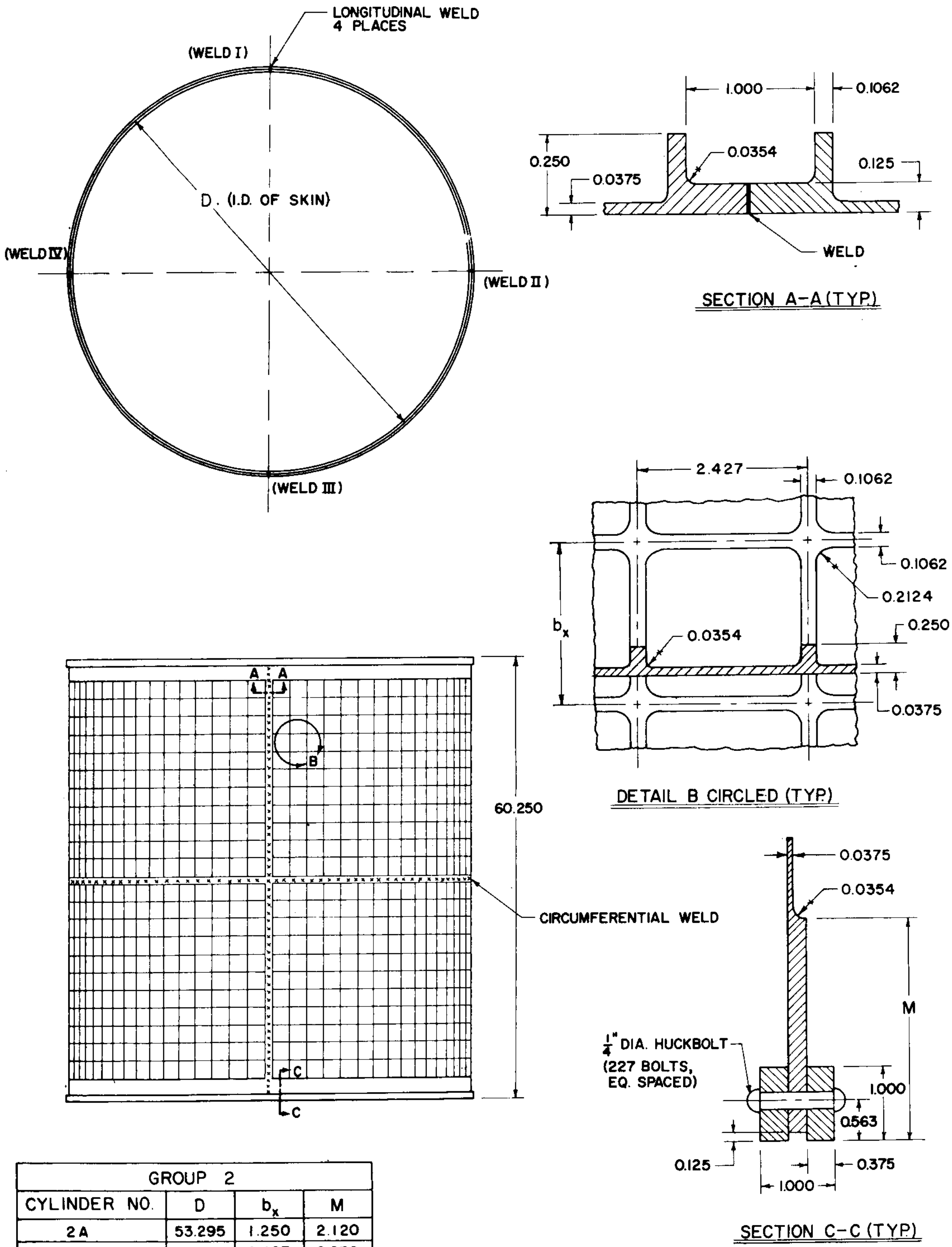

GROUP 2			
CYLINDER NO.	D	b_x	M
2A	53.295	1.250	2.120
2B-1	53.729	2.427	2.930
2B-2	52.783	2.427	2.930
2C	53.286	7.500	7.120

FIG. 2 CONT.

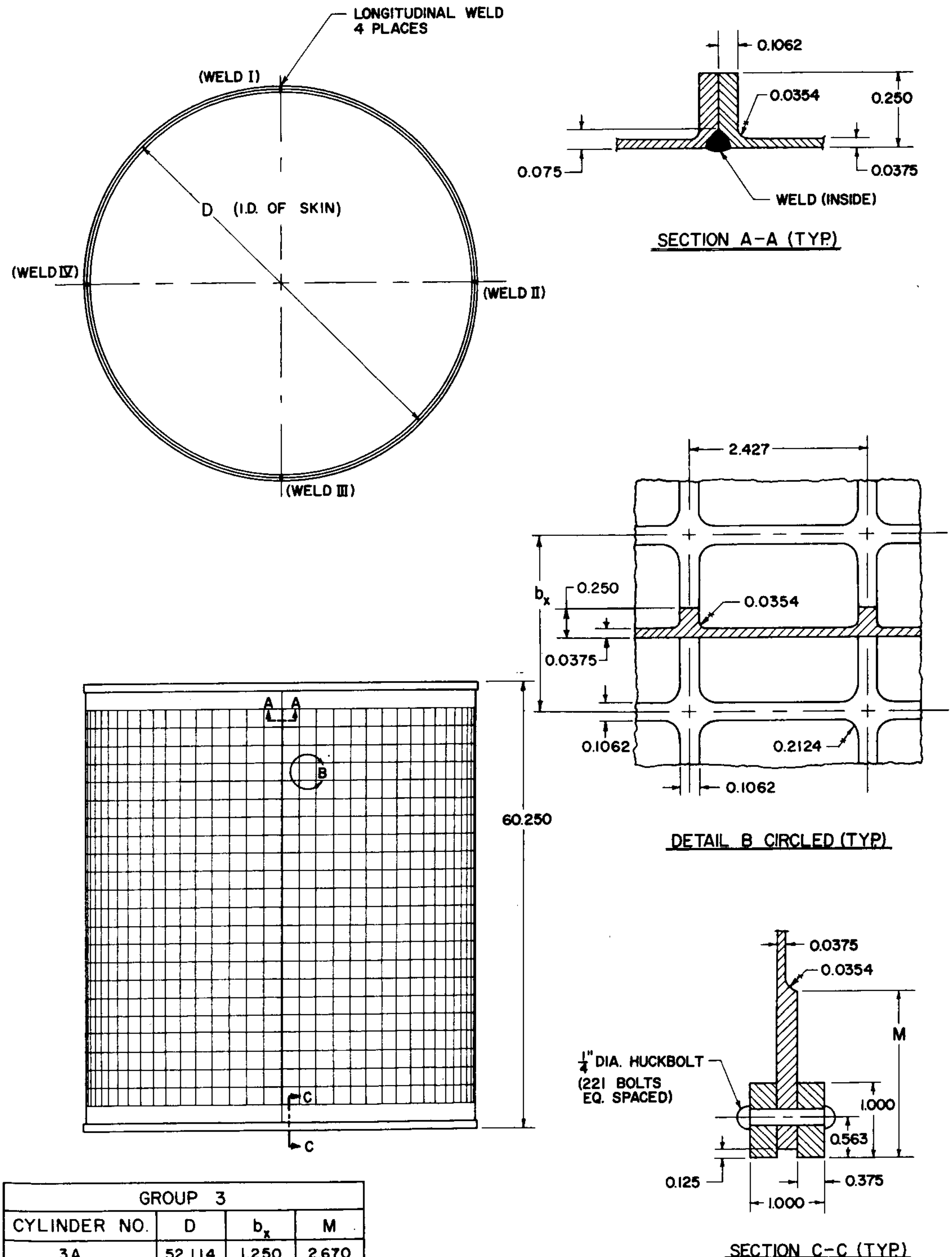

GROUP 3			
CYLINDER NO.	D	b_x	M
3A	52.114	1.250	2.670
3B-1	52.101	2.427	3.480
3B-2	52.132	2.427	3.480
3C	52.131	5.000	2.670
3D	52.152	7.500	3.930

FIG. 2 CONT.

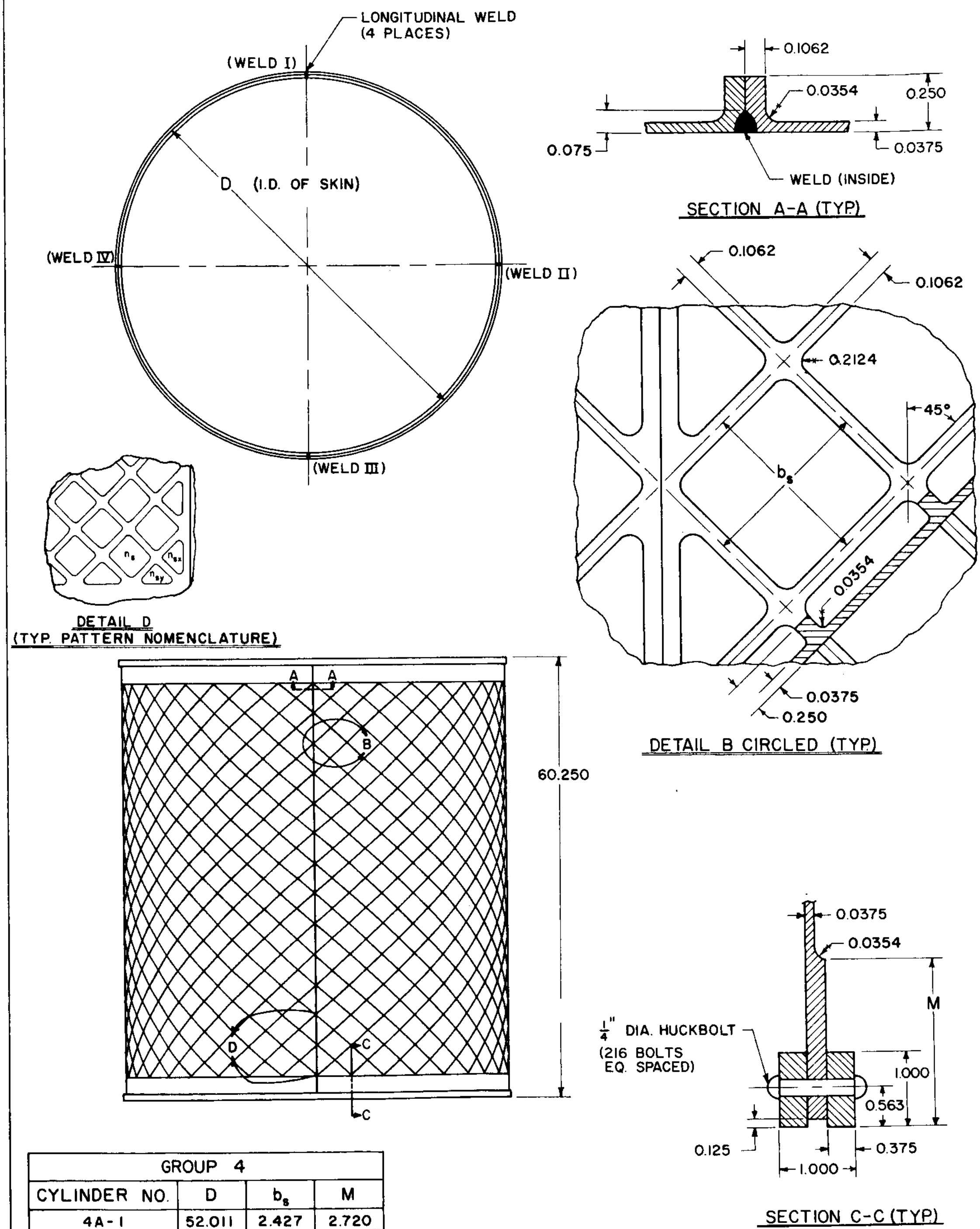

GROUP 4			
CYLINDER NO.	D	b_s	M
4A - 1	52.011	2.427	2.720
4A - 2	52.014	2.427	2.720
4B - 1	51.037	3.177	3.220
4B - 2	51.064	3.177	3.220
4C - 1	52.055	3.712	3.930
4C - 2	52.060	3.712	3.930

FIG. 2 CONT.

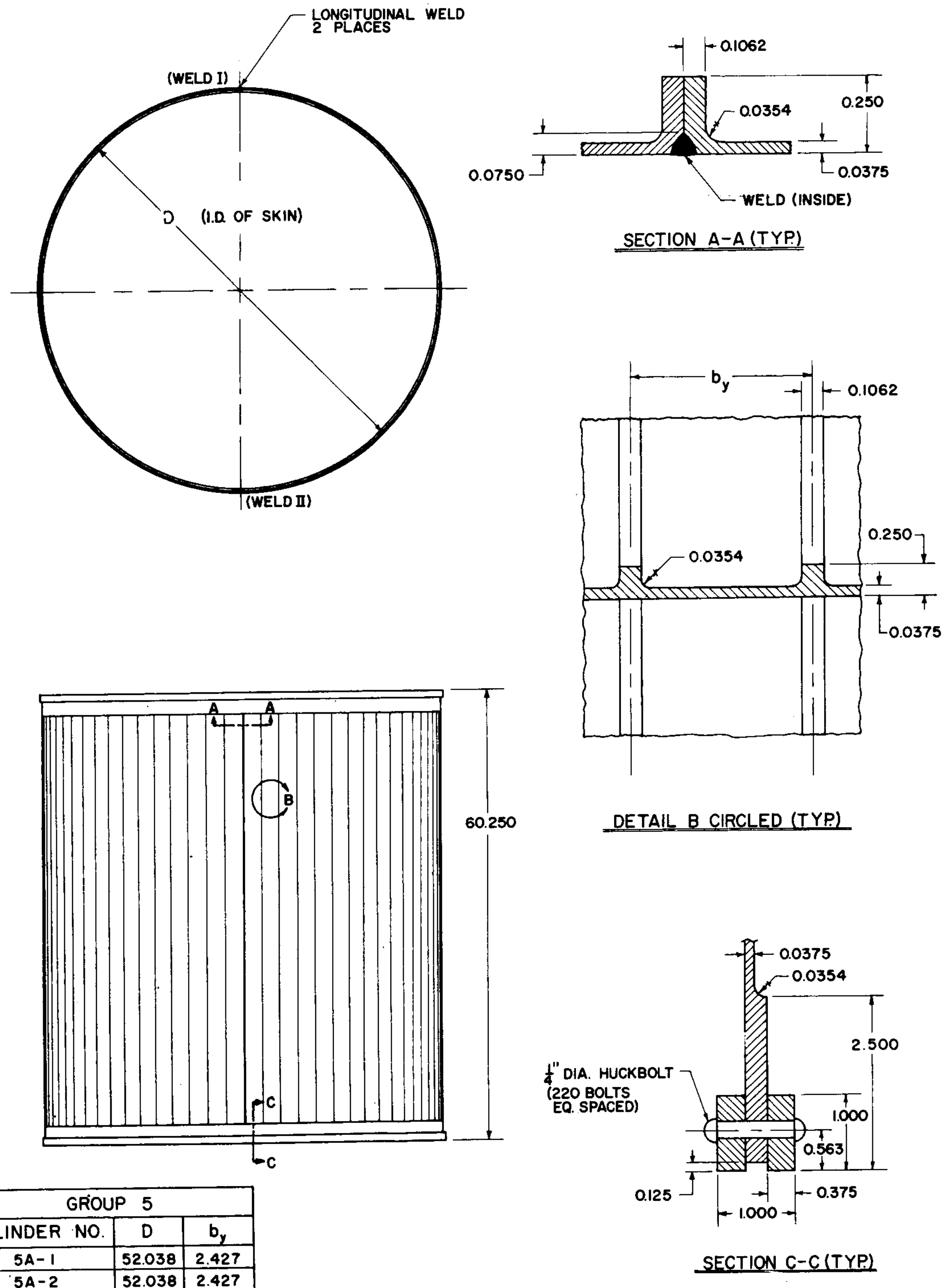

GROUP 5		
CYLINDER NO.	D	b_y
5A-1	52.038	2.427
5A-2	52.038	2.427
5B-1	51.827	1.712
5B-2	51.858	1.712
5C-1	SEE FOLLOWING PAGE	
5C-2		

FIG. 2 CONT.

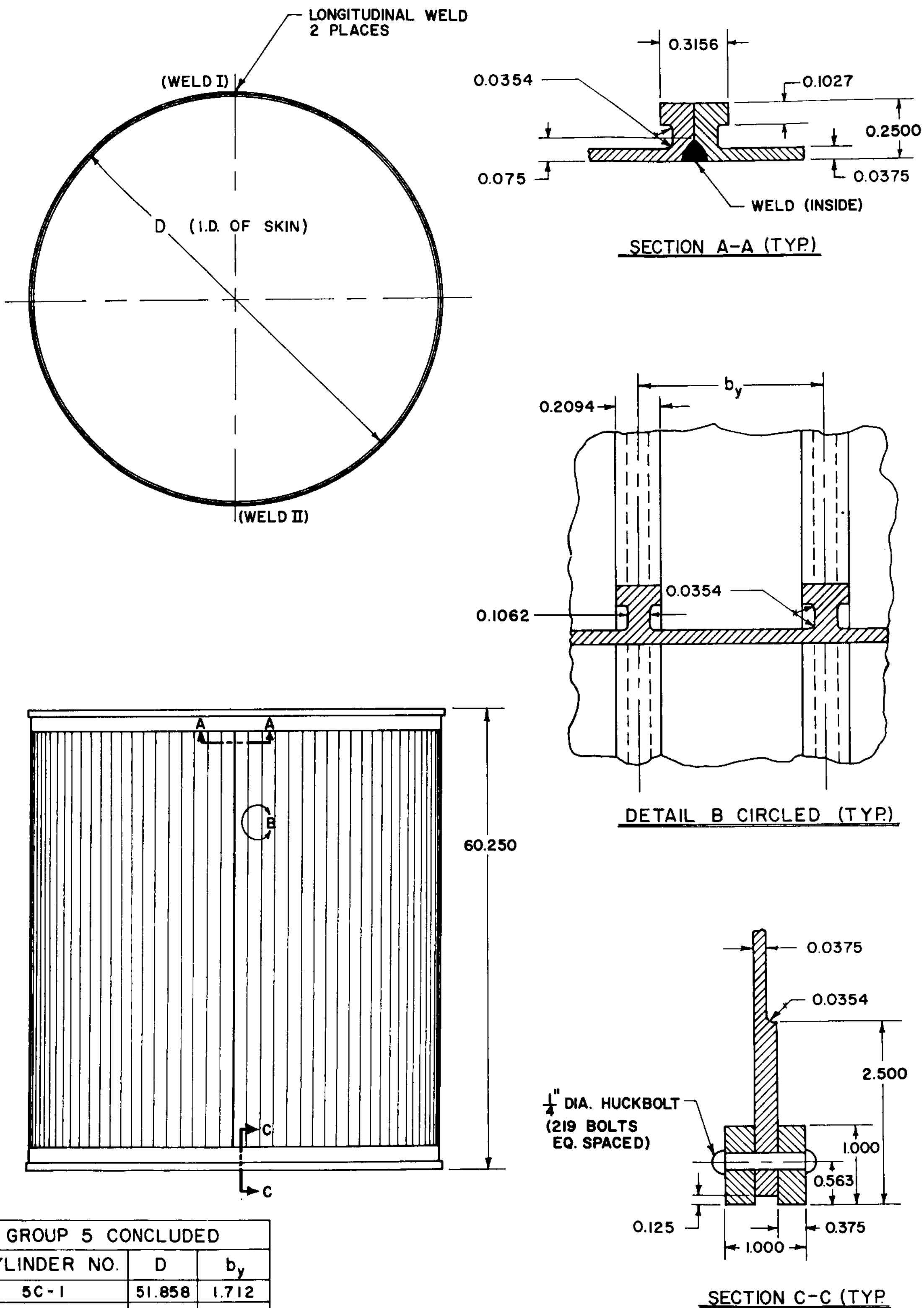

GROUP 5 CONCLUDED		
CYLINDER NO.	D	b_y
5C-1	51.858	1.712
5C-2	51.858	1.712

FIG. 2 CONCLUDED

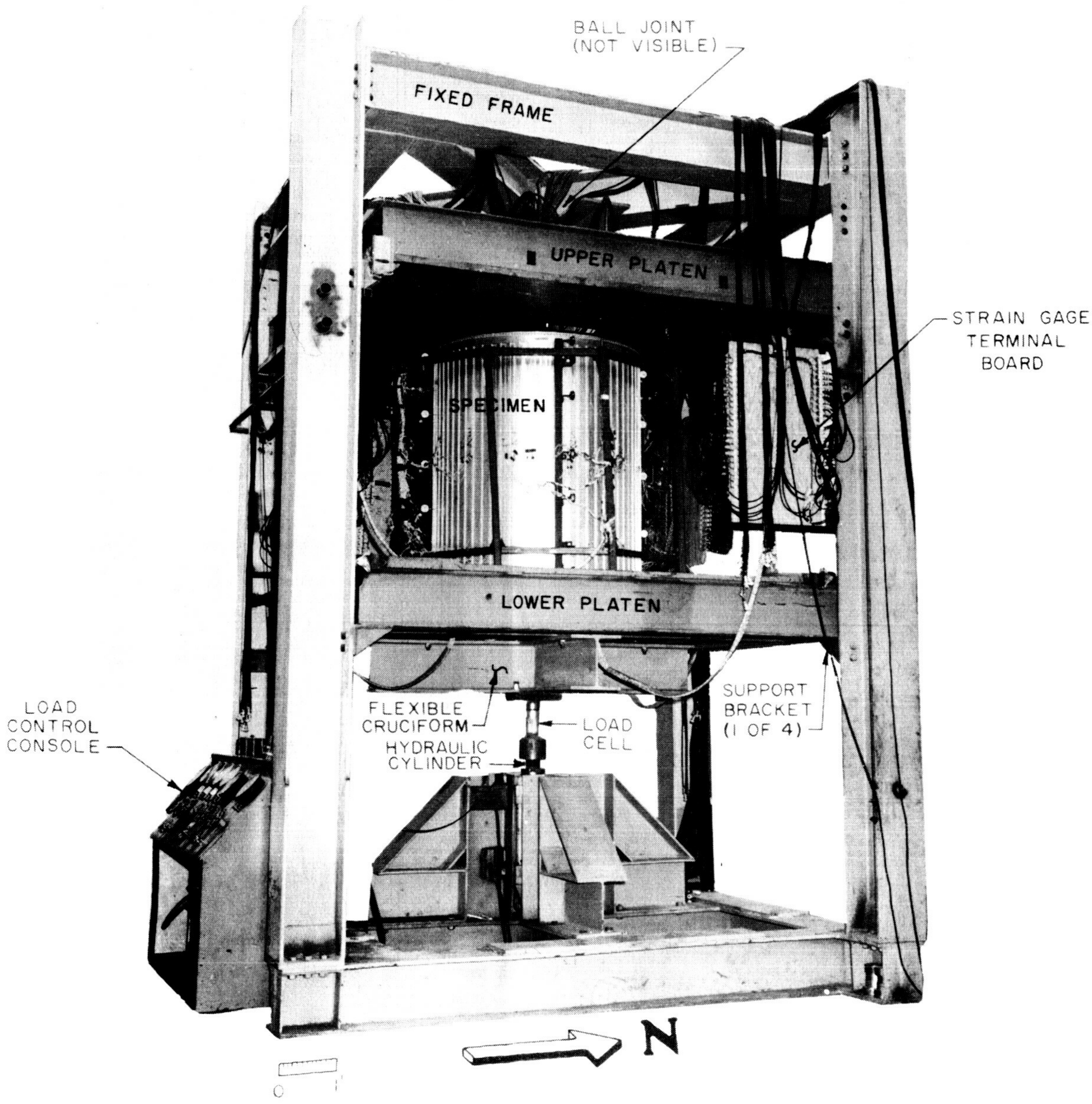

VIEW OF COMPRESSIVE LOADING MACHINE

FIG. 3

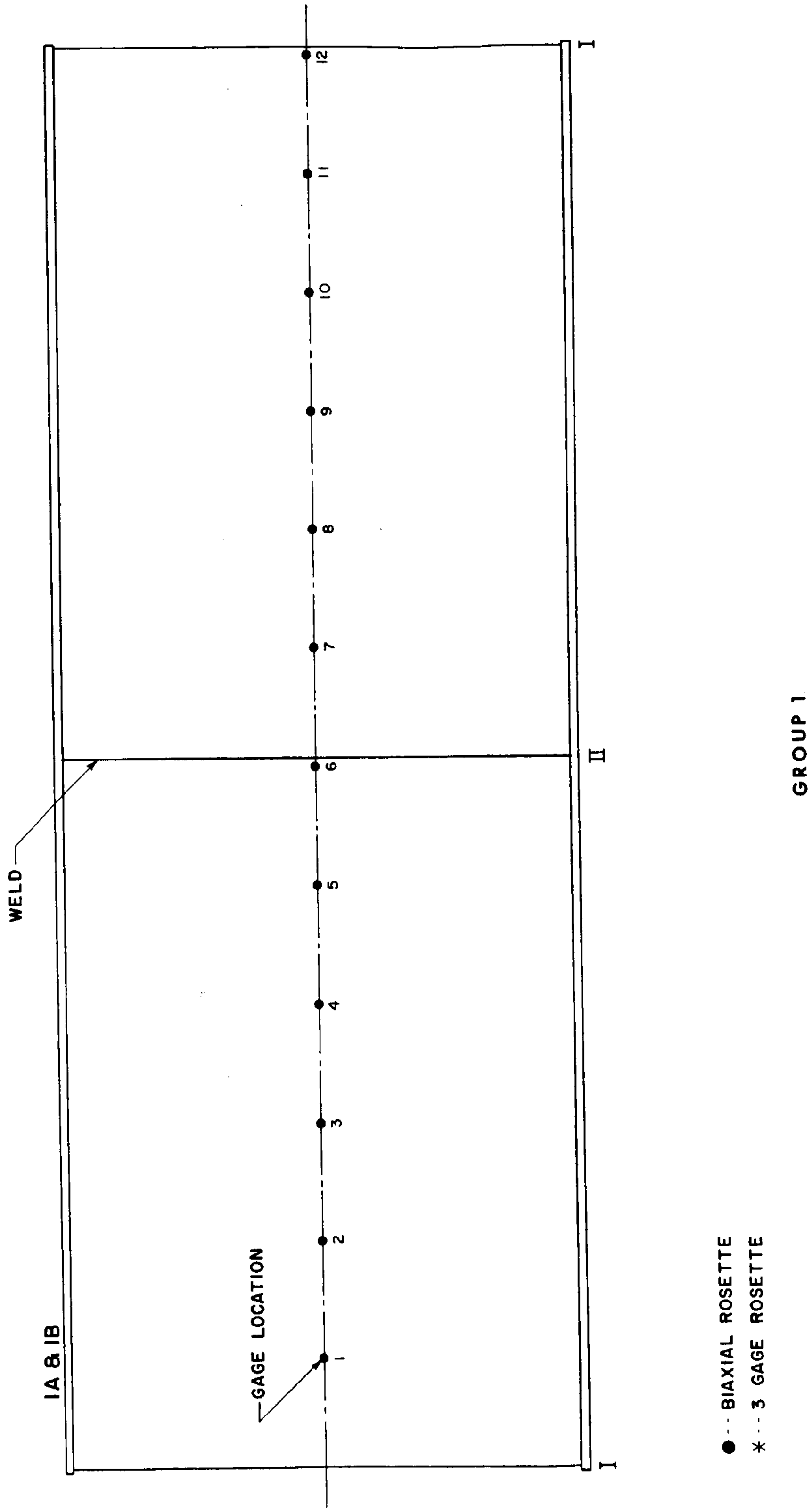

STRAIN GAGE LOCATIONS

FIG. 4

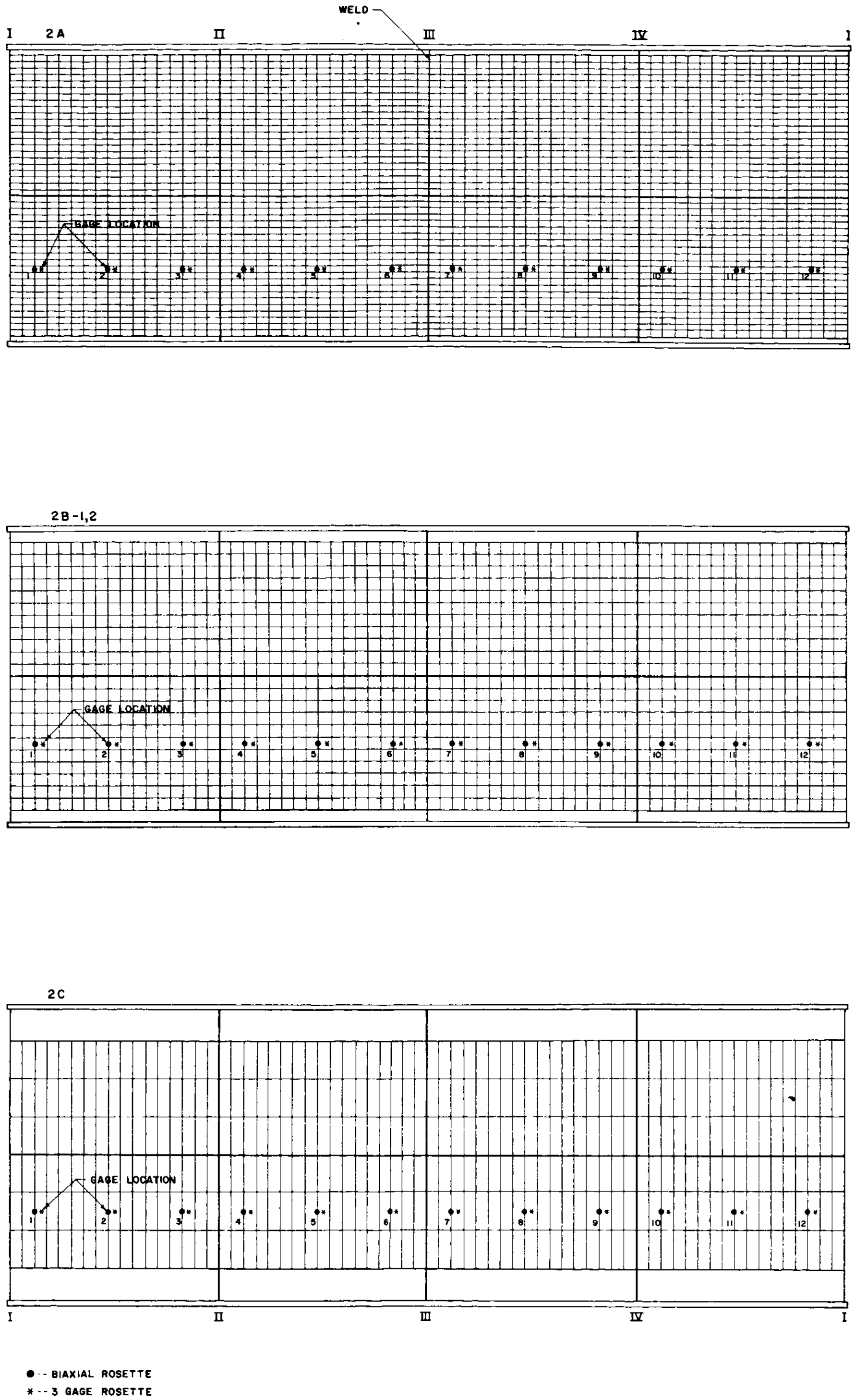
WELD
I
2A
II
III
IV
I
GAGE LOCATION
1
2
3
4
5
6
7
8
9
10
11
12
2B-1,2
GAGE LOCATION
1
2
3
4
5
6
7
8
9
10
11
12
2C
GAGE LOCATION
1
2
3
4
5
6
7
8
9
10
11
12
I
II
III
IV
I
● -- BIAXIAL ROSETTE
* -- 3 GAGE ROSETTE

FIG. 4 CONT.

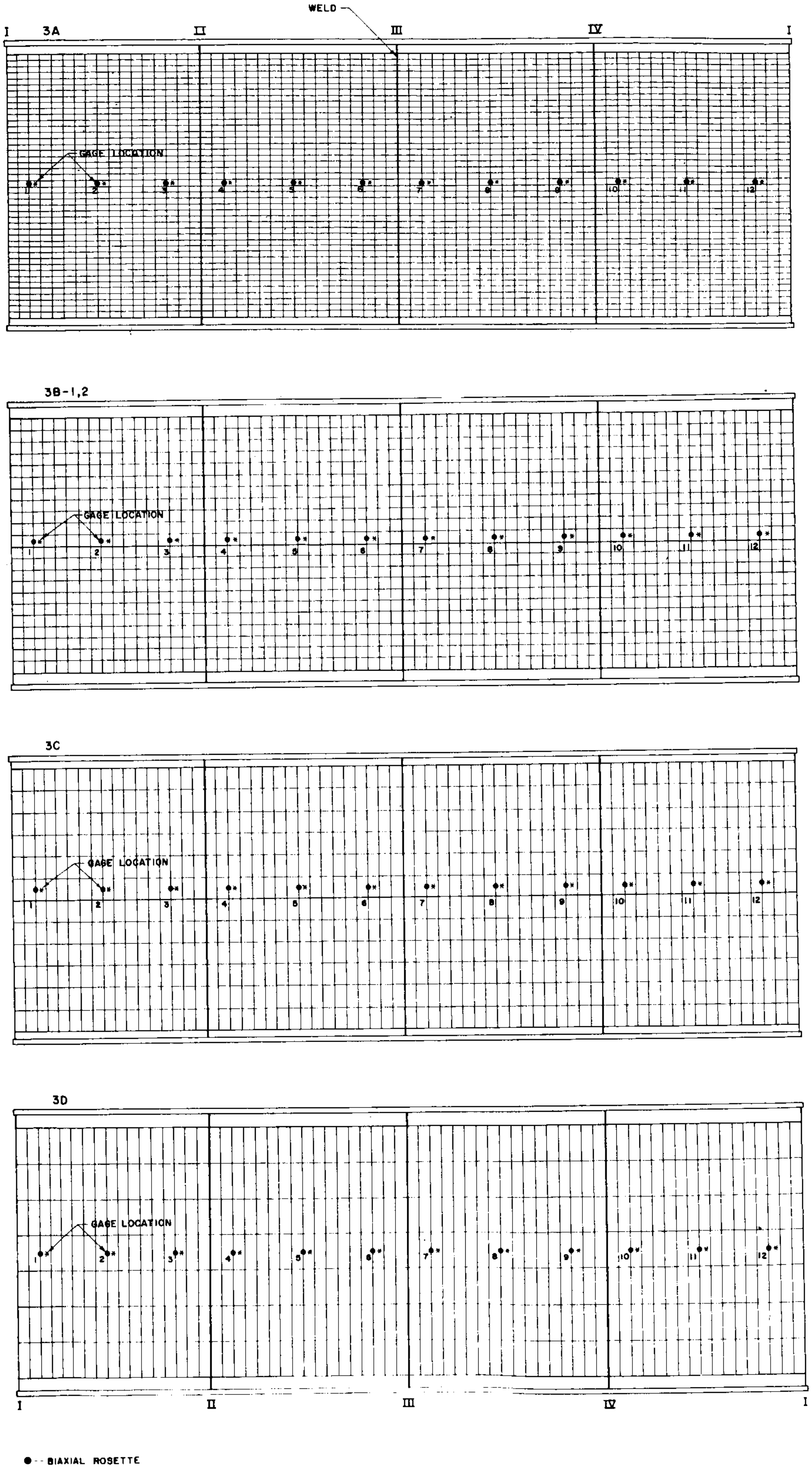
WELD
3A
I
II
III
IV
I
GAGE LOCATION
1
2
3
4
5
6
7
8
9
10
11
12
3B-1,2
GAGE LOCATION
1
2
3
4
5
6
7
8
9
10
11
12
3C
GAGE LOCATION
1
2
3
4
5
6
7
8
9
10
11
12
3D
GAGE LOCATION
1
2
3
4
5
6
7
8
9
10
11
12
I
II
III
IV
I
● -- BIAXIAL ROSETTE
x -- 3 GAGE ROSETTE

FIG. 4 CONT.

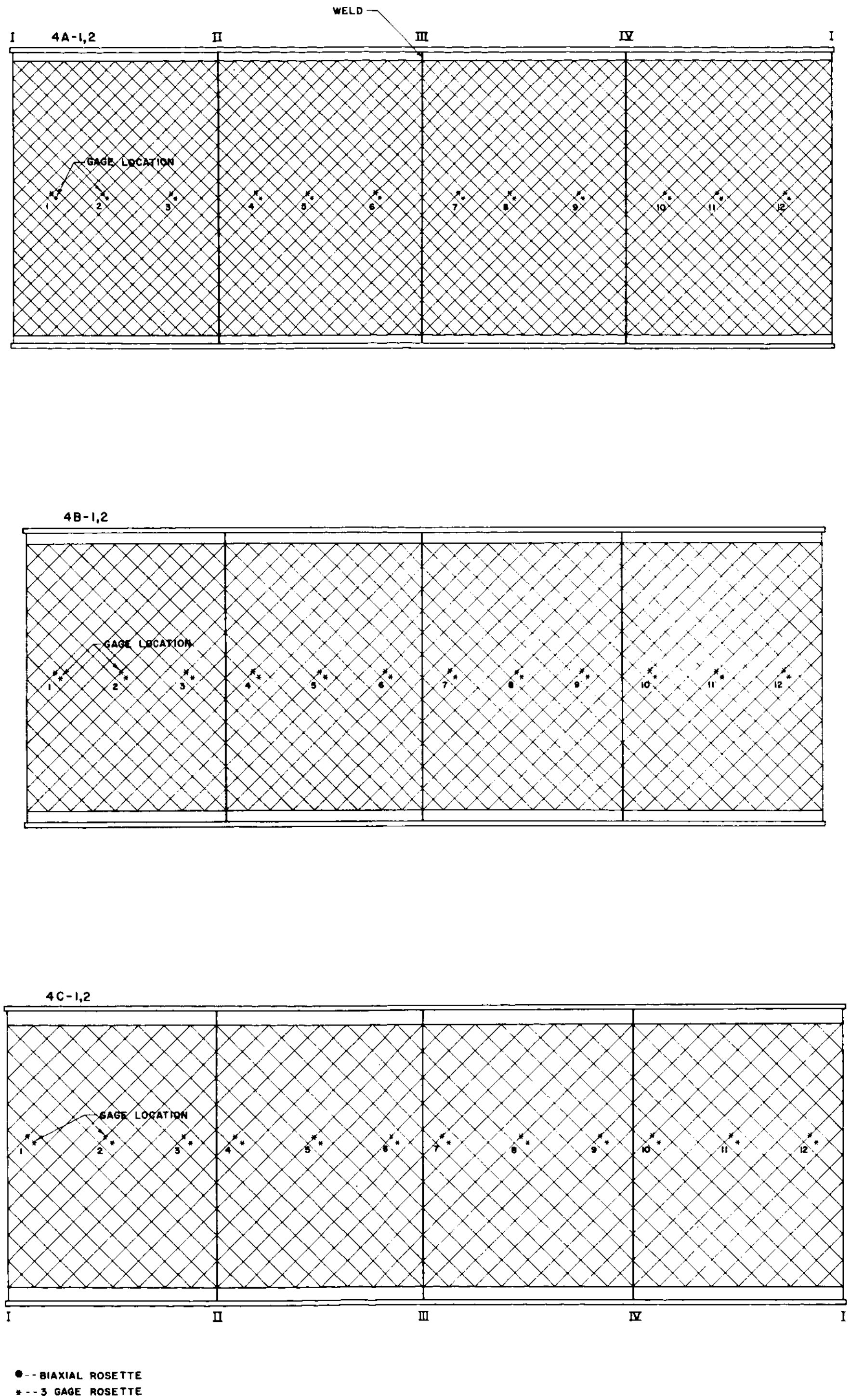
WELD
I
4A-1,2
II
III
IV
I
GAGE LOCATION
1
2
3
4
5
6
7
8
9
10
11
12
4B-1,2
GAGE LOCATION
1
2
3
4
5
6
7
8
9
10
11
12
4C-1,2
GAGE LOCATION
1
2
3
4
5
6
7
8
9
10
11
12
I
II
III
IV
I
●-- BIAXIAL ROSETTE
*-- 3 GAGE ROSETTE

FIG. 4 CONT.

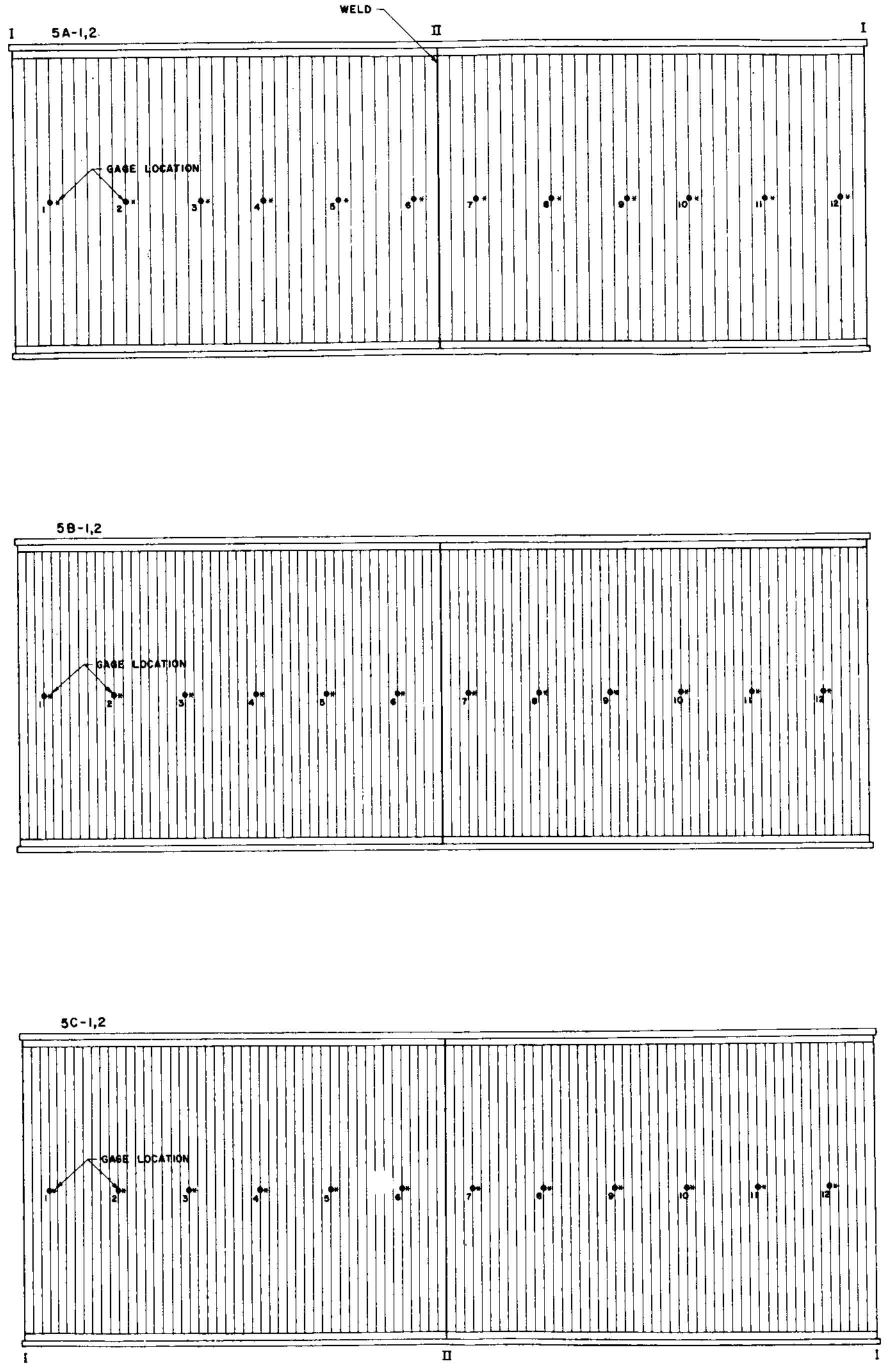

● --BIAXIAL ROSETTE
✱ --3 GAGE ROSETTE

FIG 4 CONCLUDED

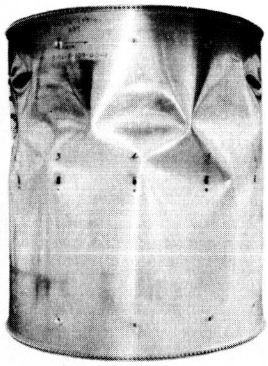

CYLINDER 1A

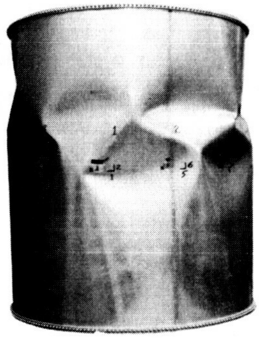

CYLINDER 1B

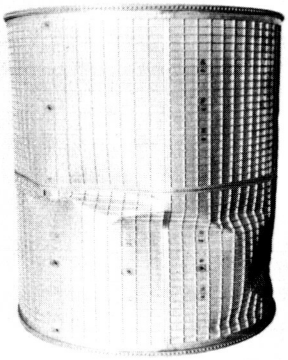

CYLINDER 2A

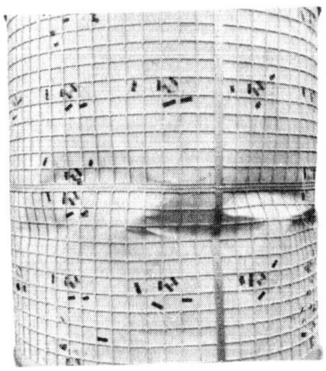

CYLINDER 2B-1

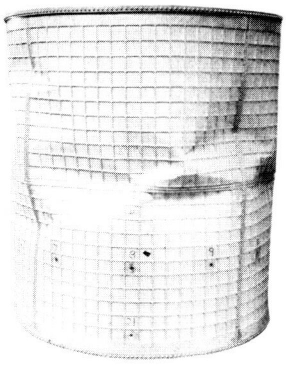

CYLINDER 2B-2

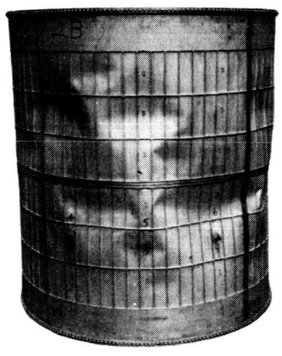

CYLINDER 2C

VIEWS OF BUCKLED CYLINDERS

FIG. 5

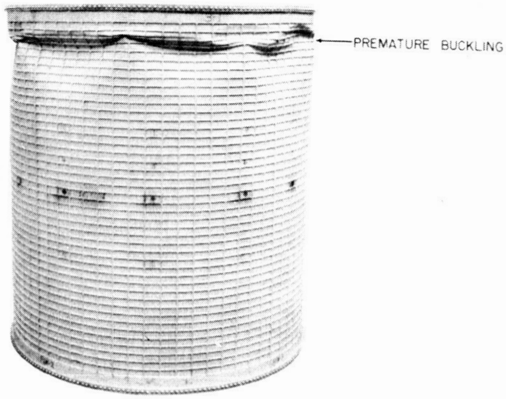

CYLINDER 3A

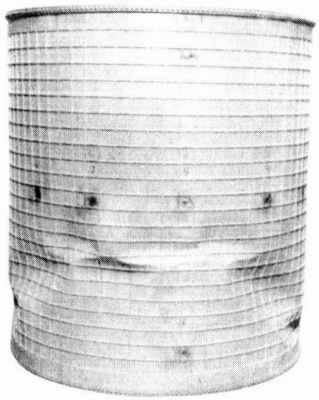

CYLINDER 3B - 1

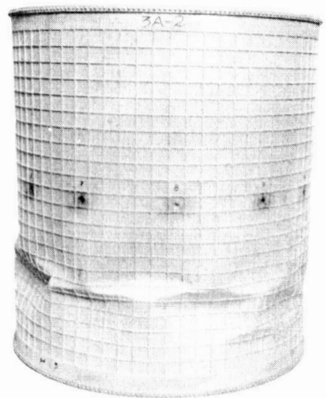

CYLINDER 3B - 2

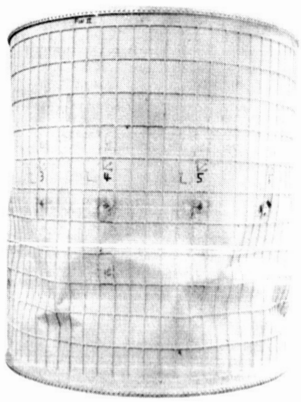

CYLINDER 3C

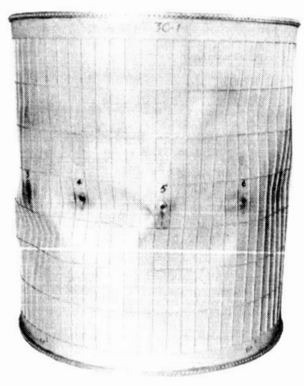

CYLINDER 3D

FIG. 5 CONT.

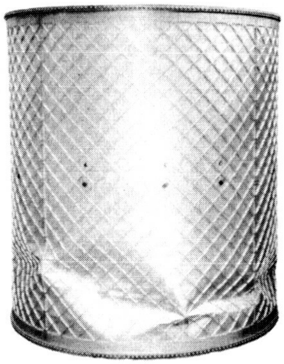

CYLINDER 4A-1

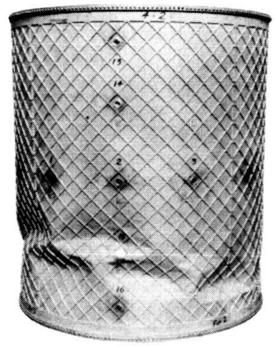

CYLINDER 4A-2

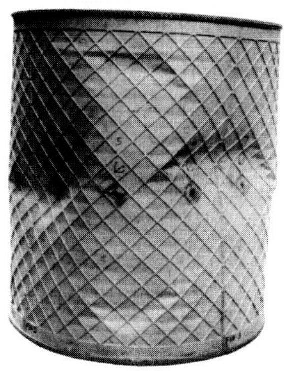

CYLINDER 4B-1

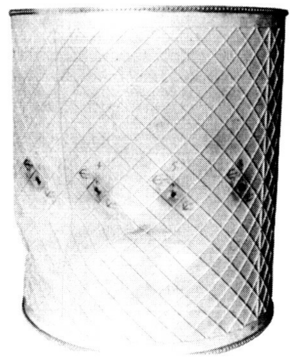

CYLINDER 4B-2

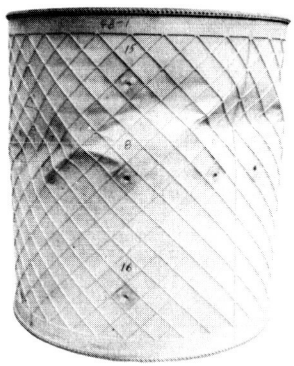

CYLINDER 4C-1

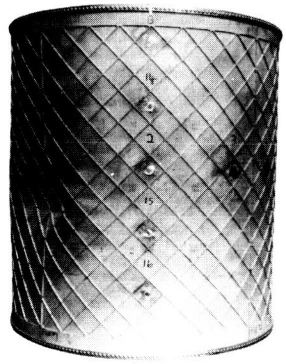

CYLINDER 4C-2

FIG. 5 CONT.

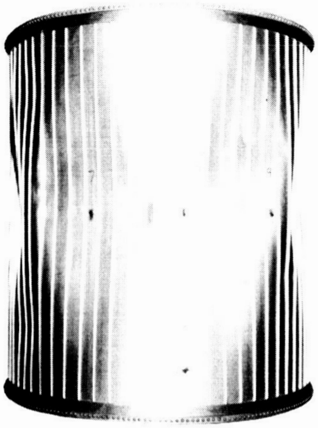

CYLINDER 5A-1

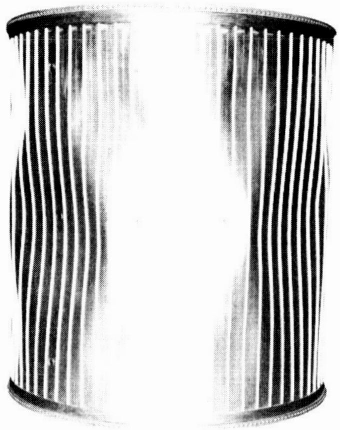

CYLINDER 5A-2

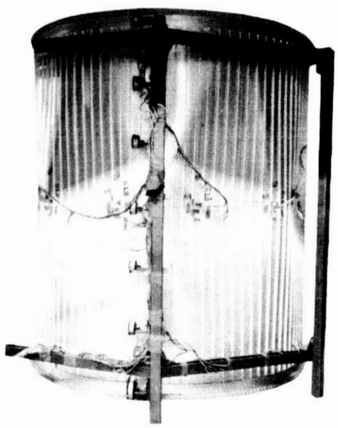

CYLINDER 5B-1

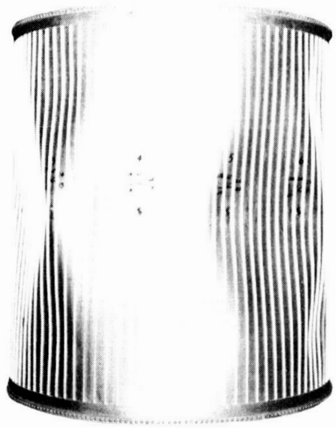

CYLINDER 5B-2

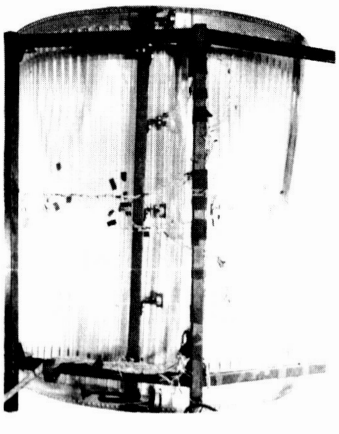

CYLINDER 5C-1

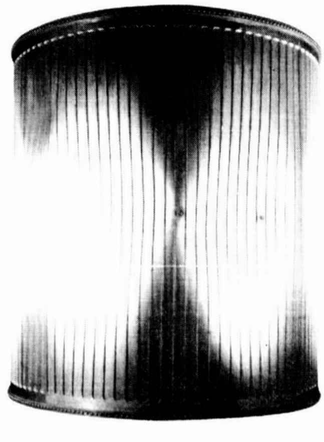

CYLINDER 5C-2

FIG. 5 CONCLUDED

Free - Body showing local end-moments in skin due to eccentricity, (neglecting effect of shear decay and frame stiffness).

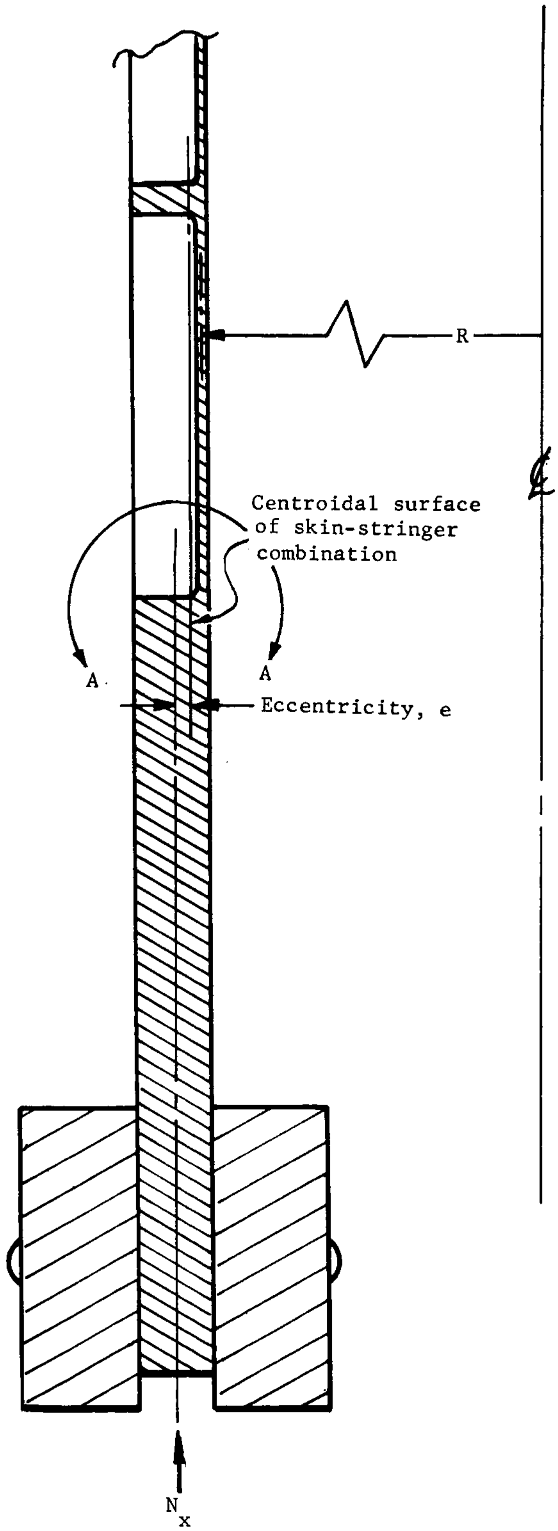

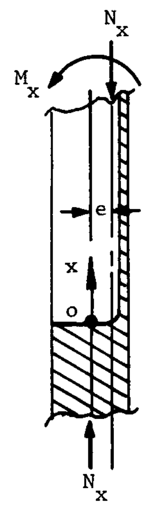

View A - A

$M_x = M_o \phi$

where $M_o = N_x e$

$$\phi = e^{-\beta x}(\cos \beta x + \sin \beta x)$$

$$\beta = \left[\frac{Et}{4R^2 D_x}\right]^{\frac{1}{4}} \qquad \text{Ref. (15)}$$

$$D_x = EI_x = 1.558 \times 10^{-4} E$$

$R = 26.2$ and $t = 0.0375$

For $M_x < 5\%$, $x \approx 4$
or End-Moment decays to 5% of its initial value within 4 inches.

END MOMENT DUE TO ECCENTRICITY

FIG. 6

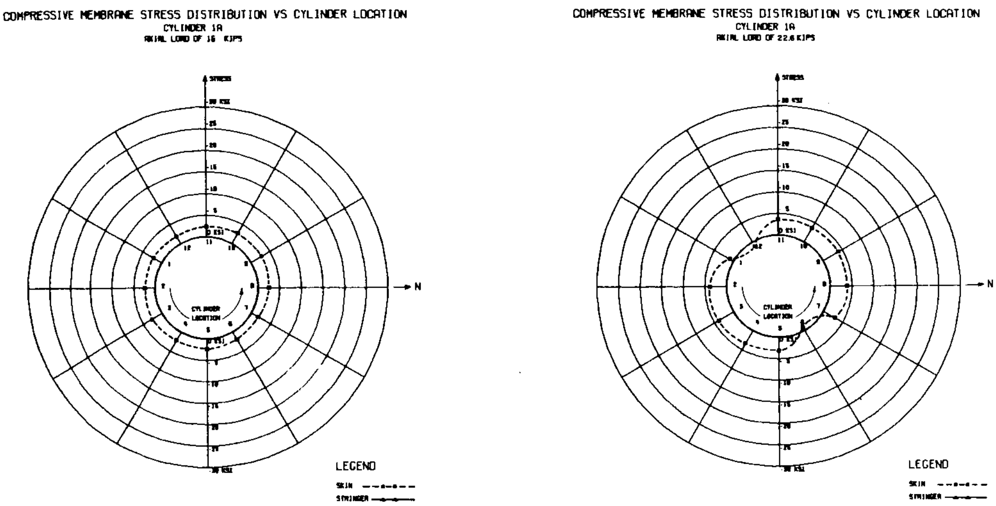

GENERAL INSTABILITY OCCURRED AT 22.9 KIPS

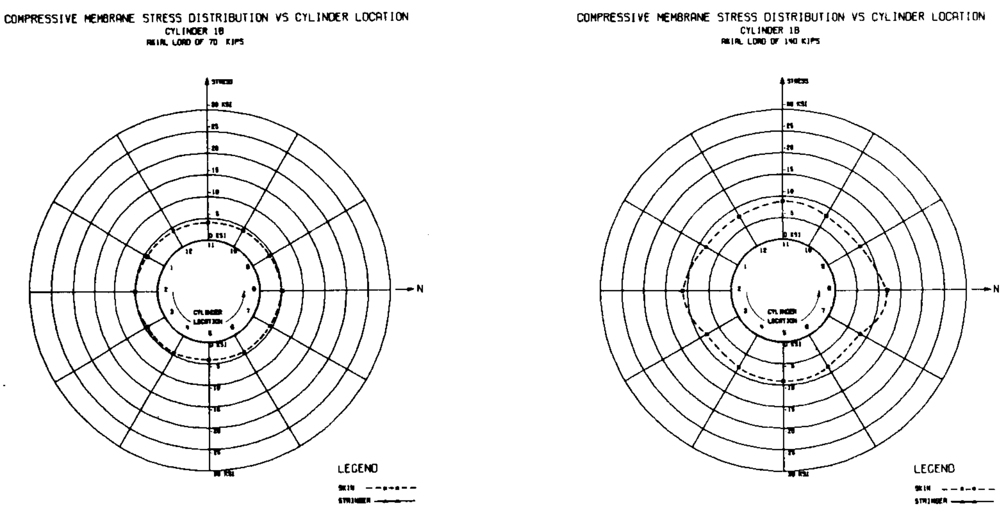

GENERAL INSTABILITY OCCURRED AT 143.5 KIPS

POLAR PLOTS OF STRESS DISTRIBUTIONS

FIG. 7

COMPRESSIVE MEMBRANE STRESS DISTRIBUTION VS CYLINDER LOCATION
CYLINDER 2A
AXIAL LOAD OF 70 KIPS

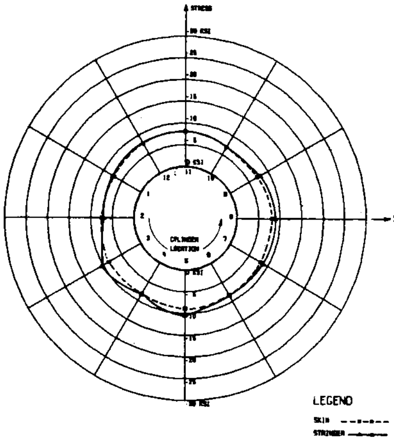

COMPRESSIVE MEMBRANE STRESS DISTRIBUTION VS CYLINDER LOCATION
CYLINDER 2A
AXIAL LOAD OF 170 KIPS

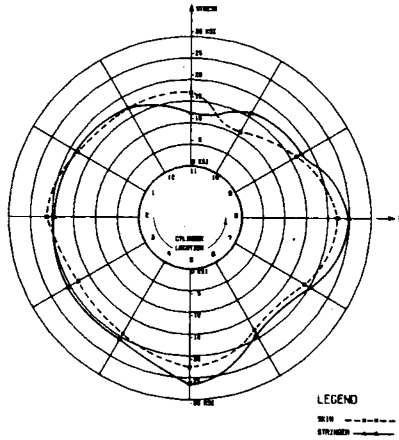

GENERAL INSTABILITY OCCURRED AT 171.5 KIPS

COMPRESSIVE MEMBRANE STRESS DISTRIBUTION VS CYLINDER LOCATION
CYLINDER 2B-1
AXIAL LOAD OF 80 KIPS

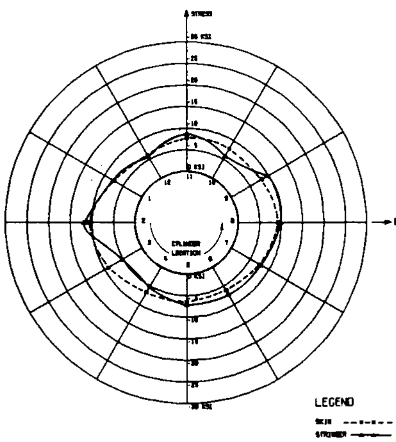

COMPRESSIVE MEMBRANE STRESS DISTRIBUTION VS CYLINDER LOCATION
CYLINDER 2B-1
AXIAL LOAD OF 117 KIPS

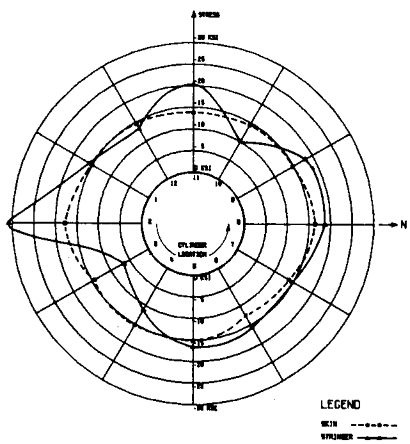

GENERAL INSTABILITY OCCURRED AT 118.3 KIPS

FIG. 7 CONT.

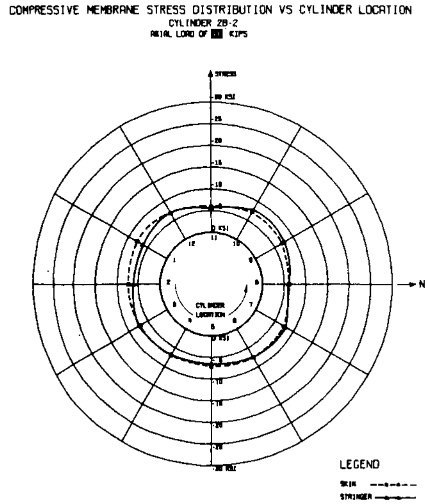

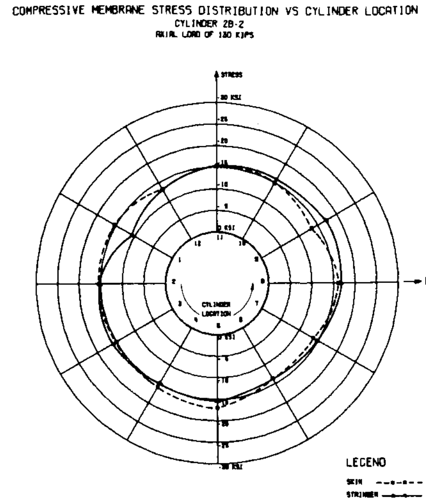

GENERAL INSTABILITY OCCURRED AT 131.5 KIPS

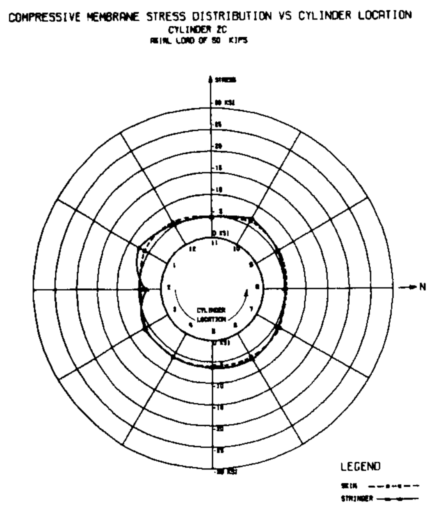

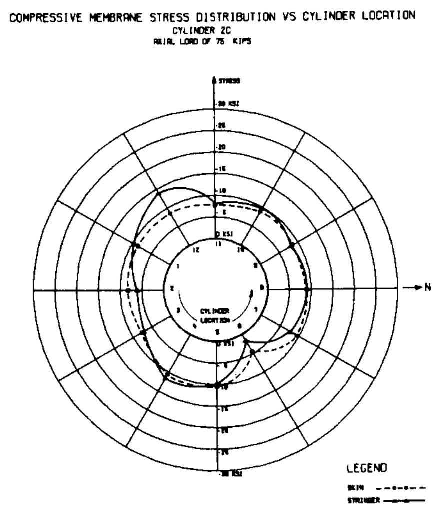

GENERAL INSTABILITY OCCURRED AT 77.2 KIPS

FIG. 7 CONT.

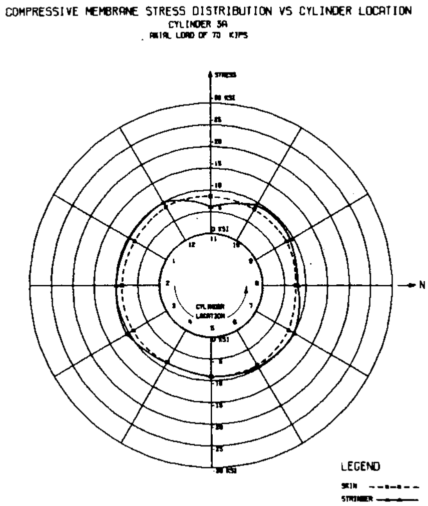

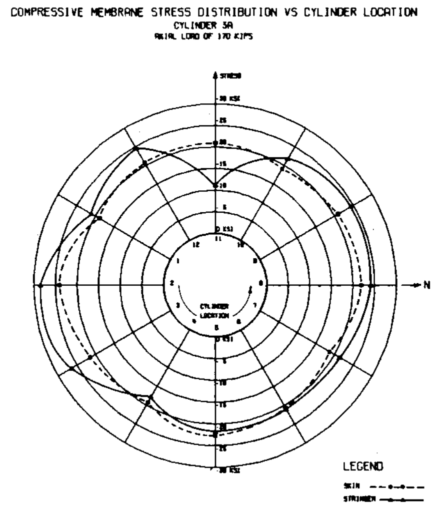

GENERAL INSTABILITY OCCURRED AT 172.1 KIPS

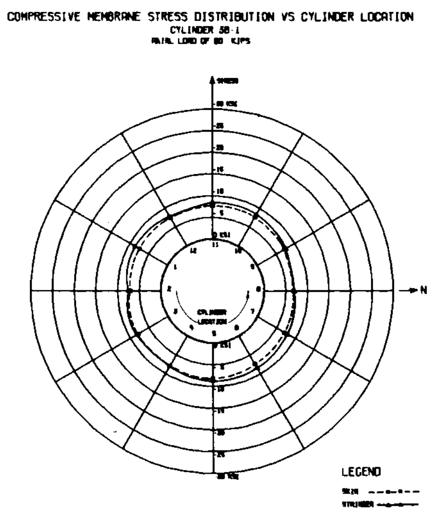

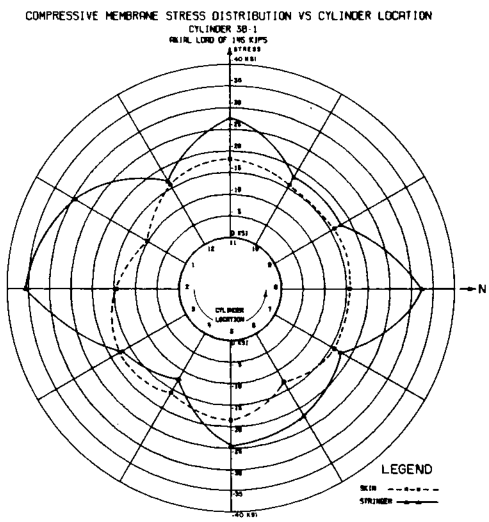

GENERAL INSTABILITY OCCURRED AT 150.0 KIPS

FIG. 7 CONT.

COMPRESSIVE MEMBRANE STRESS DISTRIBUTION VS CYLINDER LOCATION
CYLINDER 3B-2
AXIAL LOAD OF 70 KIPS

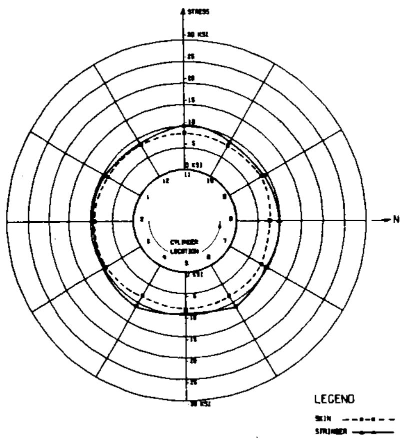

COMPRESSIVE MEMBRANE STRESS DISTRIBUTION VS CYLINDER LOCATION
CYLINDER 3B-2
AXIAL LOAD OF 150 KIPS

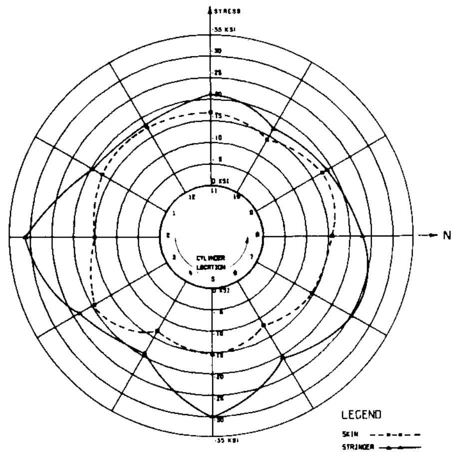

GENERAL INSTABILITY OCCURRED AT 154.7 KIPS

COMPRESSIVE MEMBRANE STRESS DISTRIBUTION VS CYLINDER LOCATION
CYLINDER 3C
AXIAL LOAD OF 80 KIPS

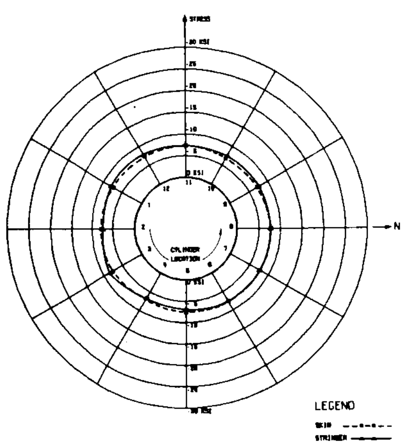

COMPRESSIVE MEMBRANE STRESS DISTRIBUTION VS CYLINDER LOCATION
CYLINDER 3C
AXIAL LOAD OF 120 KIPS

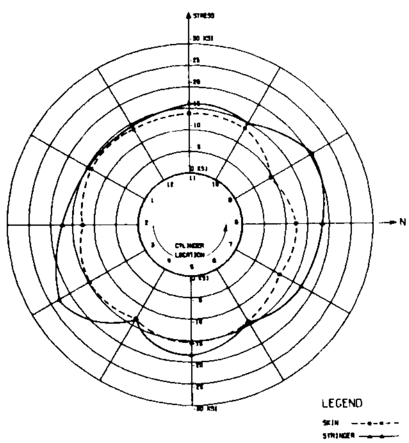

GENERAL INSTABILITY OCCURRED AT 122.2 KIPS

FIG. 7 CONT.

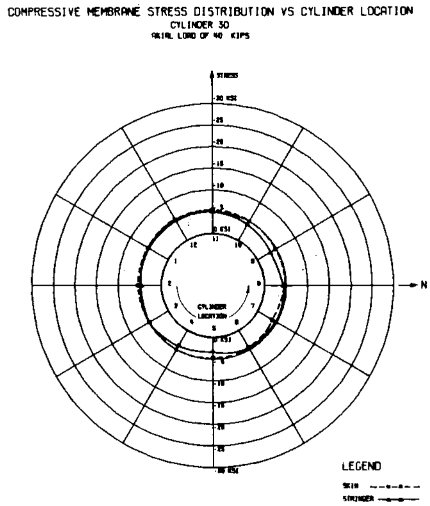

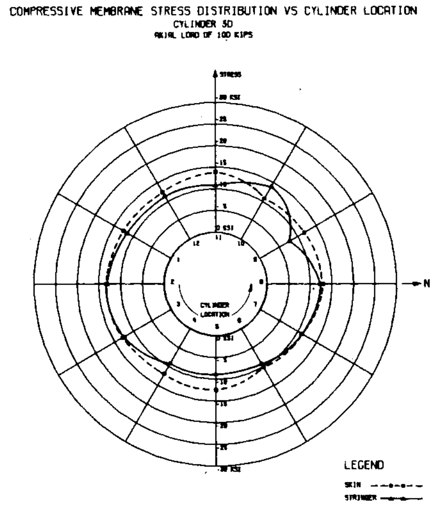

GENERAL INSTABILITY OCCURRED AT 103.9 KIPS

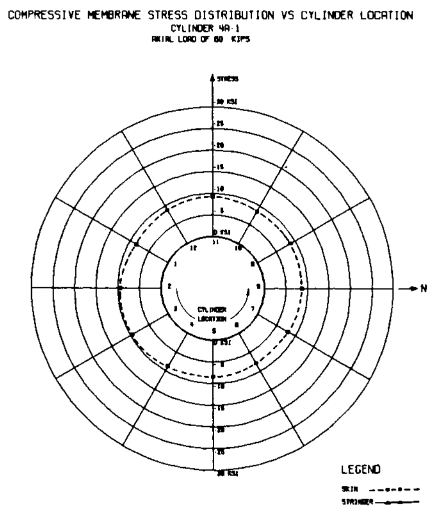

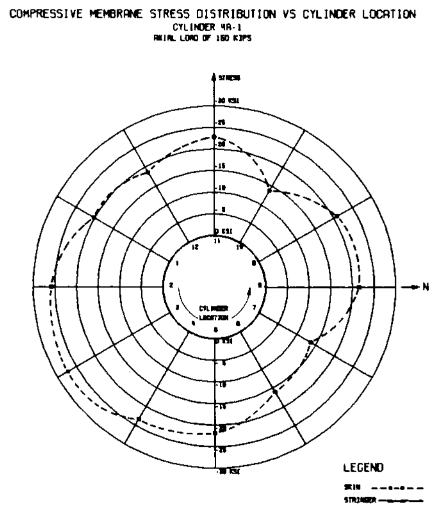

GENERAL INSTABILITY OCCURRED AT 154.0 KIPS

FIG. 7 CONT.

COMPRESSIVE MEMBRANE STRESS DISTRIBUTION VS CYLINDER LOCATION
CYLINDER 4A-2
AXIAL LOAD OF 80 KIPS

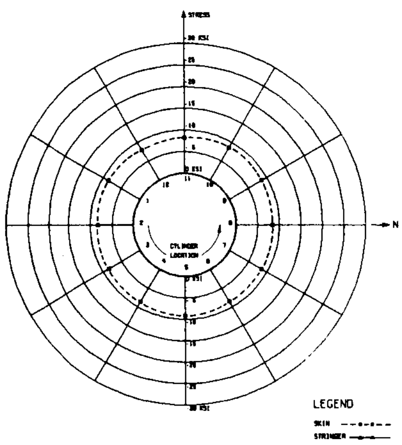

COMPRESSIVE MEMBRANE STRESS DISTRIBUTION VS CYLINDER LOCATION
CYLINDER 4A-2
AXIAL LOAD OF 160 KIPS

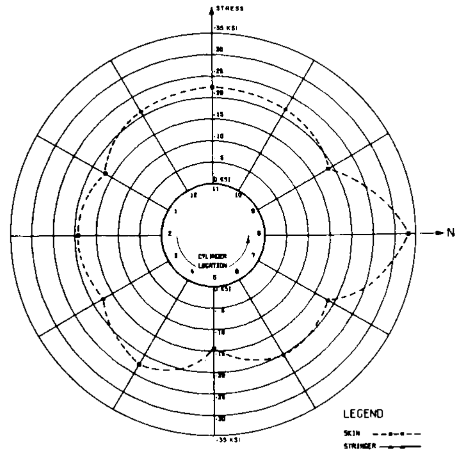

GENERAL INSTABILITY OCCURRED AT 164.8 KIPS

COMPRESSIVE MEMBRANE STRESS DISTRIBUTION VS CYLINDER LOCATION
CYLINDER 4B-1
AXIAL LOAD OF 40 KIPS

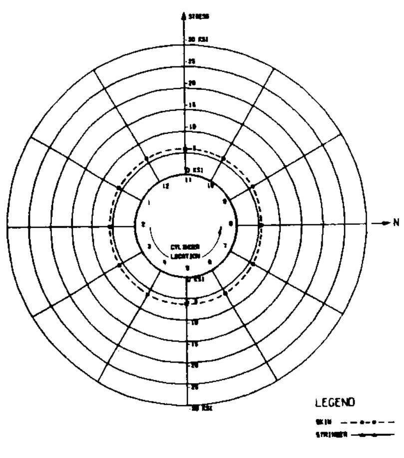

COMPRESSIVE MEMBRANE STRESS DISTRIBUTION VS CYLINDER LOCATION
CYLINDER 4B-1
AXIAL LOAD OF 105 KIPS

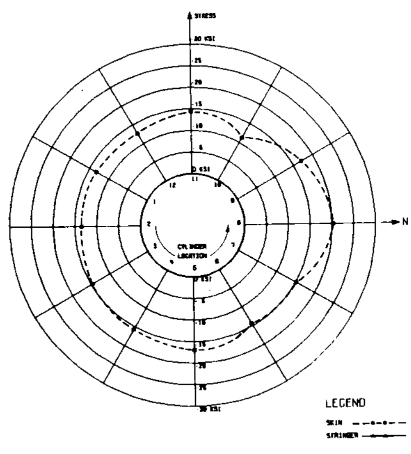

GENERAL INSTABILITY OCCURRED AT 110.0 KIPS

FIG. 7 CONT.

COMPRESSIVE MEMBRANE STRESS DISTRIBUTION VS CYLINDER LOCATION
CYLINDER 4B-2
AXIAL LOAD OF 40 KIPS

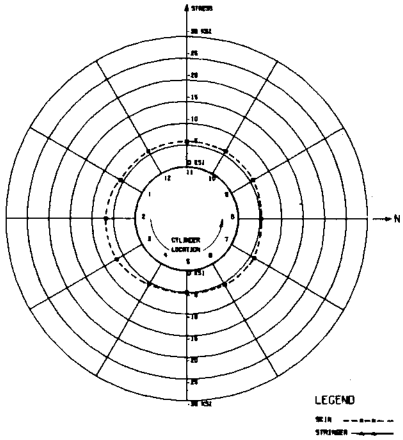

COMPRESSIVE MEMBRANE STRESS DISTRIBUTION VS CYLINDER LOCATION
CYLINDER 4B-2
AXIAL LOAD OF 100 KIPS

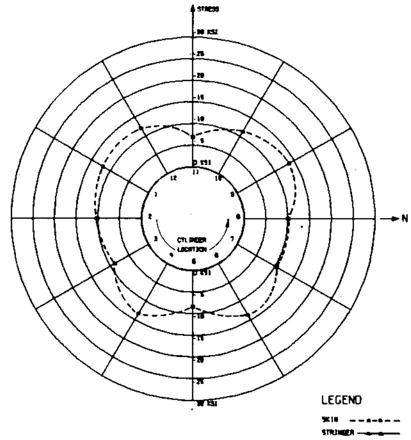

GENERAL INSTABILITY OCCURRED AT 104.3 KIPS

COMPRESSIVE MEMBRANE STRESS DISTRIBUTION VS CYLINDER LOCATION
CYLINDER 4C-1
AXIAL LOAD OF 50 KIPS

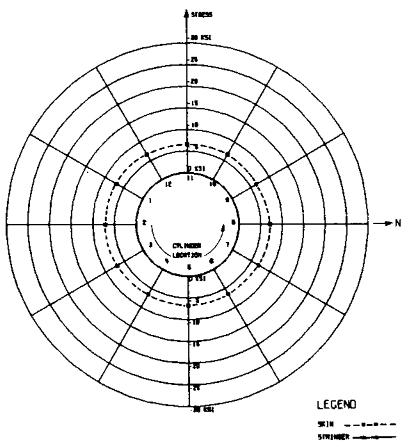

COMPRESSIVE MEMBRANE STRESS DISTRIBUTION VS CYLINDER LOCATION
CYLINDER 4C-1
AXIAL LOAD OF 96 KIPS

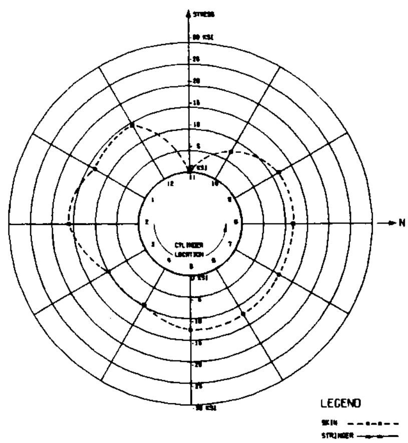

GENERAL INSTABILITY OCCURRED AT 93.4 KIPS

FIG. 7 CONT.

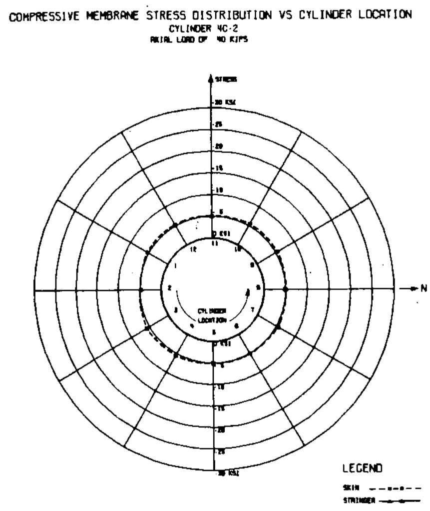

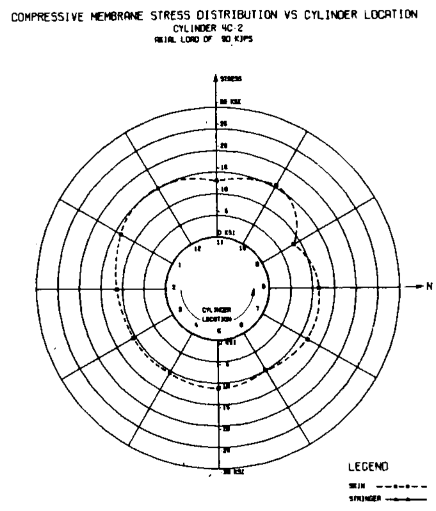

GENERAL INSTABILITY OCCURRED AT 97.3 KIPS

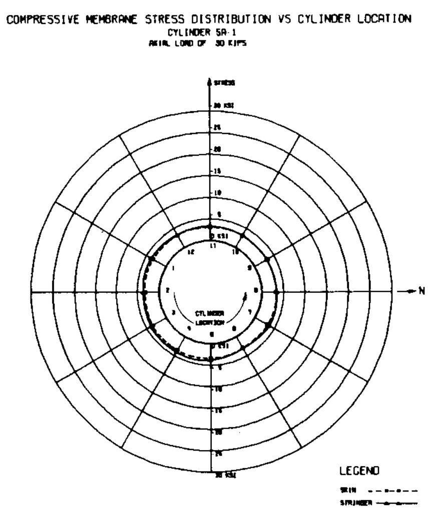

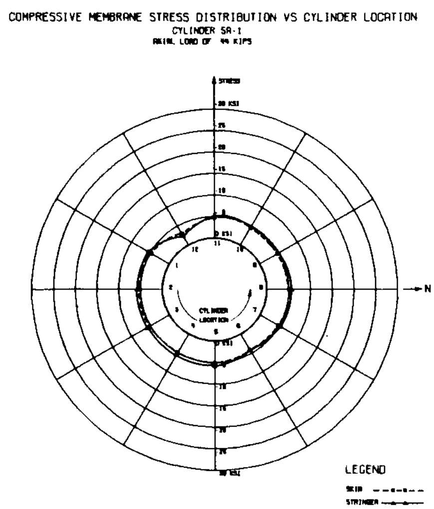

GENERAL INSTABILITY OCCURRED AT 44.3 KIPS

FIG. 7 CONT.

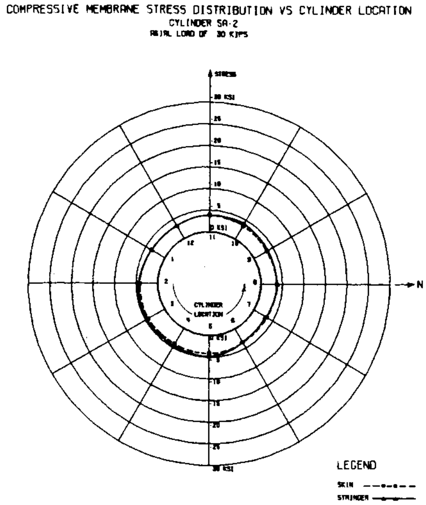

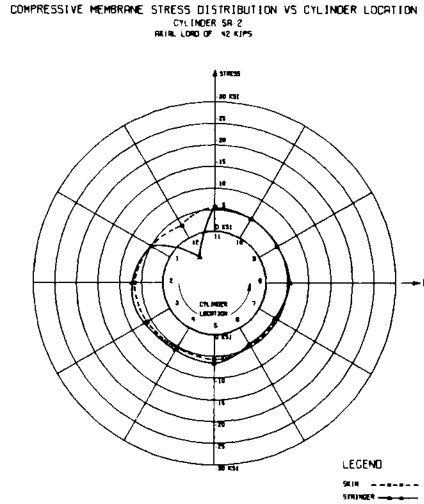

GENERAL INSTABILITY OCCURRED AT 41.9 KIPS

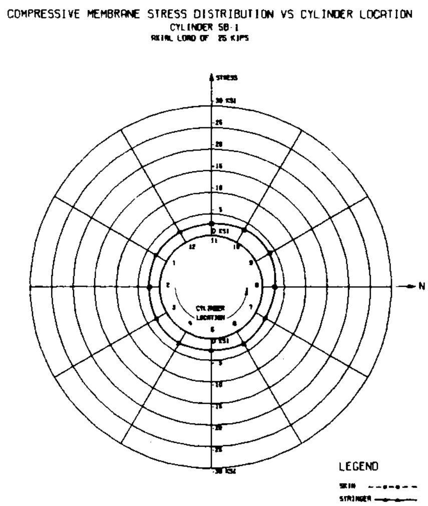

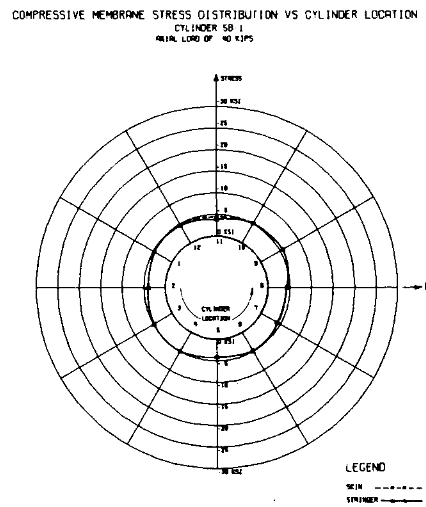

GENERAL INSTABILITY OCCURRED AT 43.7 KIPS

FIG. 7 CONT.

COMPRESSIVE MEMBRANE STRESS DISTRIBUTION VS CYLINDER LOCATION
CYLINDER SB-2
AXIAL LOAD OF 20 KIPS

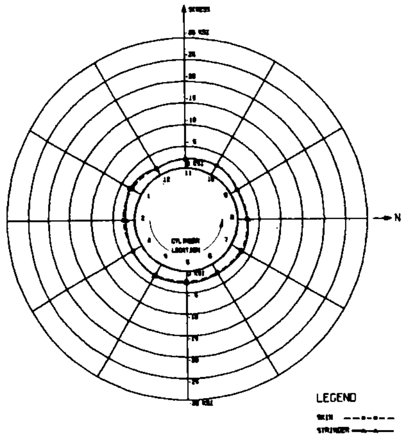

COMPRESSIVE MEMBRANE STRESS DISTRIBUTION VS CYLINDER LOCATION
CYLINDER SB-2
AXIAL LOAD OF 41 KIPS

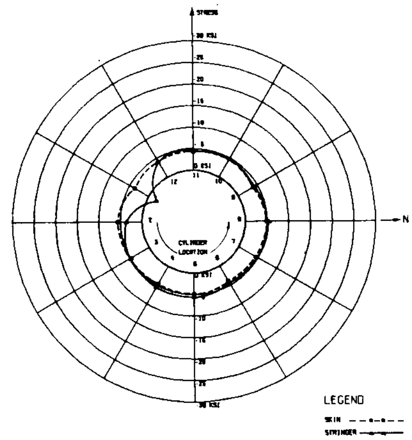

GENERAL INSTABILITY OCCURRED AT 42.0 KIPS

COMPRESSIVE MEMBRANE STRESS DISTRIBUTION VS CYLINDER LOCATION
CYLINDER SC-1
AXIAL LOAD OF 30 KIPS

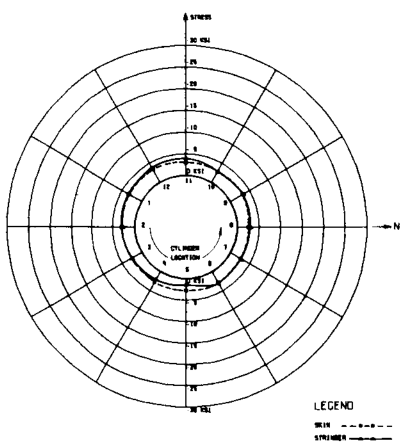

COMPRESSIVE MEMBRANE STRESS DISTRIBUTION VS CYLINDER LOCATION
CYLINDER SC-1
AXIAL LOAD OF 56 KIPS

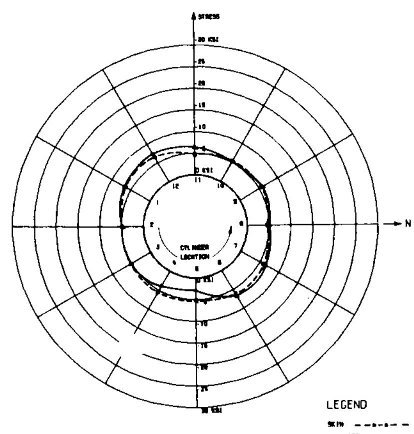

GENERAL INSTABILITY OCCURRED AT 58.7 KIPS

FIG. 7 CONT.

COMPRESSIVE MEMBRANE STRESS DISTRIBUTION VS CYLINDER LOCATION
CYLINDER SC-2
AXIAL LOAD OF 30 KIPS

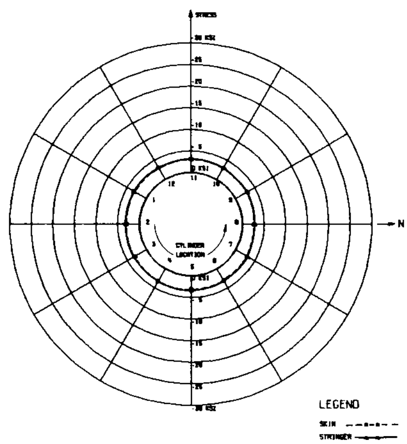

COMPRESSIVE MEMBRANE STRESS DISTRIBUTION VS CYLINDER LOCATION
CYLINDER SC-2
AXIAL LOAD OF 68 KIPS

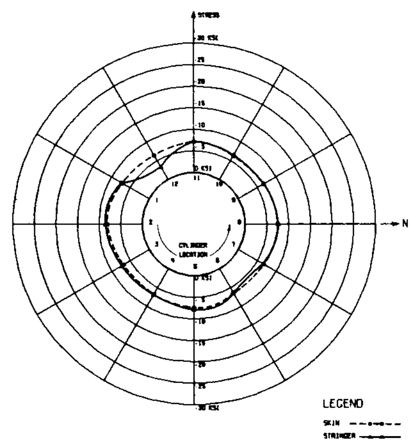

GENERAL INSTABILITY OCCURRED AT 70.0 KIPS

FIG. 7 CONCLUDED

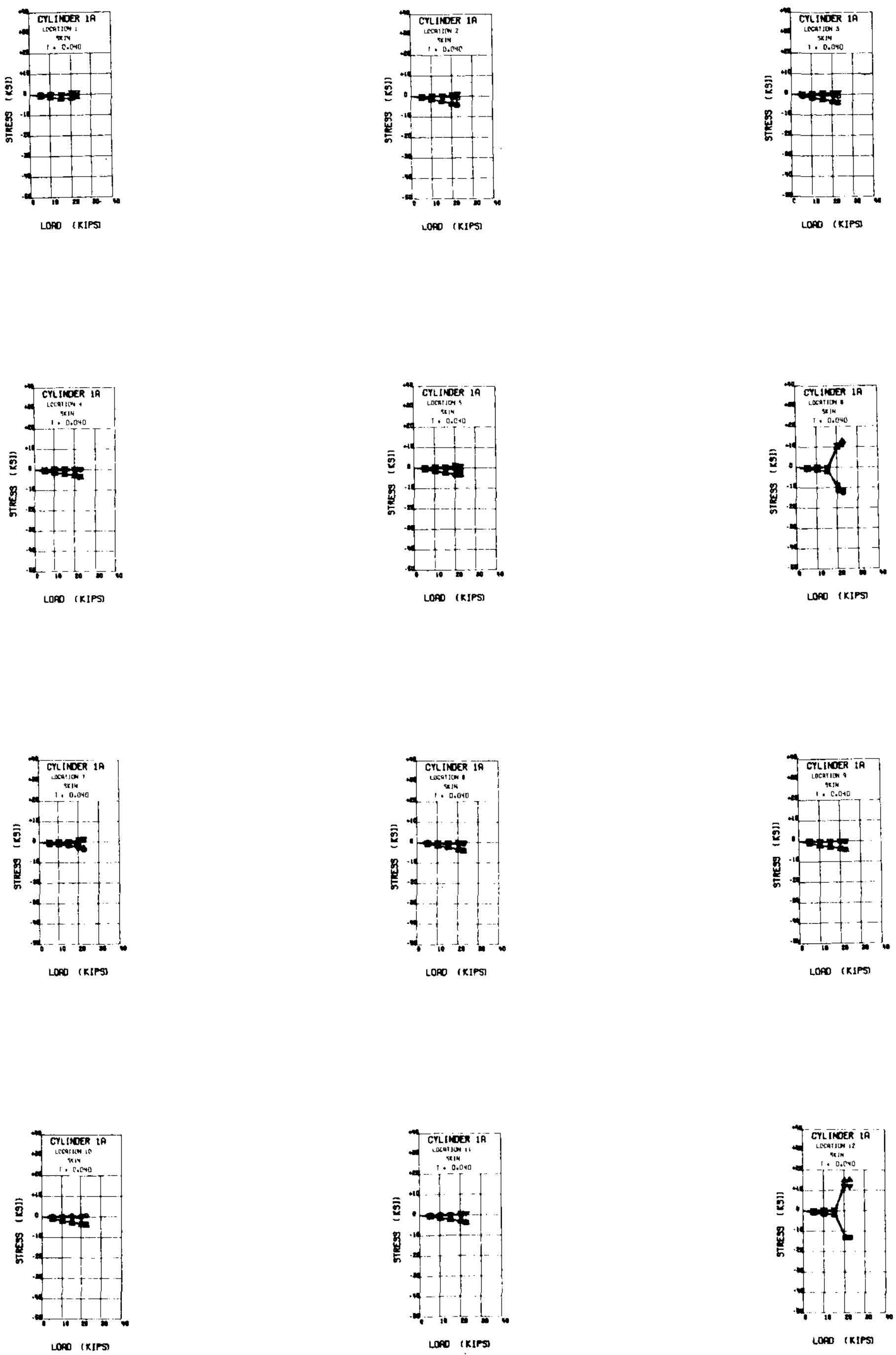

LEGEND		
ITEM	DESCRIPTION	SYMBOL
σ_1^o	MAX. OUTSIDE PRINCIPAL STRESS, (CIRCUM. DIR.)	
σ_1^i	MAX. INSIDE PRINCIPAL STRESS, (CIRCUM DIR.)	
σ_2^o	MIN. OUTSIDE PRINCIPAL STRESS, (AXIAL DIR.)	
σ_2^i	MIN. INSIDE PRINCIPAL STRESS, (AXIAL DIR.)	
θ_1^o	PRINCIPAL DIRECTION, OUTSIDE SURFACE	
θ_1^i	PRINCIPAL DIRECTION, INSIDE SURFACE	

CYLINDER 1A
(SKIN)

STRESS VS LOAD

FIG. 8

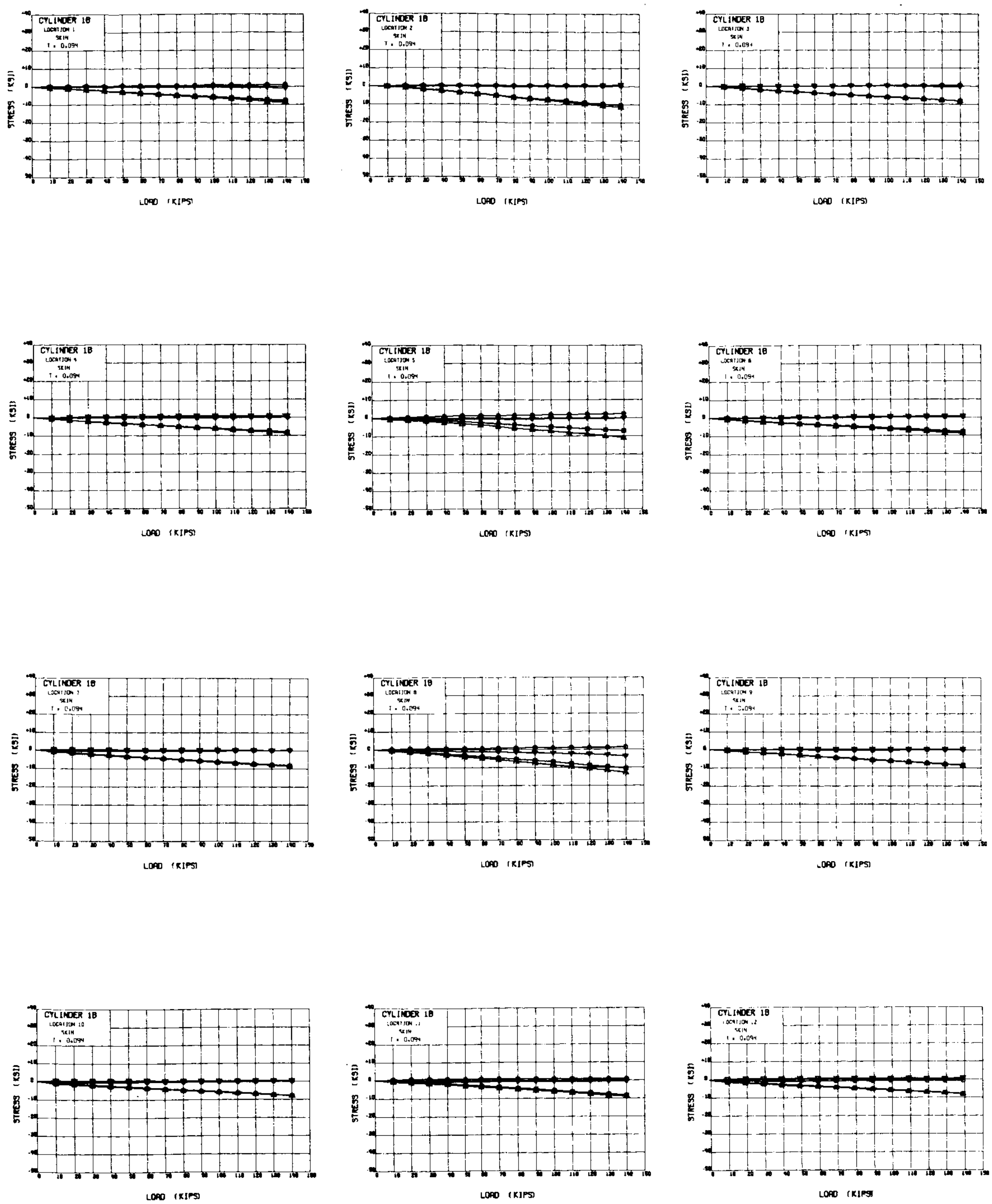

LEGEND		
ITEM	DESCRIPTION	SYMBOL
σ_1^o	MAX. OUTSIDE PRINCIPAL STRESS, (CIRCUM. DIR.)	
σ_1^i	MAX. INSIDE PRINCIPAL STRESS, (CIRCUM. DIR.)	
σ_2^o	MIN. OUTSIDE PRINCIPAL STRESS, (AXIAL DIR.)	
σ_2^i	MIN. INSIDE PRINCIPAL STRESS, (AXIAL DIR.)	
θ_1^o	PRINCIPAL DIRECTION, OUTSIDE SURFACE	
θ_1^i	PRINCIPAL DIRECTION, INSIDE SURFACE	

CYLINDER 1B
(SKIN)

FIG. 8 CONT.

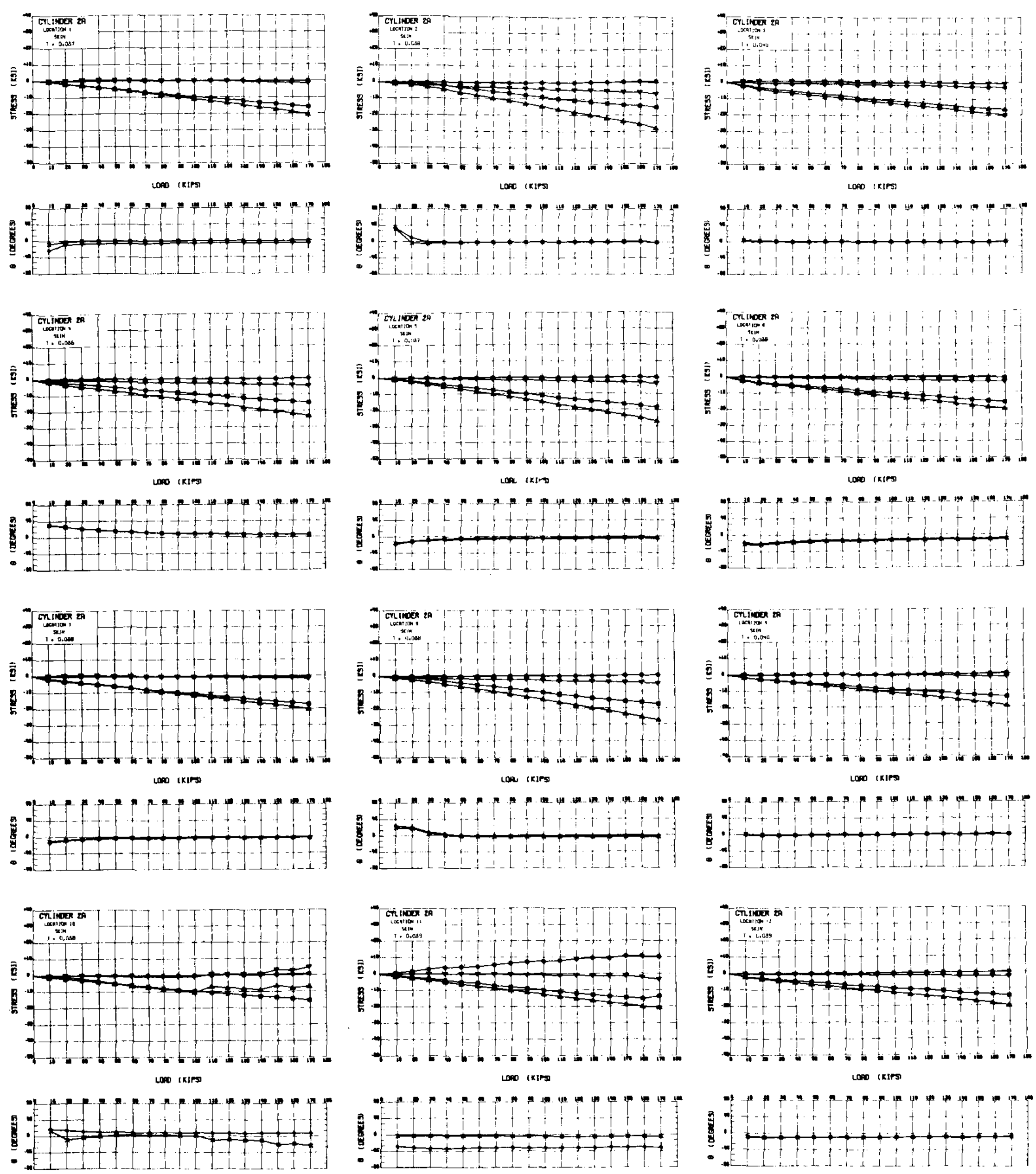

LEGEND		
ITEM	DESCRIPTION	SYMBOL
σ_1^o	MAX OUTSIDE PRINCIPAL STRESS, (CIRCUM DIR)	
σ_1^i	MAX INSIDE PRINCIPAL STRESS, (CIRCUM DIR)	
σ_2^o	MIN OUTSIDE PRINCIPAL STRESS, (AXIAL DIR)	
σ_2^i	MIN INSIDE PRINCIPAL STRESS, (AXIAL DIR)	
θ^o	PRINCIPAL DIRECTION, OUTSIDE SURFACE	
θ^i	PRINCIPAL DIRECTION, INSIDE SURFACE	

CYLINDER 2A
(SKIN)

FIG. 8 CONT.

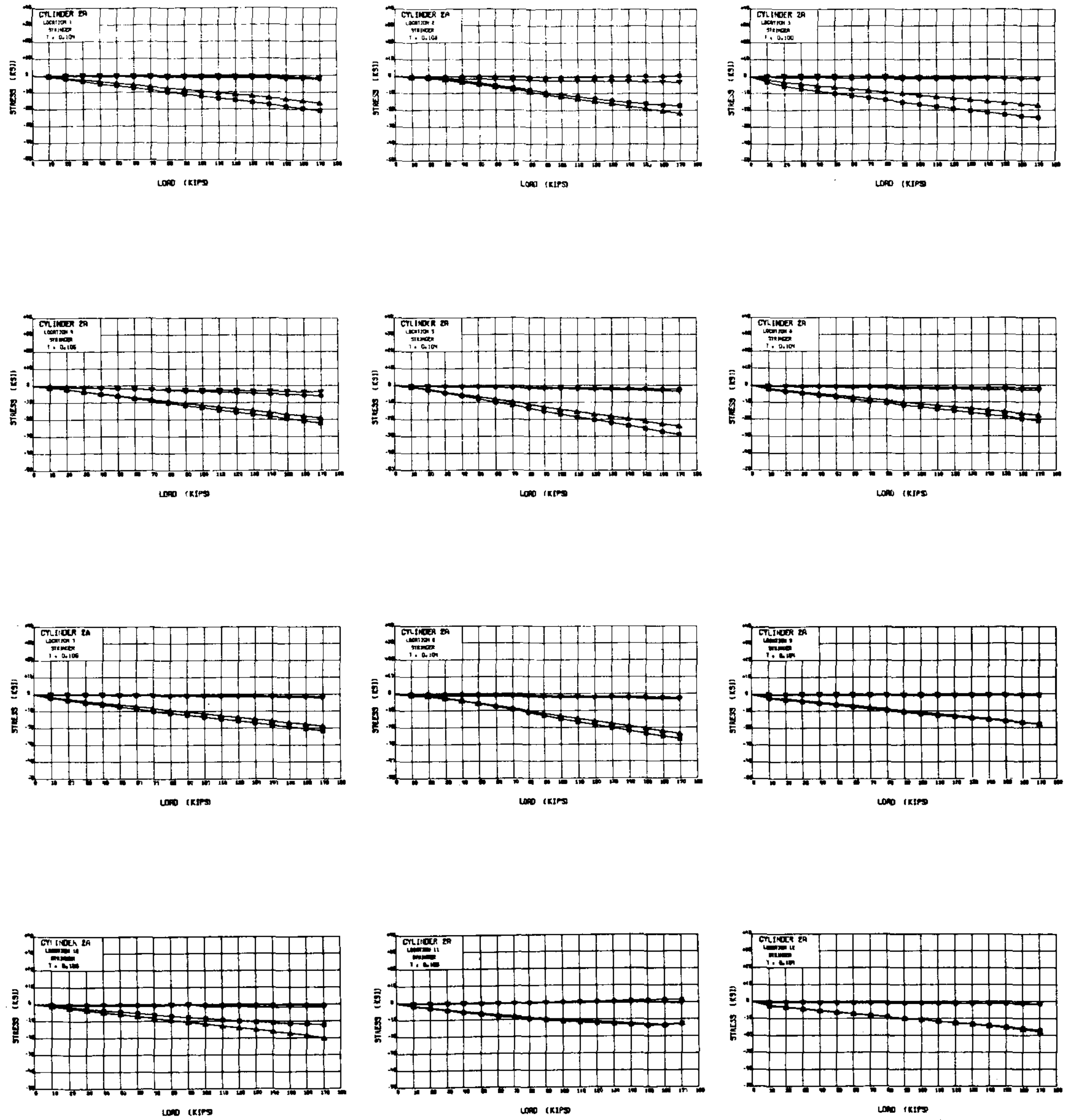

LEGEND		
ITEM	DESCRIPTION	SYMBOL
σ_1^o	MAX. OUTSIDE PRINCIPAL STRESS, (CIRCUM. DIR.)	
σ_1^i	MAX. INSIDE PRINCIPAL STRESS, (CIRCUM. DIR.)	
σ_2^o	MIN. OUTSIDE PRINCIPAL STRESS, (AXIAL DIR.)	
σ_2^i	MIN. INSIDE PRINCIPAL STRESS, (AXIAL DIR.)	
θ_1^o	PRINCIPAL DIRECTION, OUTSIDE SURFACE	
θ_1^i	PRINCIPAL DIRECTION, INSIDE SURFACE	

CYLINDER 2A
(STRINGER)

FIG. 8 CONT.

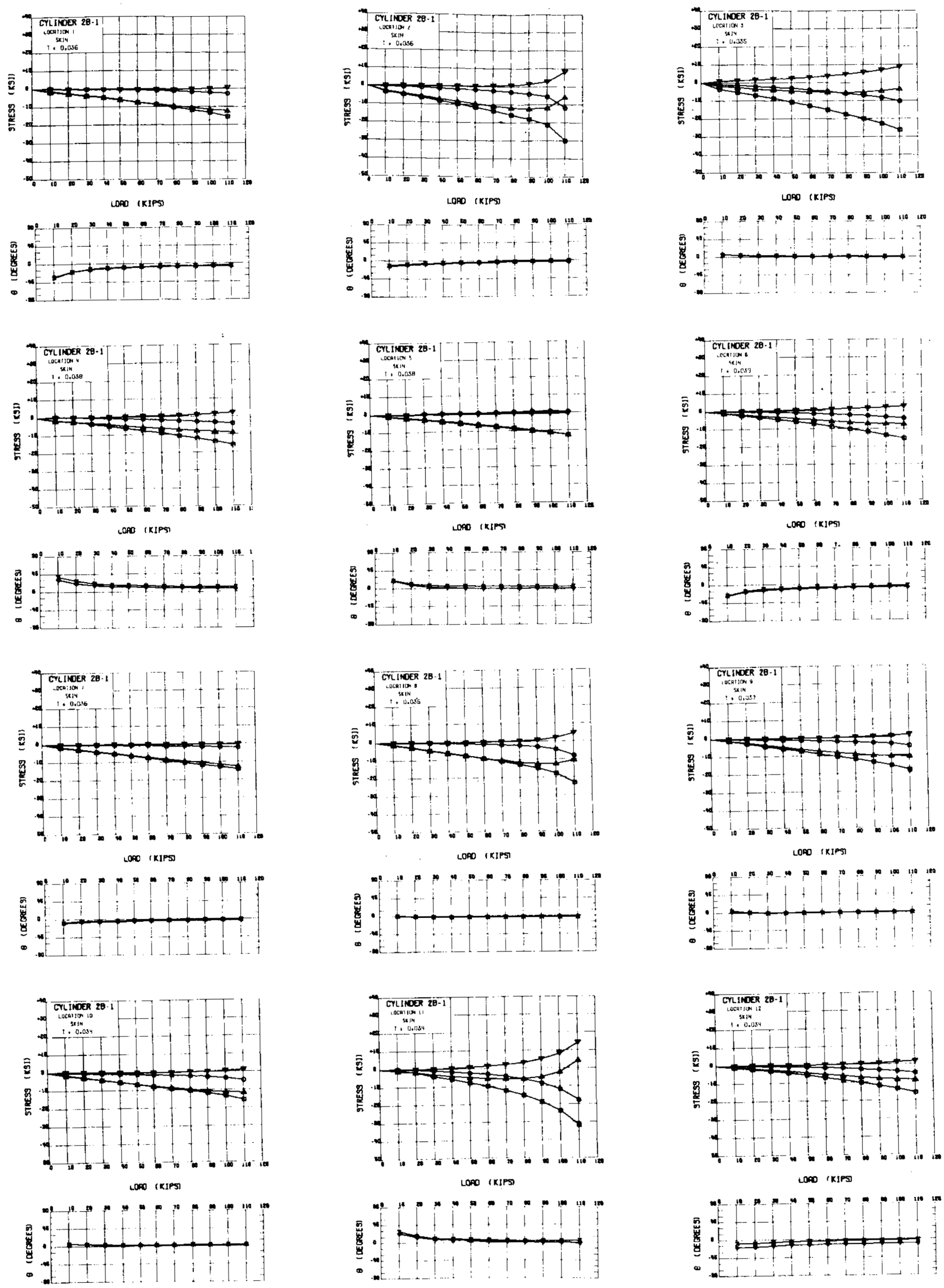

LEGEND

ITEM	DESCRIPTION	SYMBOL
σ_1^o	MAX OUTSIDE PRINCIPAL STRESS, (CIRCUM. DIR)	-o-o-
σ_1^i	MAX INSIDE PRINCIPAL STRESS, (CIRCUM DIR)	-▽-▽-
σ_2^o	MIN OUTSIDE PRINCIPAL STRESS, (AXIAL DIR)	-□-□-
σ_2^i	MIN INSIDE PRINCIPAL STRESS, (AXIAL DIR)	-△-△-
θ_i^o	PRINCIPAL DIRECTION, OUTSIDE SURFACE	-◇-◇-
θ_i^i	PRINCIPAL DIRECTION, INSIDE SURFACE	-×-×-

CYLINDER 2B-1
(SKIN)

FIG. 8 CONT.

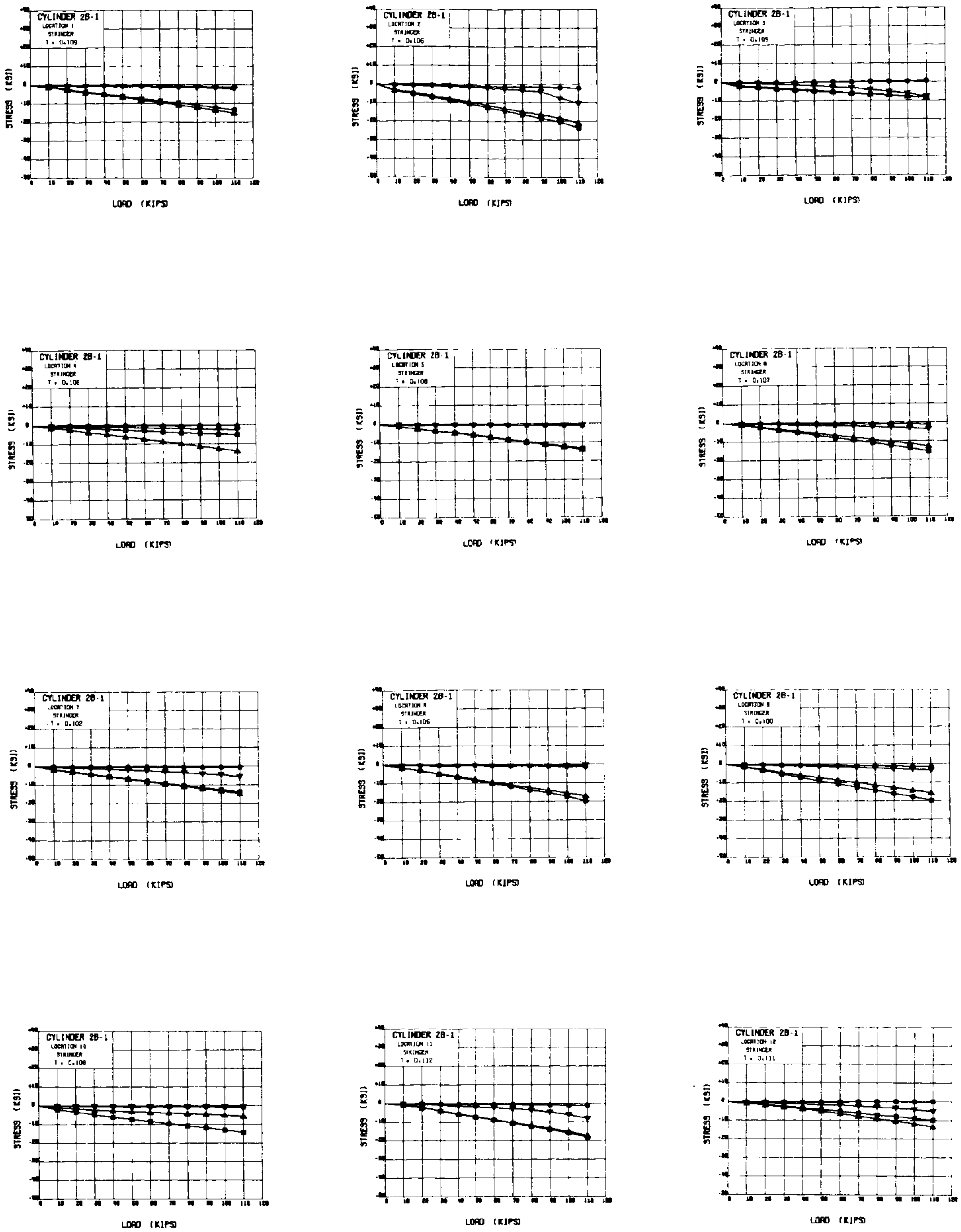

LEGEND		
ITEM	DESCRIPTION	SYMBOL
σ_1^{o}	MAX. OUTSIDE PRINCIPAL STRESS, (CIRCUM. DIR.)	
σ_1^{i}	MAX. INSIDE PRINCIPAL STRESS, (CIRCUM. DIR.)	
σ_2^{o}	MIN. OUTSIDE PRINCIPAL STRESS, (AXIAL DIR.)	
σ_2^{i}	MIN. INSIDE PRINCIPAL STRESS, (AXIAL DIR.)	
θ_1^{o}	PRINCIPAL DIRECTION, OUTSIDE SURFACE	
θ_1^{i}	PRINCIPAL DIRECTION, INSIDE SURFACE	

CYLINDER 2B-1
(STRINGER)

FIG. 8 CONT.

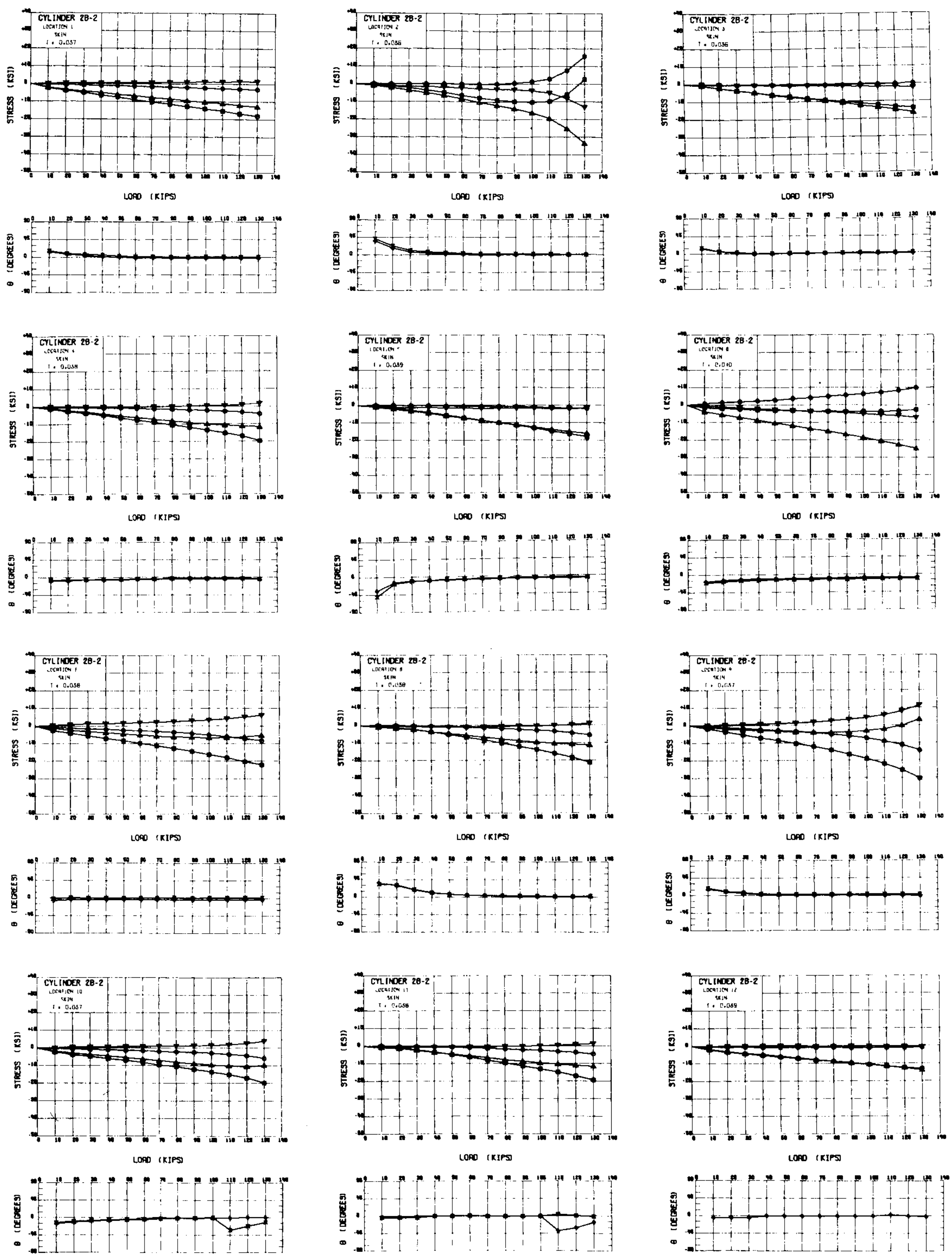

LEGEND		
ITEM	DESCRIPTION	SYMBOL
σ_1^o	MAX. OUTSIDE PRINCIPAL STRESS, (CIRCUM. DIR.)	-o-o-
σ_1^i	MAX. INSIDE PRINCIPAL STRESS, (CIRCUM. DIR.)	-▽-▽-
σ_2^o	MIN. OUTSIDE PRINCIPAL STRESS, (AXIAL DIR.)	-□-□-
σ_2^i	MIN. INSIDE PRINCIPAL STRESS, (AXIAL DIR.)	-△-△-
θ_1^o	PRINCIPAL DIRECTION, OUTSIDE SURFACE	-◇-◇-
θ_1^i	PRINCIPAL DIRECTION, INSIDE SURFACE	-x-x-

CYLINDER 2B-2
(SKIN)

FIG.8 CONT

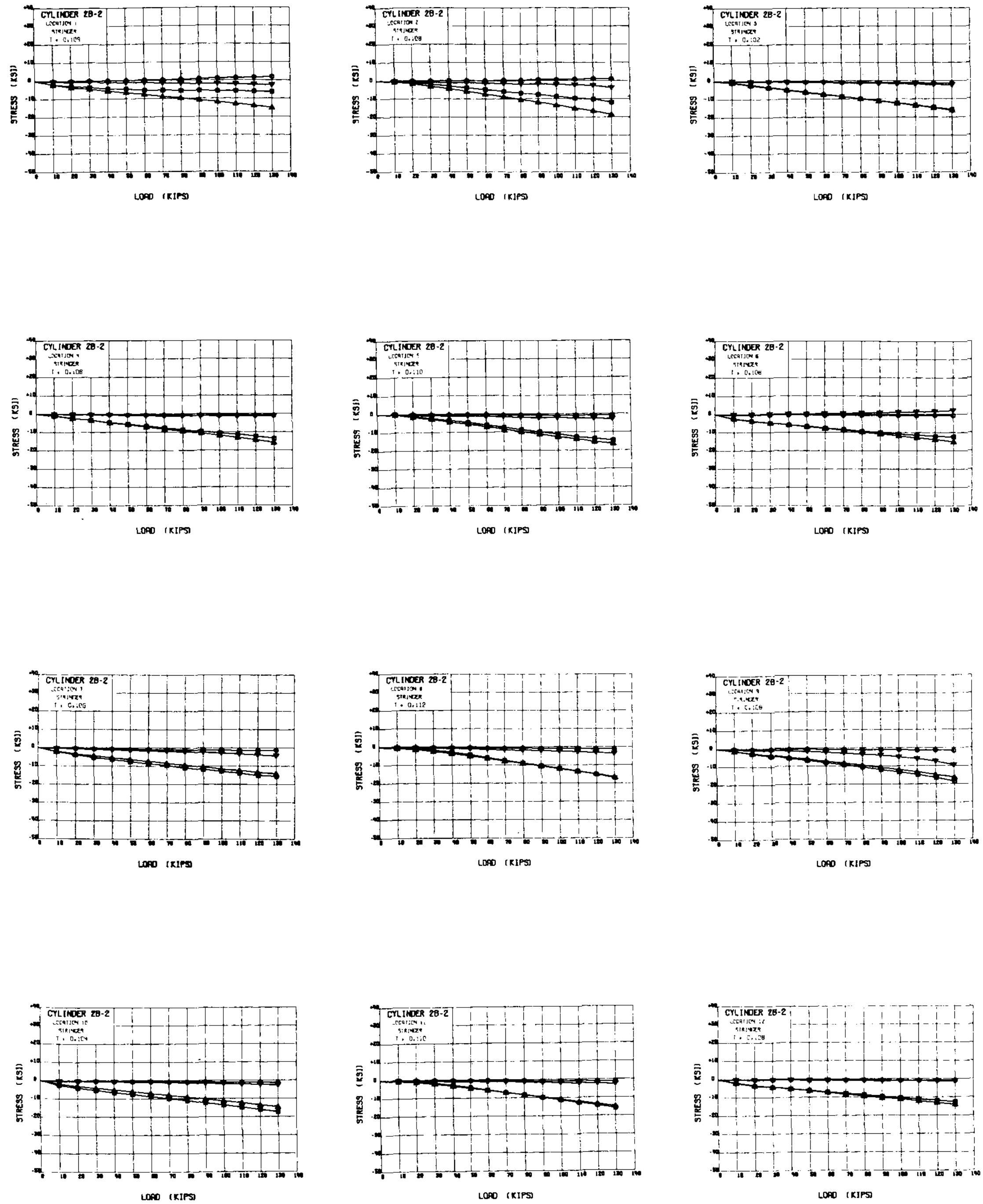

LEGEND		
ITEM	DESCRIPTION	SYMBOL
σ_1^{o}	MAX. OUTSIDE PRINCIPAL STRESS, (CIRCUM. DIR.)	-o-o-
σ_1^{i}	MAX. INSIDE PRINCIPAL STRESS, (CIRCUM. DIR.)	-▽-▽-
σ_2^{o}	MIN. OUTSIDE PRINCIPAL STRESS, (AXIAL DIR.)	-□-□-
σ_2^{i}	MIN. INSIDE PRINCIPAL STRESS, (AXIAL DIR.)	-△-△-
θ_1^{o}	PRINCIPAL DIRECTION, OUTSIDE SURFACE	-ф-ф-
θ_1^{i}	PRINCIPAL DIRECTION, INSIDE SURFACE	-x-x-

CYLINDER 2B-2
(STRINGER)

FIG. 8 CONT.

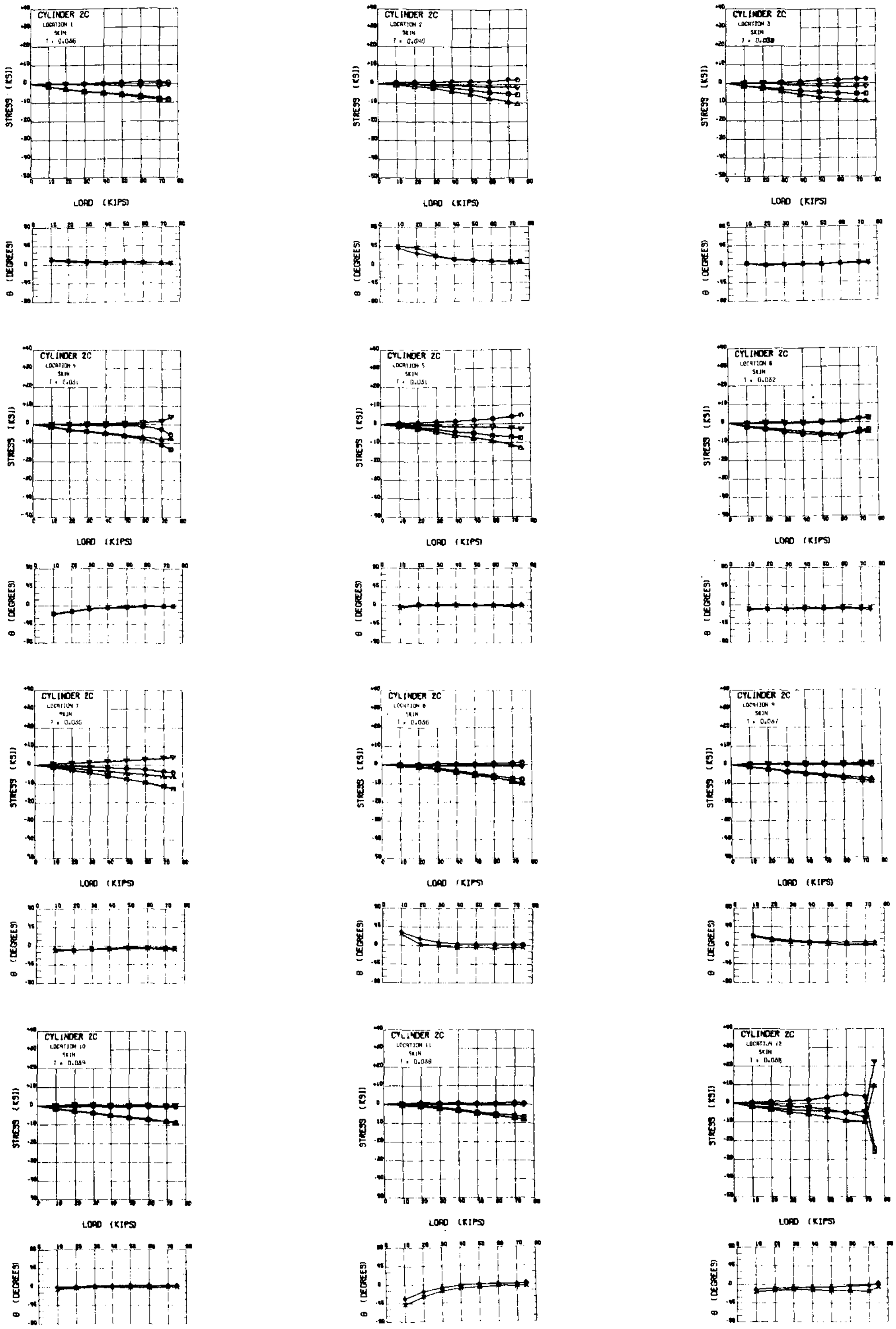

LEGEND

ITEM	DESCRIPTION	SYMBOL
σ_1^o	MAX. OUTSIDE PRINCIPAL STRESS, (CIRCUM DIR)	—o—o—
σ_1^i	MAX. INSIDE PRINCIPAL STRESS, (CIRCUM. DIR.)	—∇—∇—
σ_2^o	MIN. OUTSIDE PRINCIPAL STRESS, (AXIAL DIR)	—□—□—
σ_2^i	MIN. INSIDE PRINCIPAL STRESS, (AXIAL DIR)	—△—△—
θ_1^o	PRINCIPAL DIRECTION, OUTSIDE SURFACE	—◇—◇—
θ_1^i	PRINCIPAL DIRECTION, INSIDE SURFACE	—×—×—

CYLINDER 2C
(SKIN)

FIG. 8 CONT.

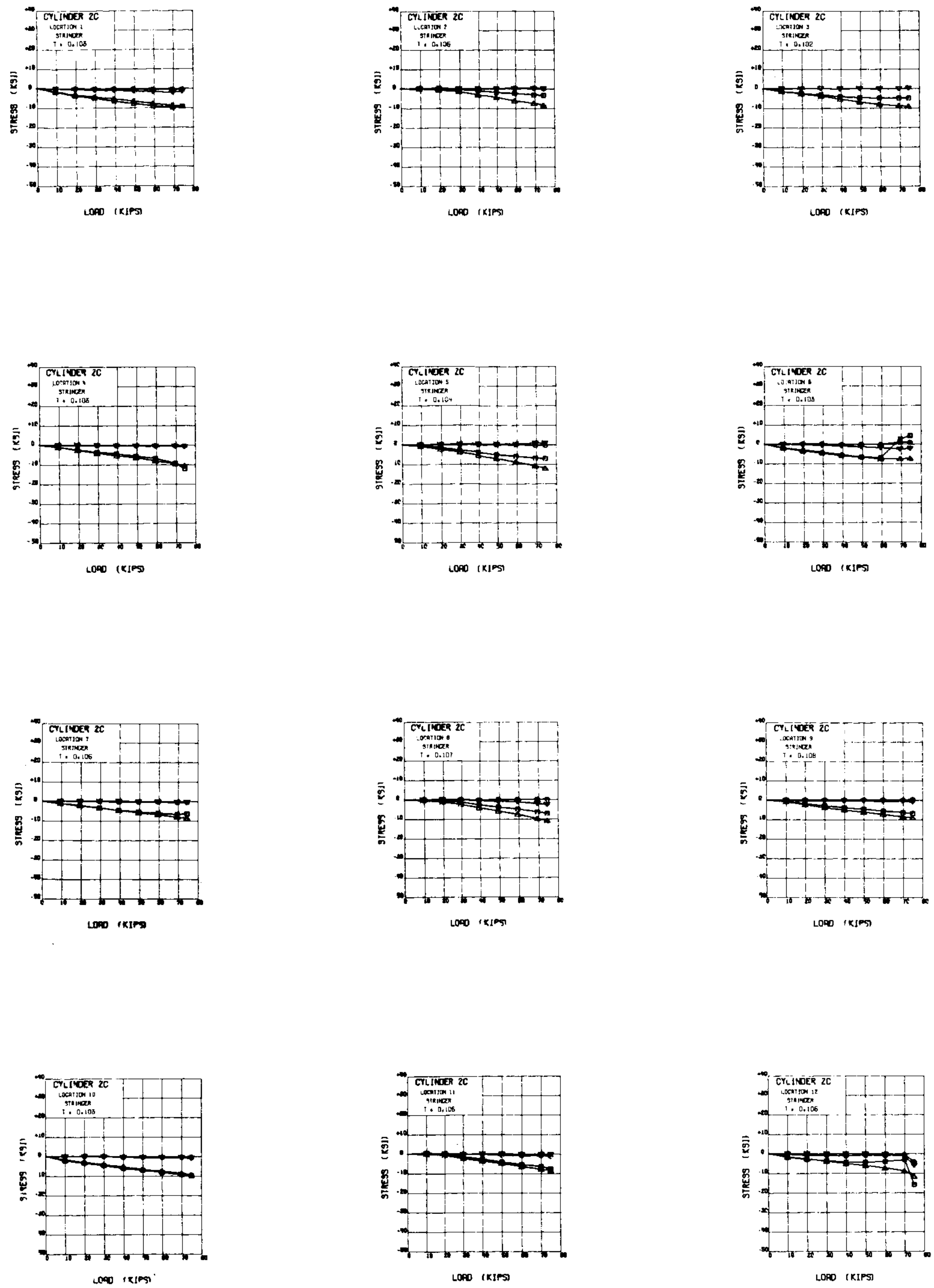

LEGEND		
ITEM	DESCRIPTION	SYMBOL
σ_1^o	MAX. OUTSIDE PRINCIPAL STRESS, (CIRCUM. DIR.)	
σ_1^i	MAX. INSIDE PRINCIPAL STRESS, (CIRCUM. DIR.)	
σ_2^o	MIN. OUTSIDE PRINCIPAL STRESS, (AXIAL DIR.)	
σ_2^i	MIN. INSIDE PRINCIPAL STRESS, (AXIAL DIR.)	
θ_1^o	PRINCIPAL DIRECTION, OUTSIDE SURFACE	
θ_1^i	PRINCIPAL DIRECTION, INSIDE SURFACE	

CYLINDER 2C
(STRINGER)

FIG. 8 CONT.

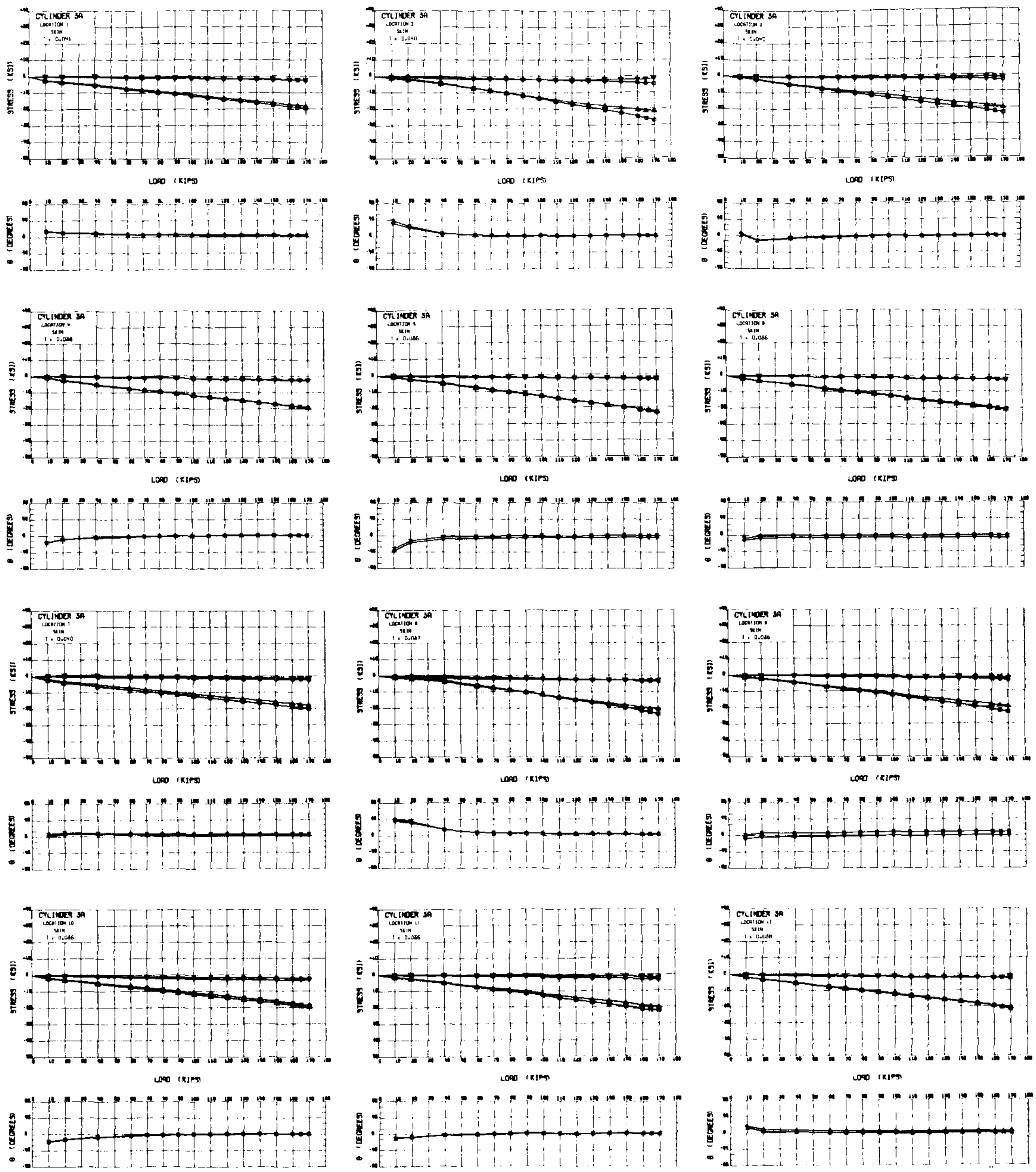

LEGEND		
ITEM	DESCRIPTION	SYMBOL
σ_1^o	MAX OUTSIDE PRINCIPAL STRESS, (CIRCUM. DIR.)	
σ_1^i	MAX INSIDE PRINCIPAL STRESS, (CIRCUM. DIR.)	
σ_2^o	MIN OUTSIDE PRINCIPAL STRESS, (AXIAL DIR.)	
σ_2^i	MIN INSIDE PRINCIPAL STRESS, (AXIAL DIR.)	
θ_1^o	PRINCIPAL DIRECTION, OUTSIDE SURFACE	
θ_1^i	PRINCIPAL DIRECTION, INSIDE SURFACE	

CYLINDER 3A
(SKIN)

FIG. 8 CONT.

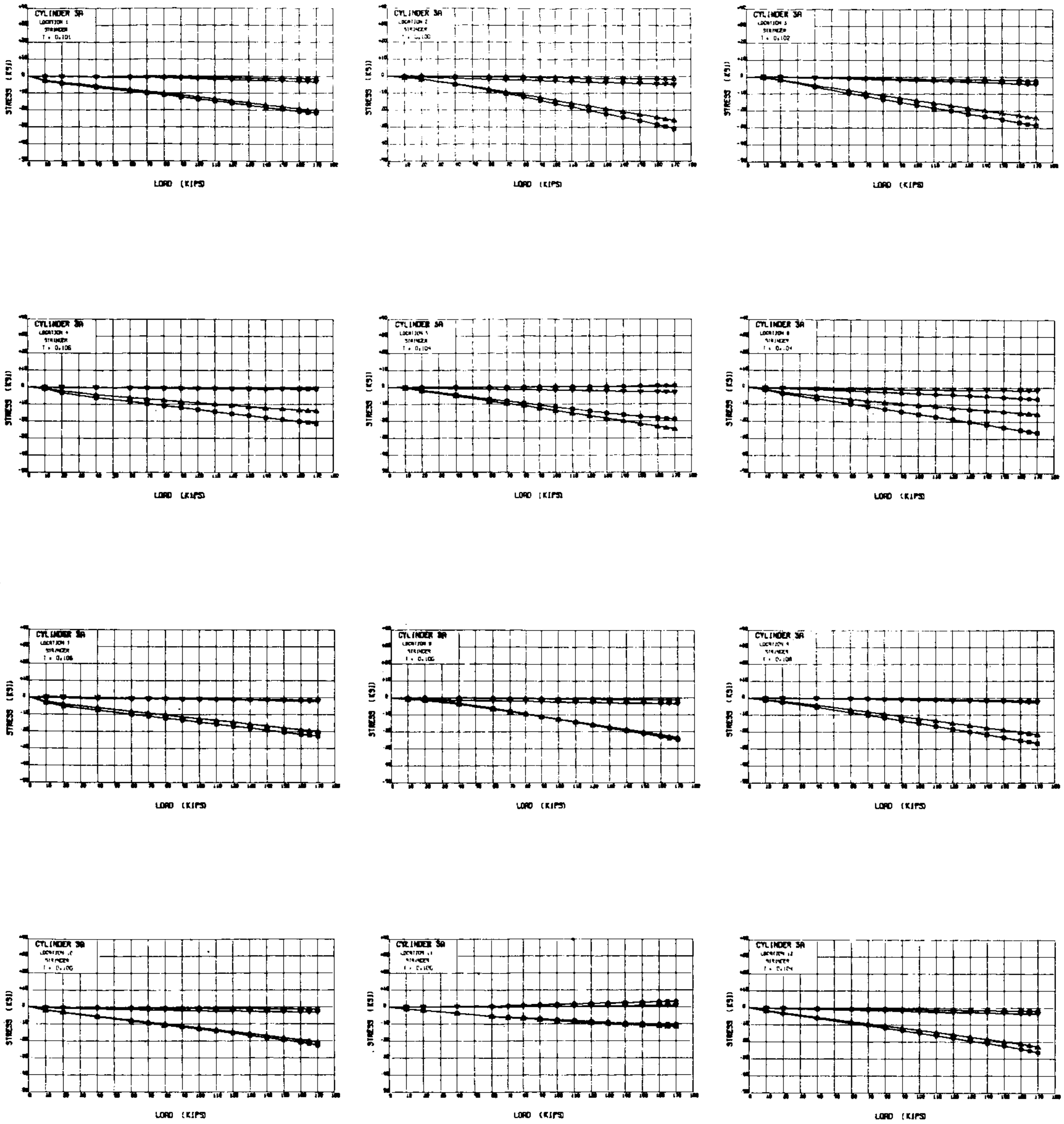

LEGEND		
ITEM	DESCRIPTION	SYMBOL
σ_1^o	MAX. OUTSIDE PRINCIPAL STRESS, (CIRCUM. DIR.)	
σ_1^i	MAX. INSIDE PRINCIPAL STRESS, (CIRCUM. DIR.)	
σ_2^o	MIN. OUTSIDE PRINCIPAL STRESS, (AXIAL DIR.)	
σ_2^i	MIN. INSIDE PRINCIPAL STRESS, (AXIAL DIR.)	
θ_i^o	PRINCIPAL DIRECTION, OUTSIDE SURFACE	
θ_i^i	PRINCIPAL DIRECTION, INSIDE SURFACE	

CYLINDER 3A
(STRINGER)

FIG. 8 CONT.

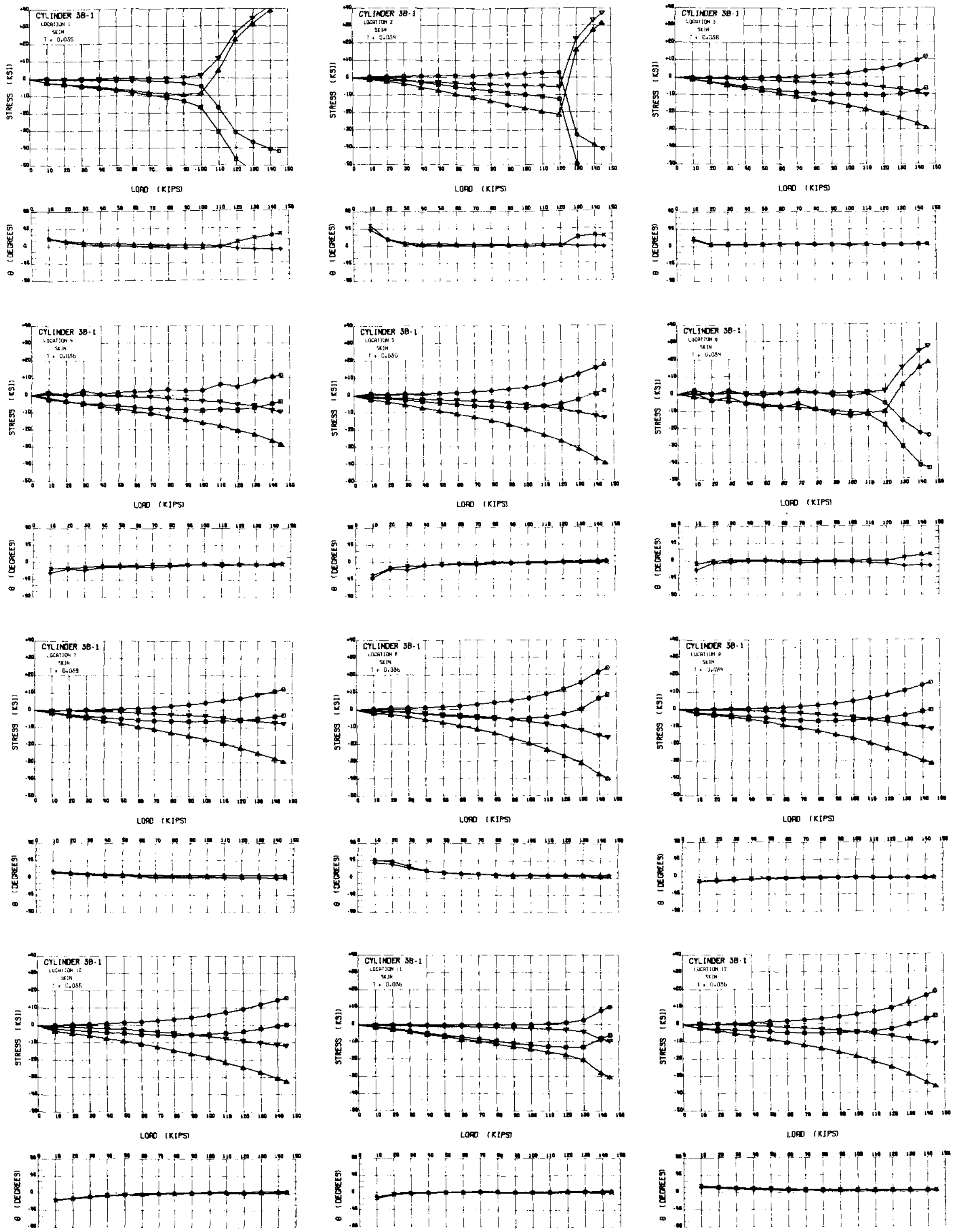

LEGEND		
ITEM	DESCRIPTION	SYMBOL
σ_1^o	MAX OUTSIDE PRINCIPAL STRESS, (CIRCUM. DIR.)	
σ_1^i	MAX INSIDE PRINCIPAL STRESS, (CIRCUM. DIR.)	
σ_2^o	MIN OUTSIDE PRINCIPAL STRESS, (AXIAL DIR.)	
σ_2^i	MIN INSIDE PRINCIPAL STRESS, (AXIAL DIR.)	
θ_1^o	PRINCIPAL DIRECTION, OUTSIDE SURFACE	
θ_1^i	PRINCIPAL DIRECTION, INSIDE SURFACE	

CYLINDER 3B-1
(SKIN)

FIG. 8 CONT.

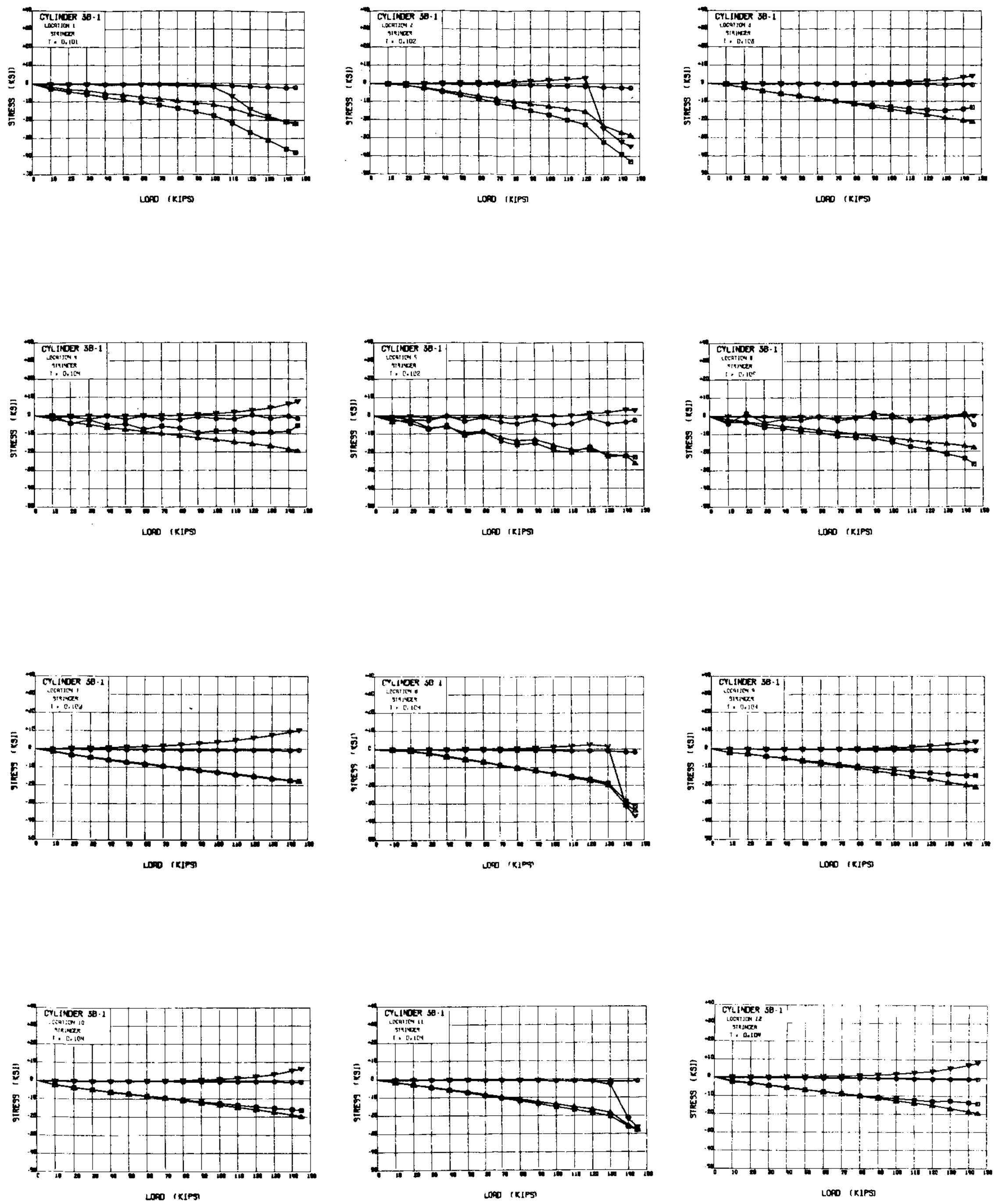

LEGEND		
ITEM	DESCRIPTION	SYMBOL
σ_1^o	MAX. OUTSIDE PRINCIPAL STRESS, (CIRCUM. DIR.)	-θ-θ-
σ_1^i	MAX. INSIDE PRINCIPAL STRESS, (CIRCUM. DIR.)	-▽-▽-
σ_2^o	MIN. OUTSIDE PRINCIPAL STRESS, (AXIAL DIR.)	-⊟-⊟-
σ_2^i	MIN. INSIDE PRINCIPAL STRESS, (AXIAL DIR.)	-△-△-
θ_1^o	PRINCIPAL DIRECTION, OUTSIDE SURFACE	-ɸ-ɸ-
θ_1^i	PRINCIPAL DIRECTION, INSIDE SURFACE	-×-×-

CYLINDER 3B-1
(STRINGER)

FIG. 8 CONT.

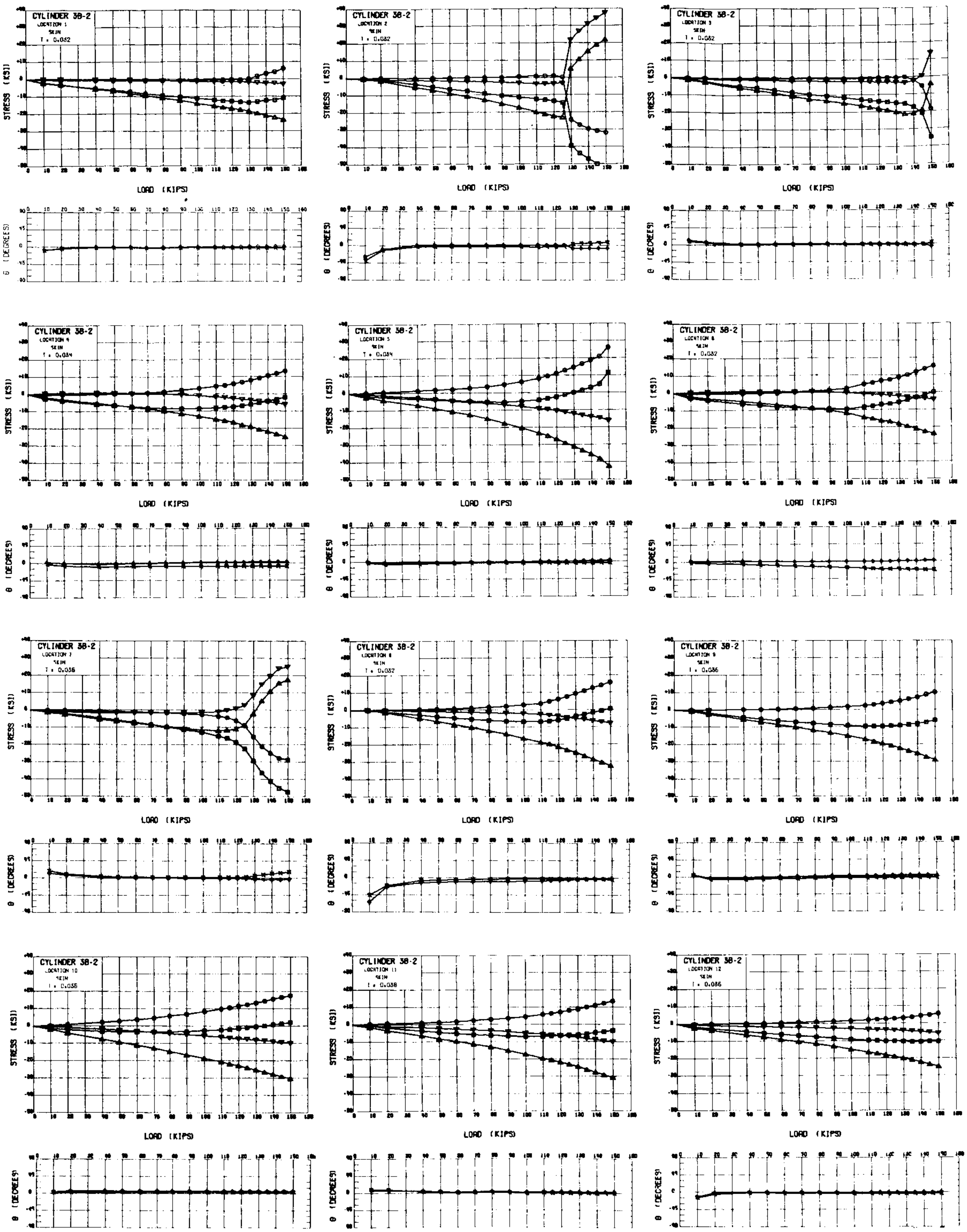

LEGEND		
ITEM	DESCRIPTION	SYMBOL
σ_1^o	MAX. OUTSIDE PRINCIPAL STRESS, (CIRCUM. DIR.)	-○-
σ_1^i	MAX. INSIDE PRINCIPAL STRESS, (CIRCUM. DIR.)	-▽-
σ_2^o	MIN. OUTSIDE PRINCIPAL STRESS, (AXIAL DIR.)	-□-
σ_2^i	MIN. INSIDE PRINCIPAL STRESS, (AXIAL DIR.)	-△-
θ_1^o	PRINCIPAL DIRECTION, OUTSIDE SURFACE	-◇-
θ_1^i	PRINCIPAL DIRECTION, INSIDE SURFACE	-×-

CYLINDER 3B-2
(SKIN)

FIG. 8 CONT.

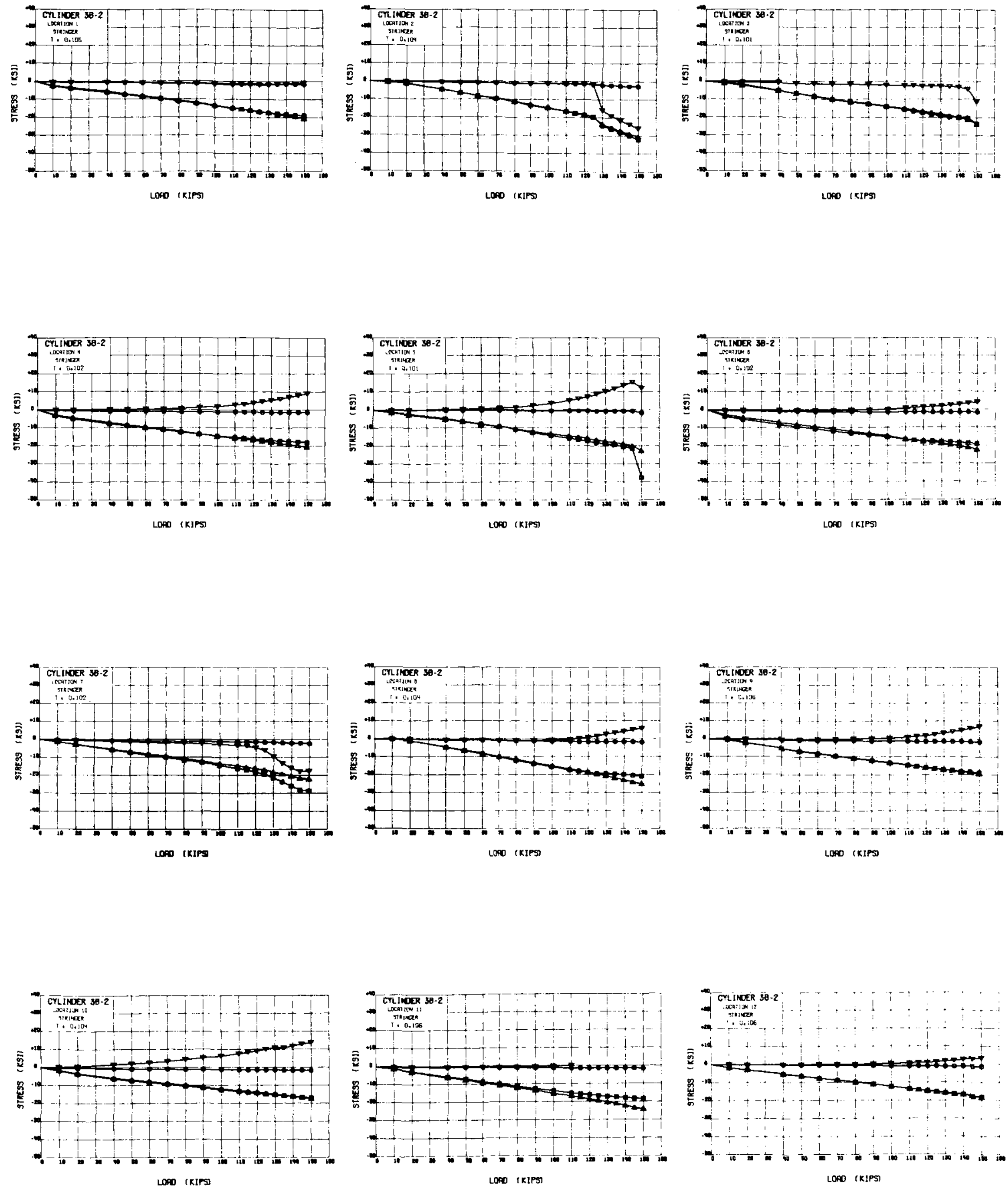

LEGEND		
ITEM	DESCRIPTION	SYMBOL
σ_1^o	MAX. OUTSIDE PRINCIPAL STRESS, (CIRCUM. DIR.)	-○-○-
σ_1^i	MAX. INSIDE PRINCIPAL STRESS, (CIRCUM. DIR.)	-▽-▽-
σ_2^o	MIN. OUTSIDE PRINCIPAL STRESS, (AXIAL DIR.)	-□-□-
σ_2^i	MIN. INSIDE PRINCIPAL STRESS, (AXIAL DIR.)	-△-△-
θ_1^o	PRINCIPAL DIRECTION, OUTSIDE SURFACE	-◇-◇-
θ_1^i	PRINCIPAL DIRECTION, INSIDE SURFACE	-x-x-

CYLINDER 3B-2
(STRINGER)

FIG. 8 CONT.

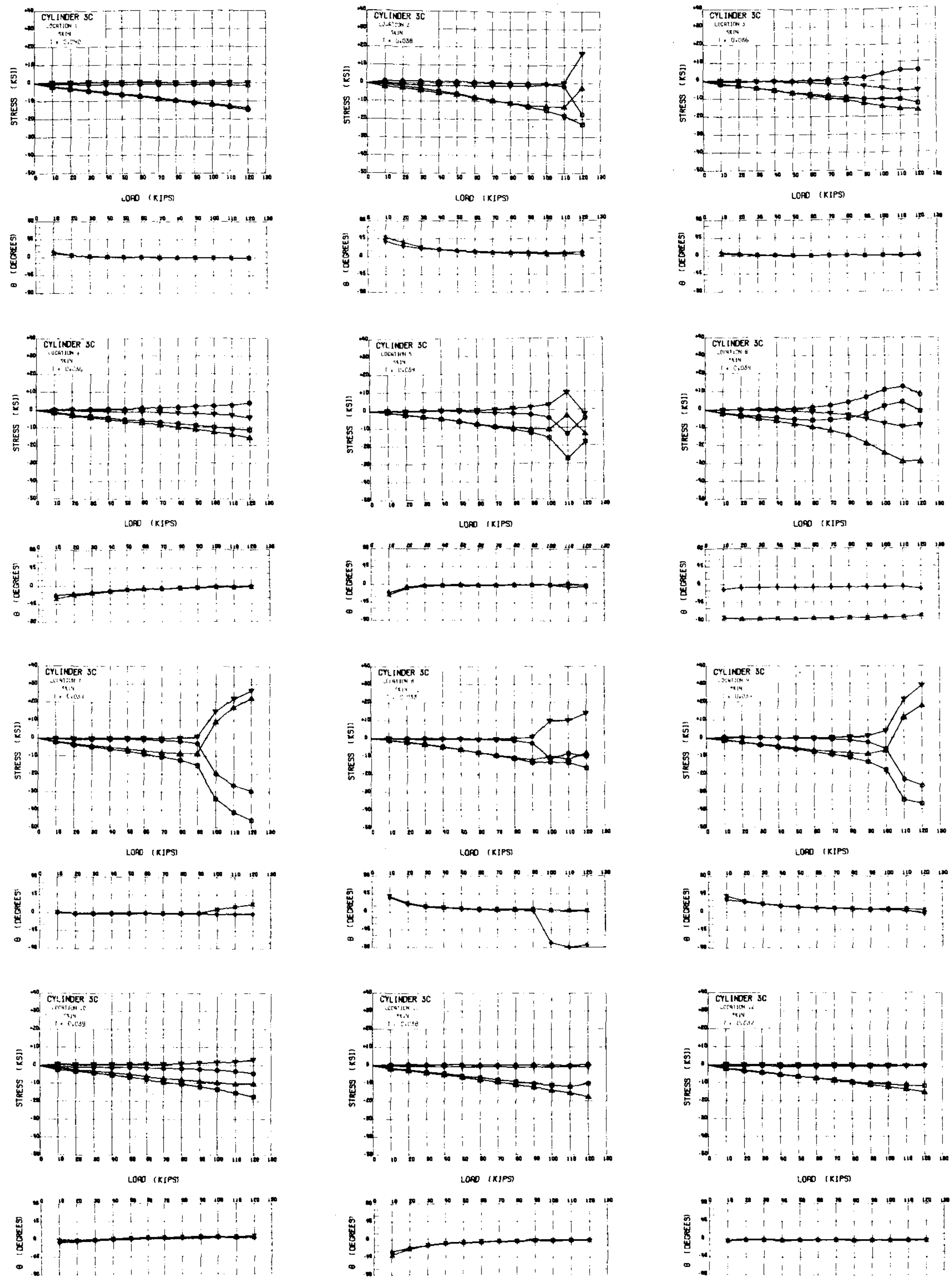

LEGEND		
ITEM	DESCRIPTION	SYMBOL
σ_1^o	MAX. OUTSIDE PRINCIPAL STRESS, (CIRCUM. DIR.)	-○-○-
σ_1^i	MAX. INSIDE PRINCIPAL STRESS, (CIRCUM DIR.)	-▽-▽-
σ_2^o	MIN. OUTSIDE PRINCIPAL STRESS, (AXIAL DIR.)	-□-□-
σ_2^i	MIN. INSIDE PRINCIPAL STRESS, (AXIAL DIR.)	-△-△-
θ_1^o	PRINCIPAL DIRECTION, OUTSIDE SURFACE	-◇-◇-
θ_1^i	PRINCIPAL DIRECTION, INSIDE SURFACE	-✕-✕-

CYLINDER 3C (SKIN)

FIG. 8 CONT.

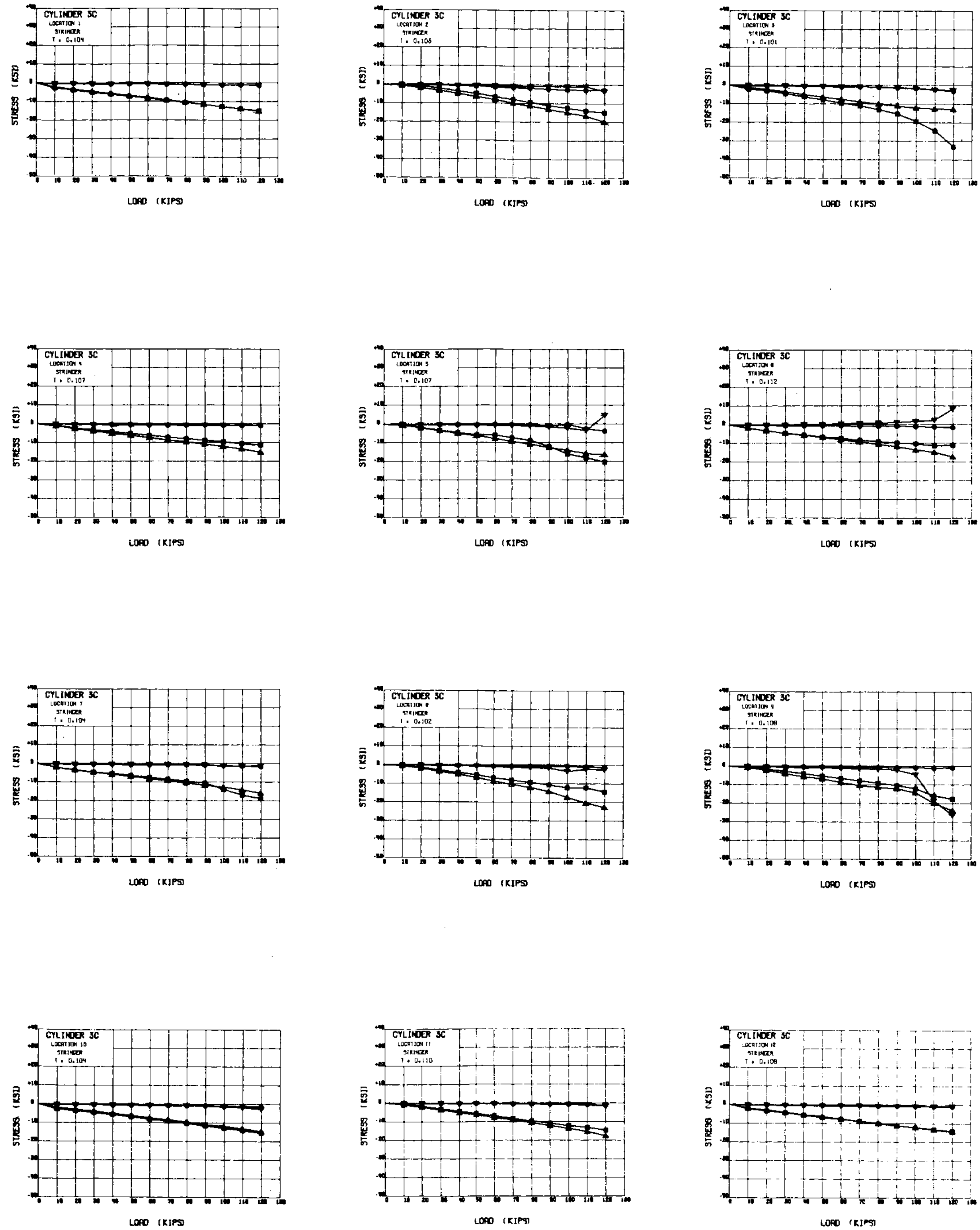

LEGEND		
ITEM	DESCRIPTION	SYMBOL
σ_1^o	MAX. OUTSIDE PRINCIPAL STRESS, (CIRCUM. DIR.)	
σ_1^i	MAX. INSIDE PRINCIPAL STRESS, (CIRCUM. DIR.)	
σ_2^o	MIN. OUTSIDE PRINCIPAL STRESS, (AXIAL DIR.)	
σ_2^i	MIN. INSIDE PRINCIPAL STRESS, (AXIAL DIR.)	
θ_1^o	PRINCIPAL DIRECTION, OUTSIDE SURFACE	
θ_1^i	PRINCIPAL DIRECTION, INSIDE SURFACE	

CYLINDER 3C (STRINGER)

FIG. 8 CONT.

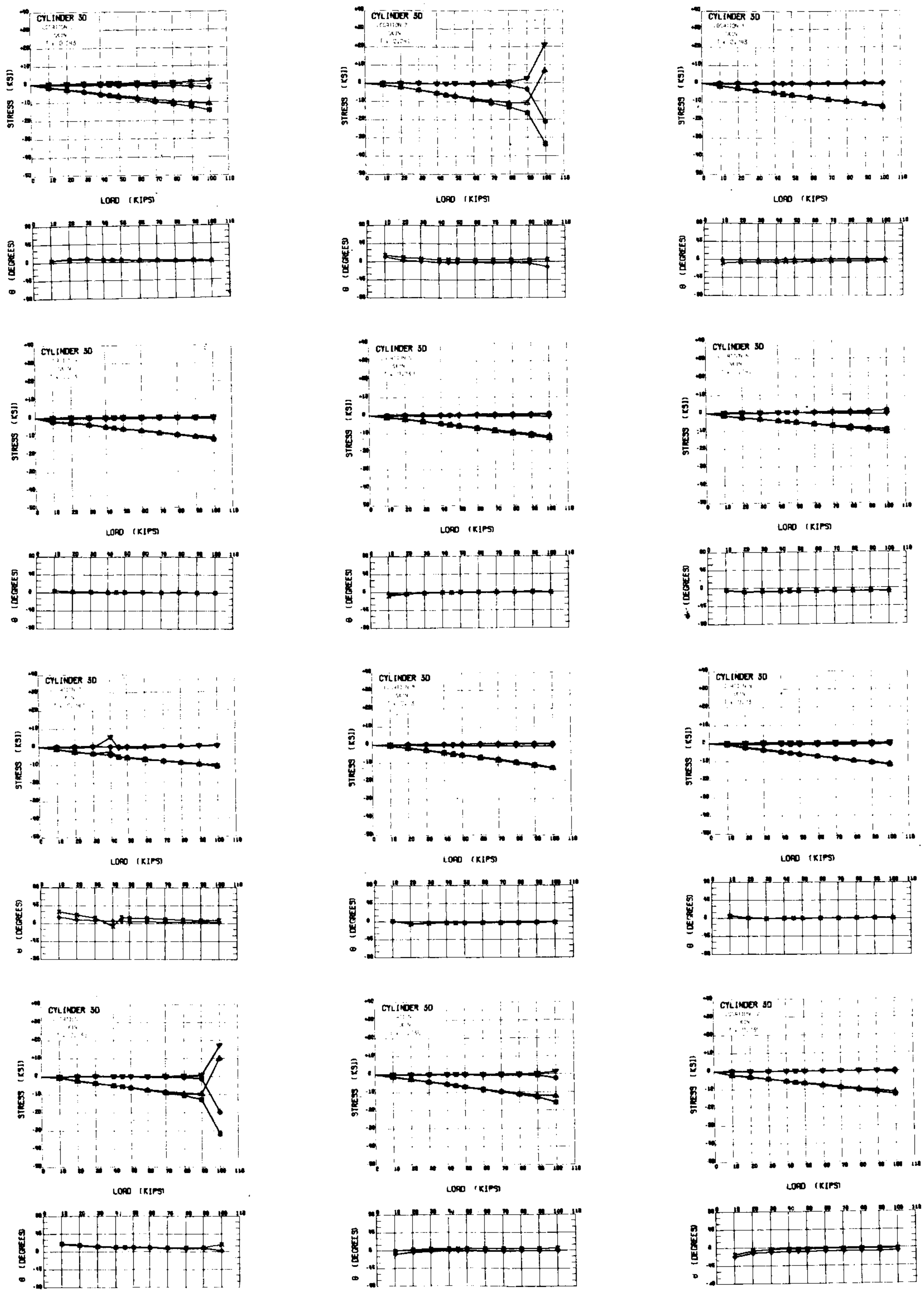

LEGEND		
ITEM	DESCRIPTION	SYMBOL
σ_1^o	MAX. OUTSIDE PRINCIPAL STRESS, (CIRCUM. DIR.)	
σ_1^i	MAX. INSIDE PRINCIPAL STRESS, (CIRCUM. DIR.)	
σ_2^o	MIN. OUTSIDE PRINCIPAL STRESS, (AXIAL DIR.)	
σ_2^i	MIN. INSIDE PRINCIPAL STRESS, (AXIAL DIR.)	
θ^o	PRINCIPAL DIRECTION, OUTSIDE SURFACE	
θ^i	PRINCIPAL DIRECTION, INSIDE SURFACE	

CYLINDER 3D
(SKIN)

FIG. 8 CONT.

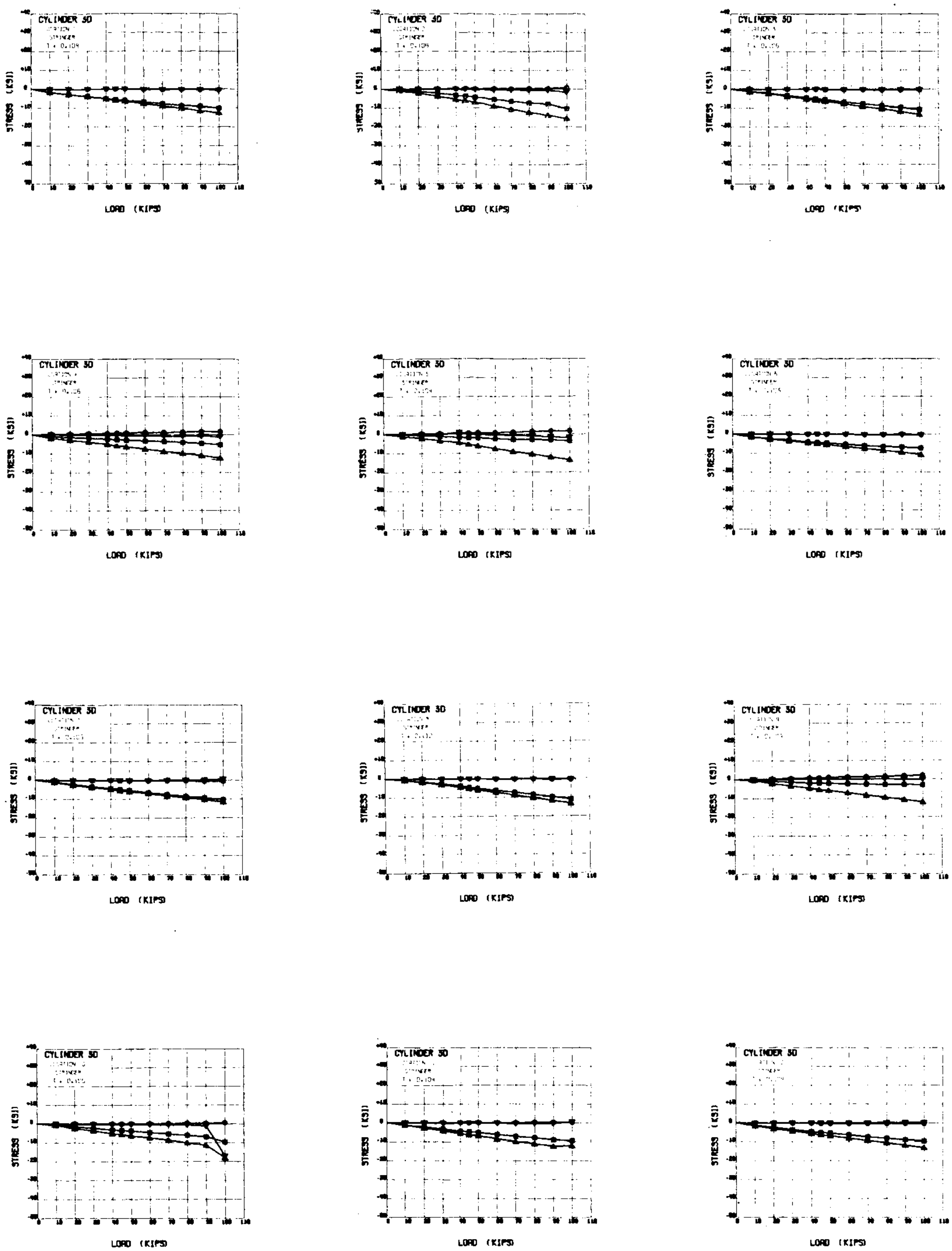

LEGEND		
ITEM	DESCRIPTION	SYMBOL
σ_1^o	MAX. OUTSIDE PRINCIPAL STRESS, (CIRCUM. DIR.)	
σ_1^i	MAX. INSIDE PRINCIPAL STRESS, (CIRCUM. DIR.)	
σ_2^o	MIN. OUTSIDE PRINCIPAL STRESS, (AXIAL DIR.)	
σ_2^i	MIN. INSIDE PRINCIPAL STRESS, (AXIAL DIR.)	
θ_1^o	PRINCIPAL DIRECTION, OUTSIDE SURFACE	
θ_1^i	PRINCIPAL DIRECTION, INSIDE SURFACE	

CYLINDER 3D (STRINGER)

FIG. 8 CONT.

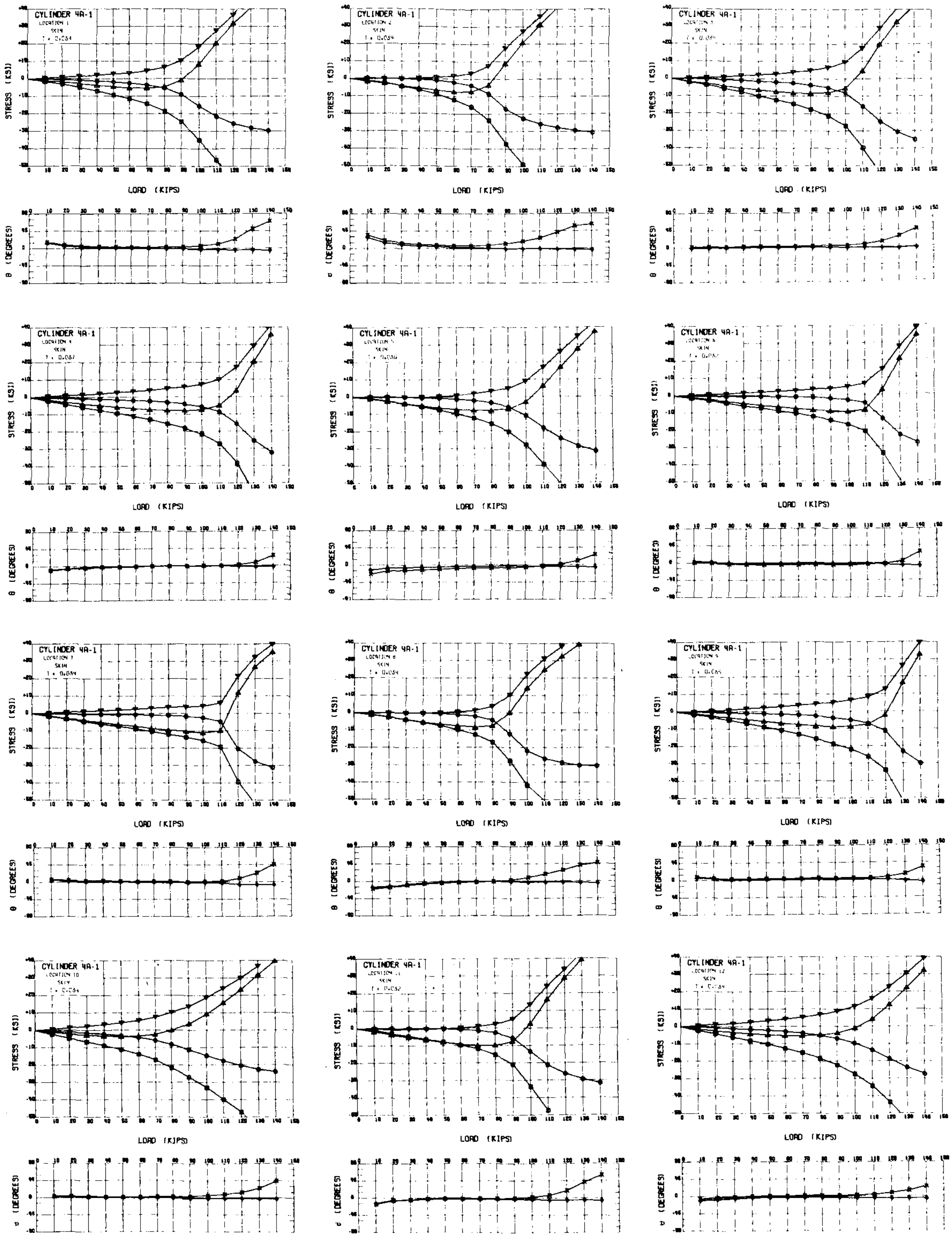

LEGEND

ITEM	DESCRIPTION	SYMBOL
σ_1^o	MAX. OUTSIDE PRINCIPAL STRESS, (CIRCUM. DIR.)	-o-o-
σ_1^i	MAX. INSIDE PRINCIPAL STRESS, (CIRCUM. DIR.)	-▽-▽-
σ_2^o	MIN. OUTSIDE PRINCIPAL STRESS, (AXIAL DIR.)	-□-□-
σ_2^i	MIN. INSIDE PRINCIPAL STRESS, (AXIAL DIR.)	-△-△-
θ_1^o	PRINCIPAL DIRECTION, OUTSIDE SURFACE	-◇-◇-
θ_1^i	PRINCIPAL DIRECTION, INSIDE SURFACE	-x-x-

CYLINDER 4A-1
(SKIN)

FIG.8 CONT.

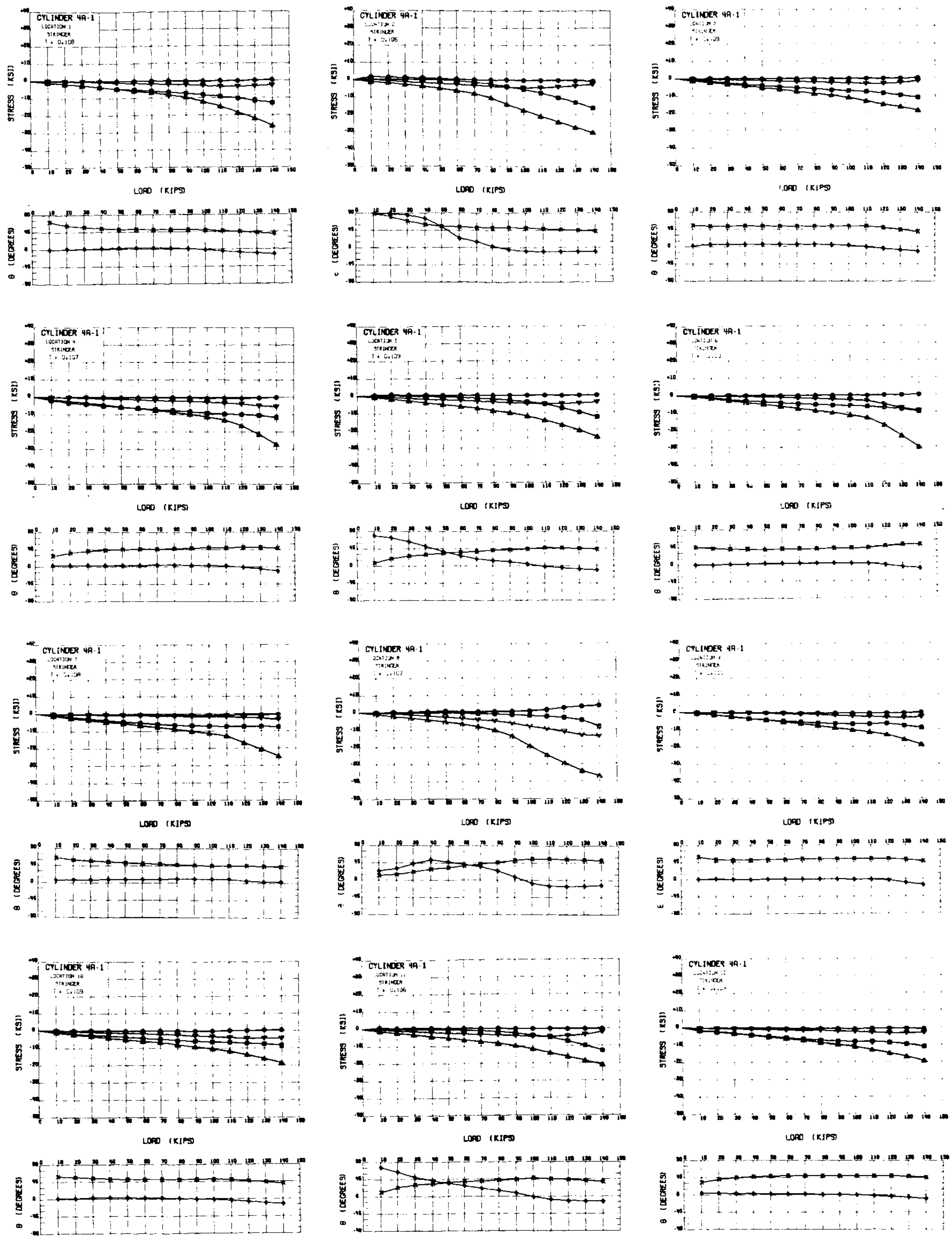

LEGEND		
ITEM	DESCRIPTION	SYMBOL
σ_1^o	MAX. OUTSIDE PRINCIPAL STRESS, (CIRCUM. DIR.)	-⊖-⊖-
σ_1^i	MAX. INSIDE PRINCIPAL STRESS, (CIRCUM. DIR.)	-▽-▽-
σ_2^o	MIN. OUTSIDE PRINCIPAL STRESS, (AXIAL DIR.)	-⊟-⊟-
σ_2^i	MIN. INSIDE PRINCIPAL STRESS, (AXIAL DIR.)	-△-△-
θ_1^o	PRINCIPAL DIRECTION, OUTSIDE SURFACE	-◇-◇-
θ_1^i	PRINCIPAL DIRECTION, INSIDE SURFACE	-×-×-

CYLINDER 4A-1 (STRINGER)

FIG. 8 CONT.

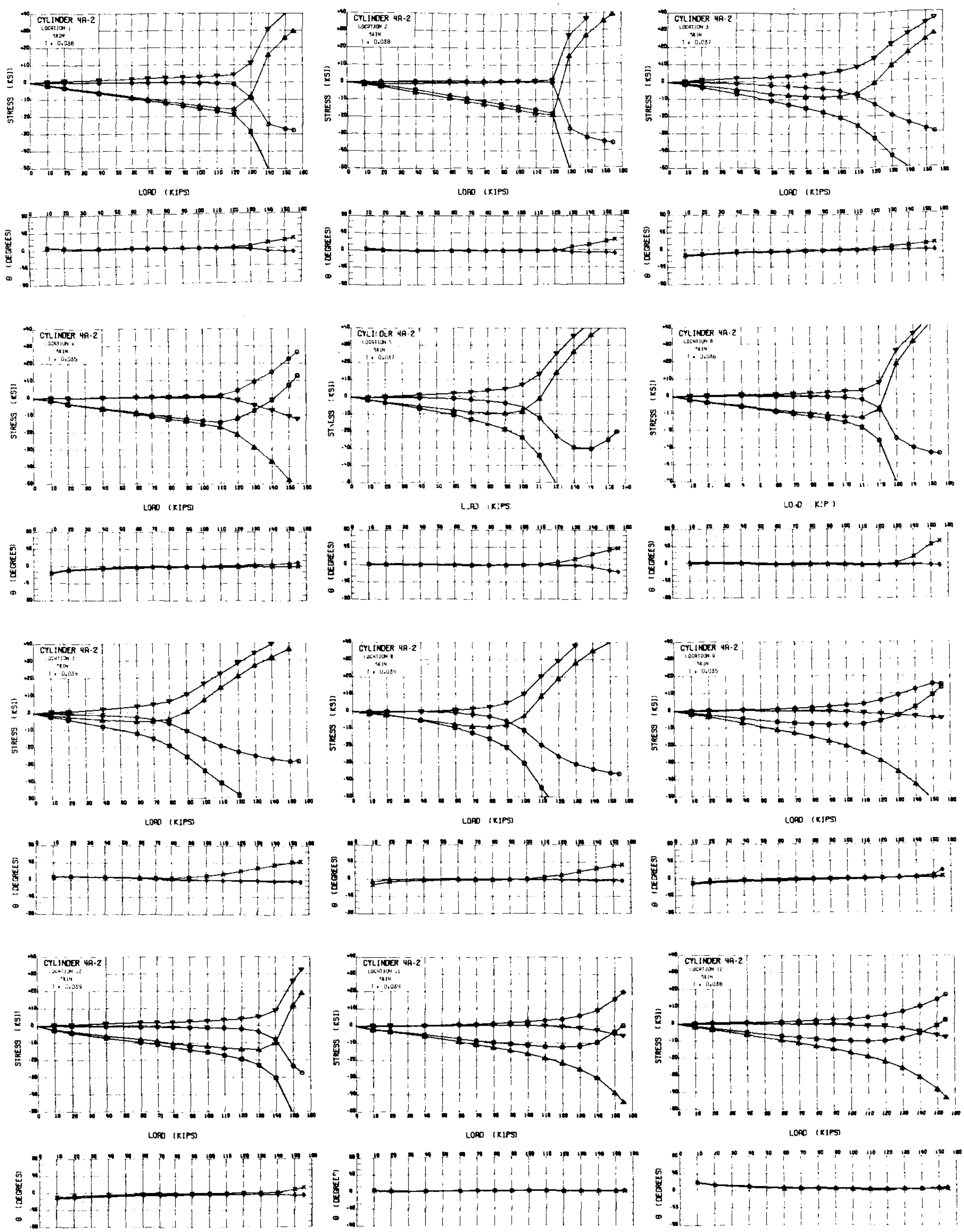

LEGEND		
ITEM	DESCRIPTION	SYMBOL
$\sigma_1^{\,o}$	MAX. OUTSIDE PRINCIPAL STRESS, (CIRCUM. DIR.)	-○-
$\sigma_1^{\,i}$	MAX. INSIDE PRINCIPAL STRESS, (CIRCUM. DIR.)	-▽-
$\sigma_2^{\,o}$	MIN. OUTSIDE PRINCIPAL STRESS, (AXIAL DIR.)	-□-
$\sigma_2^{\,i}$	MIN. INSIDE PRINCIPAL STRESS, (AXIAL DIR.)	-△-
θ^{o}	PRINCIPAL DIRECTION, OUTSIDE SURFACE	-◇-
θ^{i}	PRINCIPAL DIRECTION, INSIDE SURFACE	-×-

CYLINDER 4A-2
(SKIN)

FIG. 8 CONT.

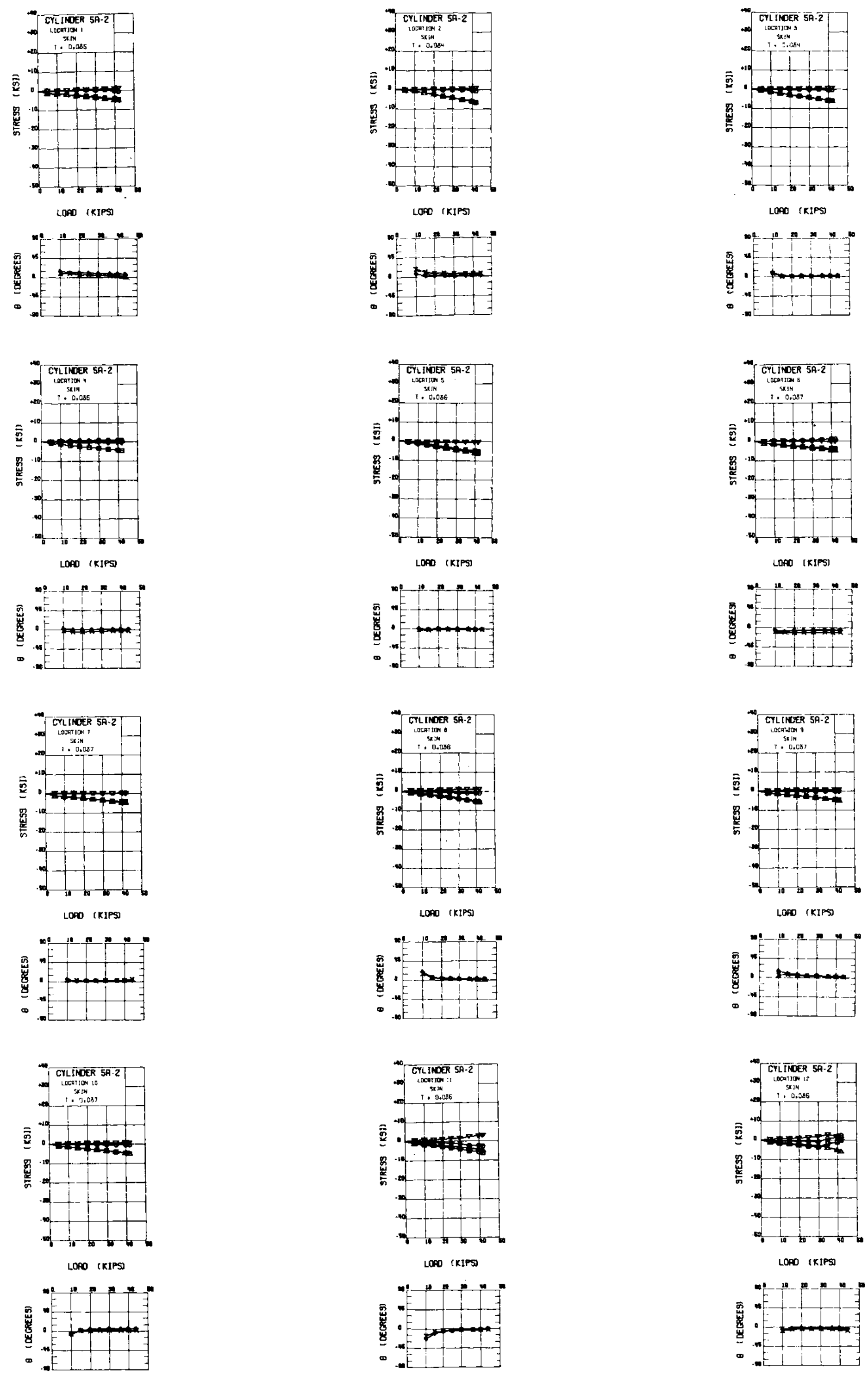

LEGEND		
ITEM	DESCRIPTION	SYMBOL
$\sigma_1^{\,o}$	MAX. OUTSIDE PRINCIPAL STRESS, (CIRCUM. DIR.)	-o-o-
$\sigma_1^{\,i}$	MAX. INSIDE PRINCIPAL STRESS, (CIRCUM. DIR.)	-▽-▽-
$\sigma_2^{\,o}$	MIN. OUTSIDE PRINCIPAL STRESS, (AXIAL DIR.)	-□-□-
$\sigma_2^{\,i}$	MIN. INSIDE PRINCIPAL STRESS, (AXIAL DIR.)	-△-△-
$\theta_1^{\,o}$	PRINCIPAL DIRECTION, OUTSIDE SURFACE	-◇-◇-
$\theta_1^{\,i}$	PRINCIPAL DIRECTION, INSIDE SURFACE	-×-×-

CYLINDER 5A-2
(SKIN)

FIG. 8 CONT.

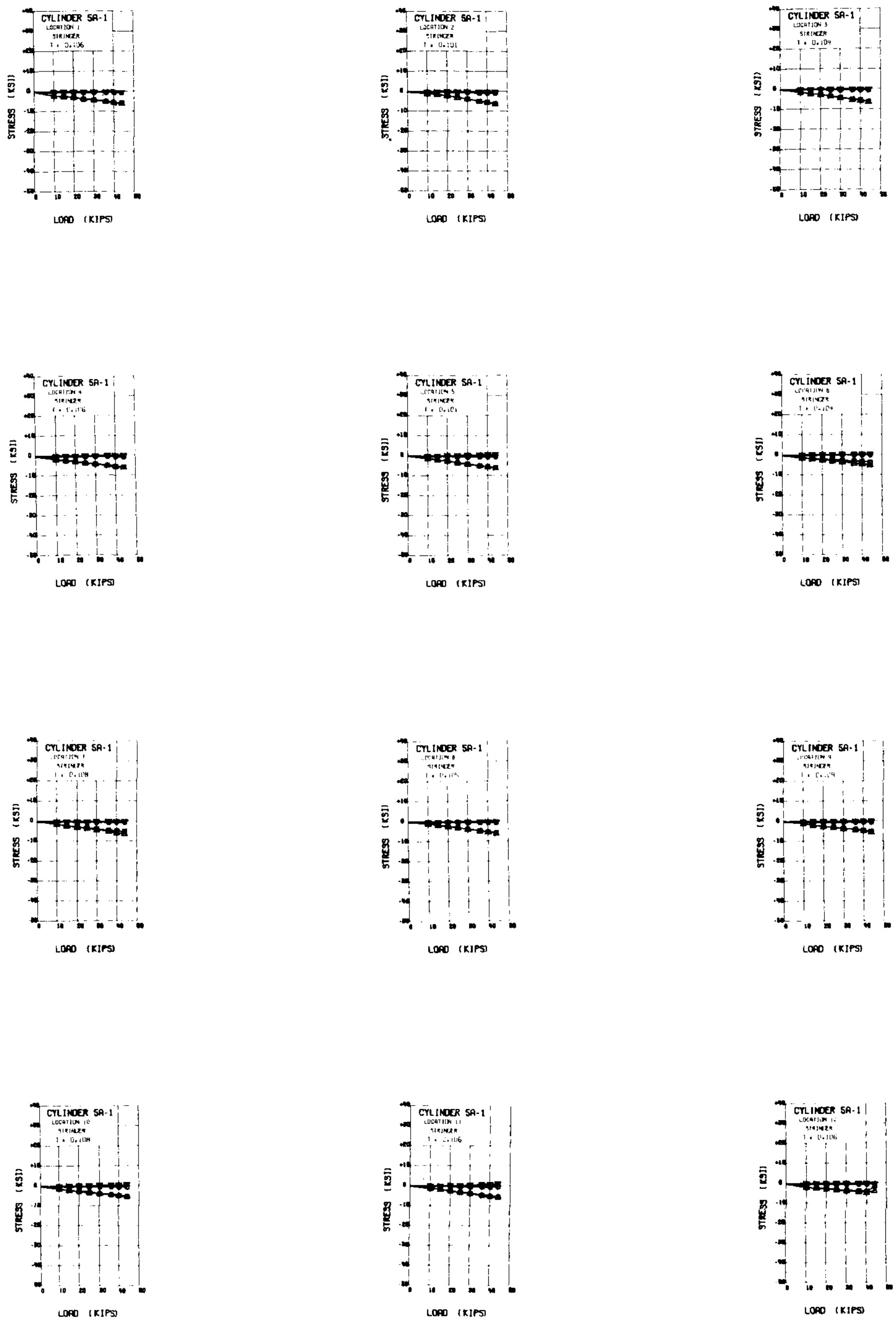

LEGEND		
ITEM	DESCRIPTION	SYMBOL
σ_1^o	MAX OUTSIDE PRINCIPAL STRESS, (CIRCUM DIR)	-o-o-
σ_1^i	MAX INSIDE PRINCIPAL STRESS, (CIRCUM DIR)	-▽-▽-
σ_2^o	MIN OUTSIDE PRINCIPAL STRESS, (AXIAL DIR)	-□-□-
σ_2^i	MIN INSIDE PRINCIPAL STRESS, (AXIAL DIR)	-△-△-
θ_1^o	PRINCIPAL DIRECTION, OUTSIDE SURFACE	-◇-◇-
θ_1^i	PRINCIPAL DIRECTION, INSIDE SURFACE	-×-×-

CYLINDER 5A-1
(STRINGER)

FIG. 8 CONT.

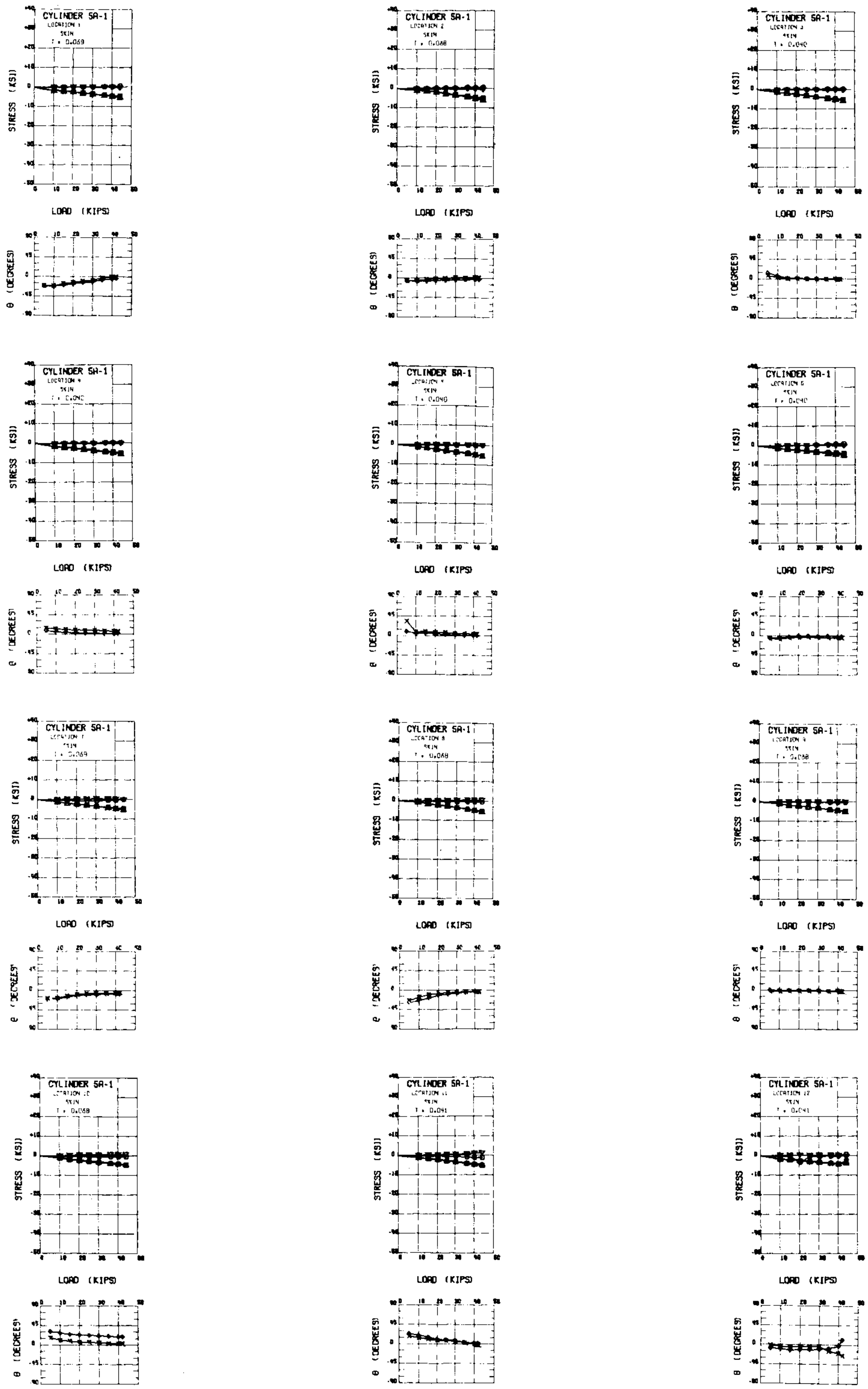

LEGEND		
ITEM	DESCRIPTION	SYMBOL
σ_1^o	MAX. OUTSIDE PRINCIPAL STRESS, (CIRCUM. DIR.)	-o-o-
σ_1^i	MAX. INSIDE PRINCIPAL STRESS, (CIRCUM. DIR.)	-▽-▽-
σ_2^o	MIN. OUTSIDE PRINCIPAL STRESS, (AXIAL DIR.)	-□-□-
σ_2^i	MIN. INSIDE PRINCIPAL STRESS, (AXIAL DIR.)	-△-△-
θ_1^o	PRINCIPAL DIRECTION, OUTSIDE SURFACE	-◇-◇-
θ_1^i	PRINCIPAL DIRECTION, INSIDE SURFACE	-×-×-

CYLINDER 5A-1
(SKIN)

FIG.8 CONT.

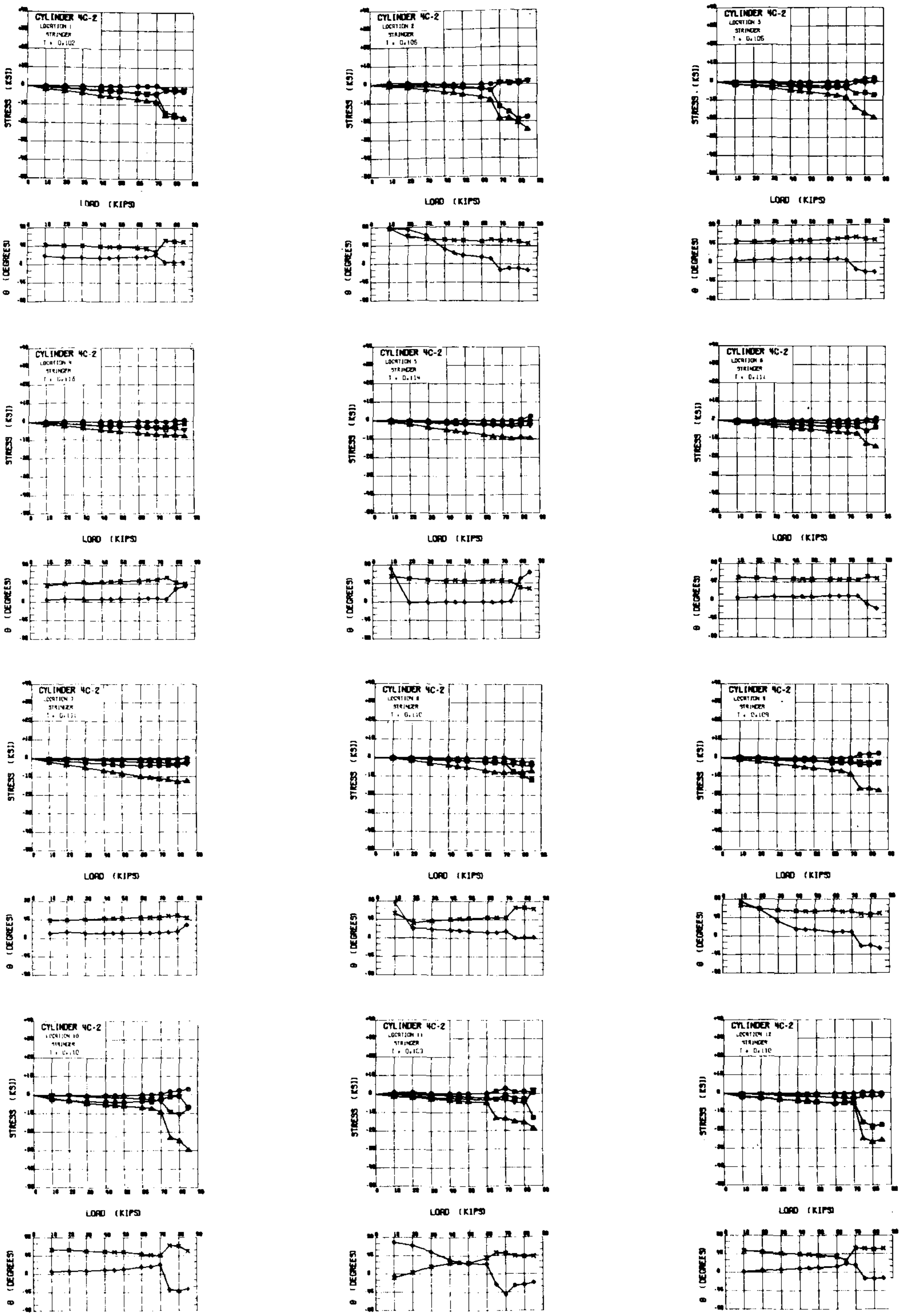

LEGEND		
ITEM	DESCRIPTION	SYMBOL
σ_1^o	MAX OUTSIDE PRINCIPAL STRESS, (CIRCUM. DIR)	
σ_1^i	MAX. INSIDE PRINCIPAL STRESS, (CIRCUM DIR)	
σ_2^o	MIN OUTSIDE PRINCIPAL STRESS, (AXIAL DIR)	
σ_2^i	MIN INSIDE PRINCIPAL STRESS, (AXIAL DIR)	
θ_1^o	PRINCIPAL DIRECTION, OUTSIDE SURFACE	
θ_1^i	PRINCIPAL DIRECTION, INSIDE SURFACE	

CYLINDER 4C-2
(STRINGER)

FIG. 8 CONT.

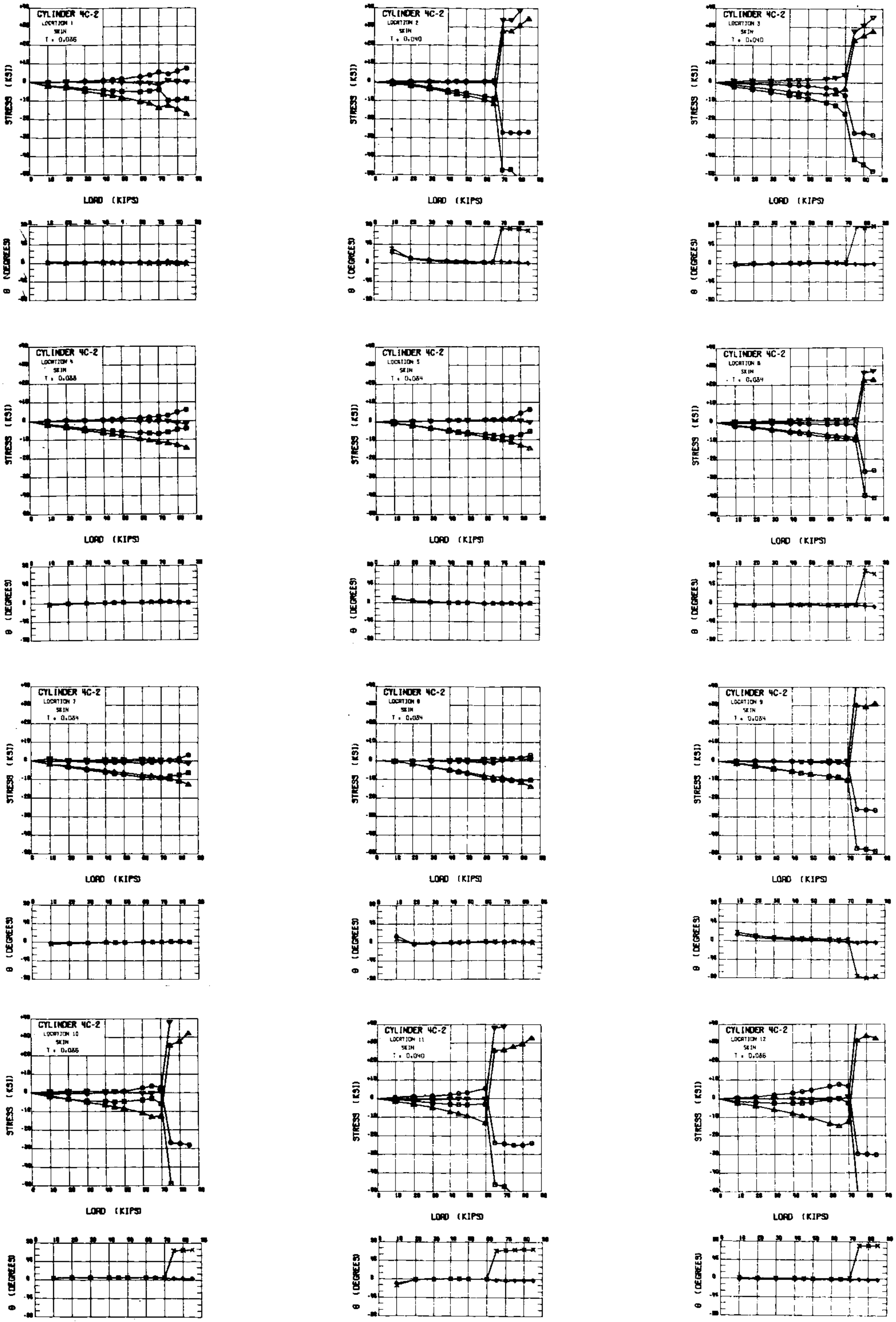

LEGEND		
ITEM	DESCRIPTION	SYMBOL
σ_1^o	MAX. OUTSIDE PRINCIPAL STRESS, (CIRCUM. DIR.)	
σ_1^i	MAX. INSIDE PRINCIPAL STRESS, (CIRCUM. DIR.)	
σ_2^o	MIN. OUTSIDE PRINCIPAL STRESS, (AXIAL DIR.)	
σ_2^i	MIN. INSIDE PRINCIPAL STRESS, (AXIAL DIR.)	
θ_1^o	PRINCIPAL DIRECTION, OUTSIDE SURFACE	
θ_1^i	PRINCIPAL DIRECTION, INSIDE SURFACE	

CYLINDER 4C-2
(SKIN)

FIG. 8 CONT.

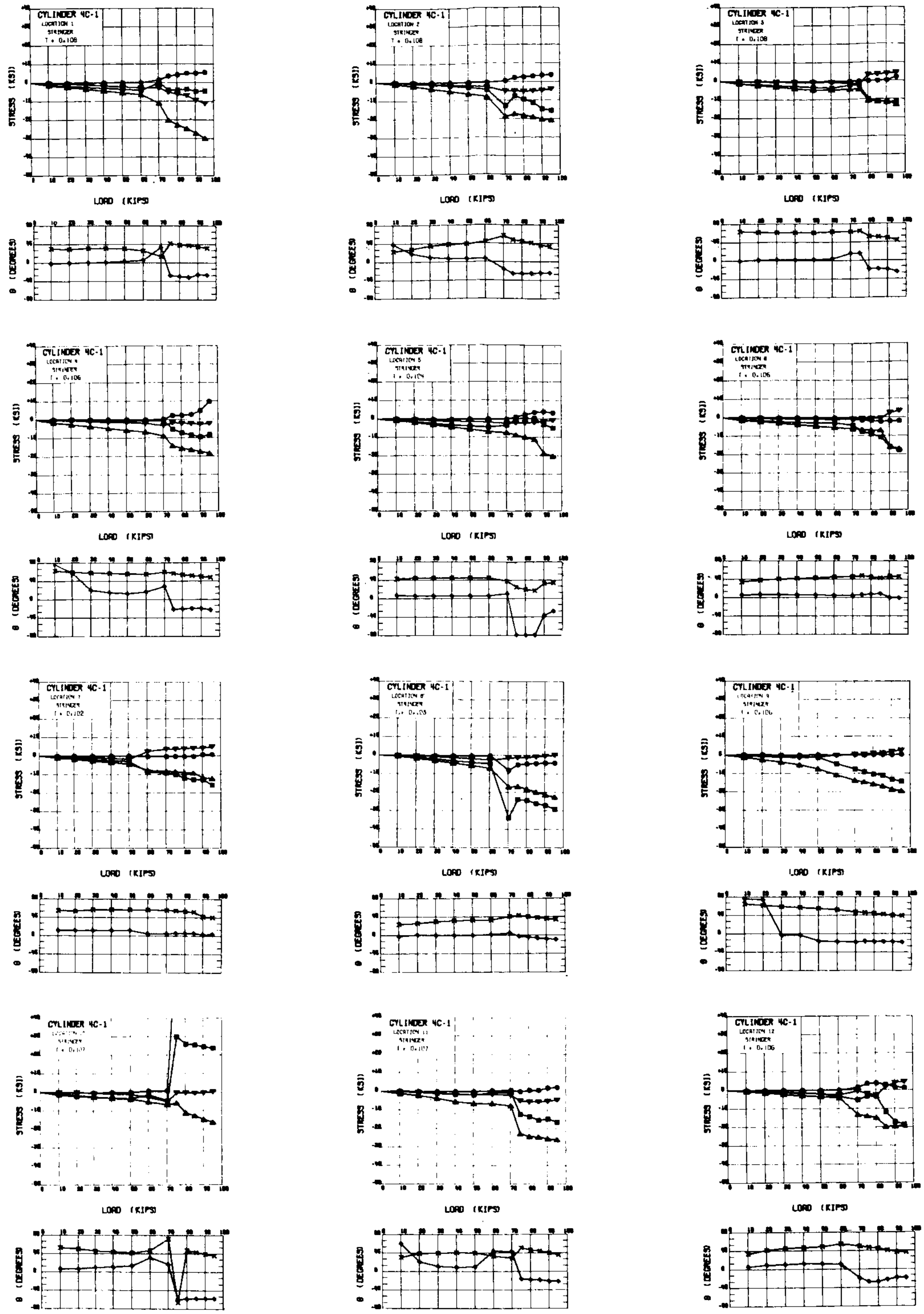

LEGEND		
ITEM	DESCRIPTION	SYMBOL
$\sigma_1^{\,o}$	MAX. OUTSIDE PRINCIPAL STRESS, (CIRCUM. DIR.)	-⊖-⊖-
$\sigma_1^{\,i}$	MAX. INSIDE PRINCIPAL STRESS, (CIRCUM. DIR.)	-▽-▽-
$\sigma_2^{\,o}$	MIN. OUTSIDE PRINCIPAL STRESS, (AXIAL DIR.)	-⊟-⊟-
$\sigma_2^{\,i}$	MIN. INSIDE PRINCIPAL STRESS, (AXIAL DIR.)	-△-△-
$\theta_1^{\,o}$	PRINCIPAL DIRECTION, OUTSIDE SURFACE	-⊖-⊖-
$\theta_1^{\,i}$	PRINCIPAL DIRECTION, INSIDE SURFACE	-×-×-

CYLINDER 4C-1
(STRINGER)

FIG. 8 CONT.

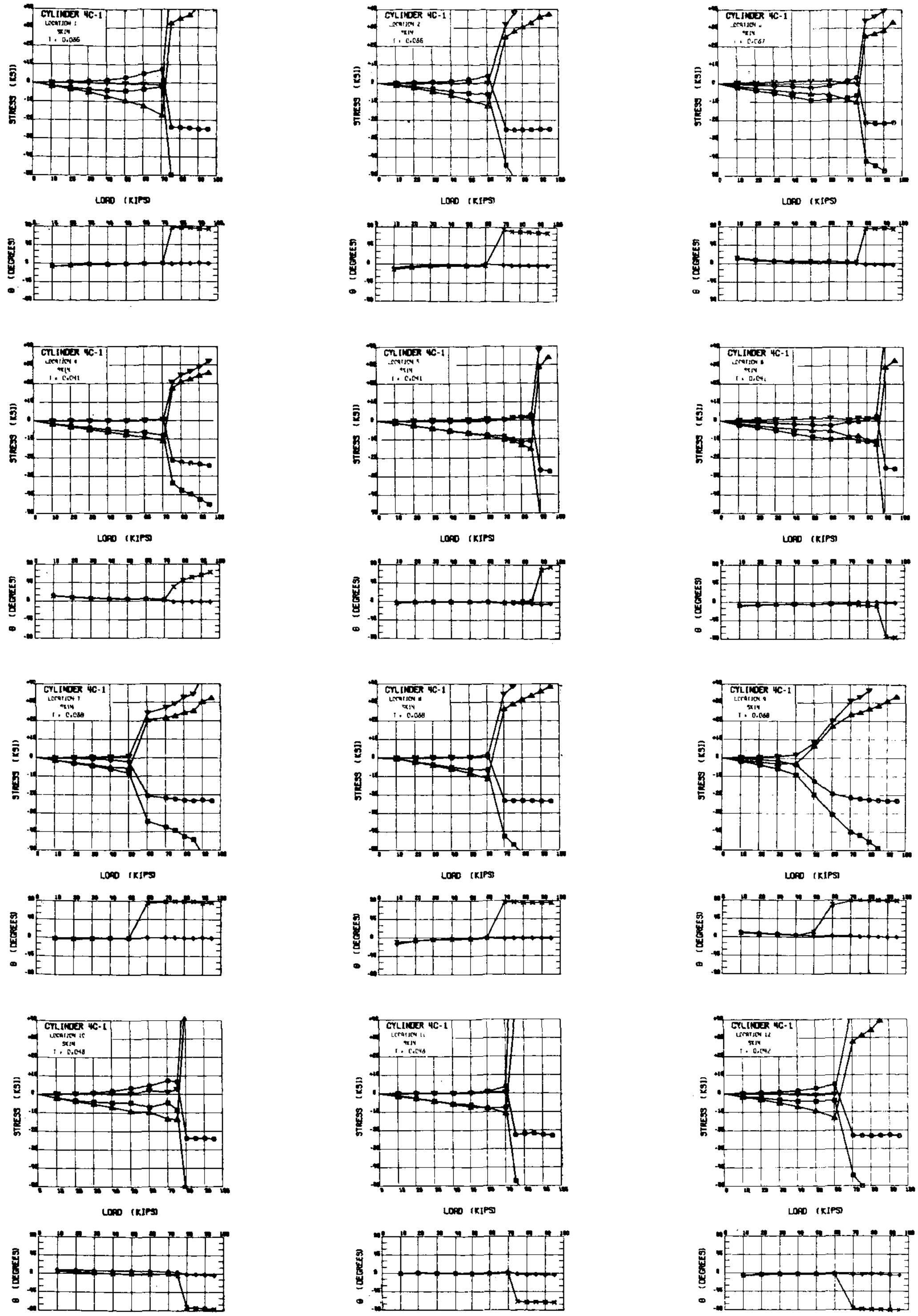

LEGEND		
ITEM	DESCRIPTION	SYMBOL
σ_1^o	MAX. OUTSIDE PRINCIPAL STRESS, (CIRCUM. DIR.)	
σ_1^i	MAX. INSIDE PRINCIPAL STRESS, (CIRCUM. DIR.)	
σ_2^o	MIN. OUTSIDE PRINCIPAL STRESS, (AXIAL DIR.)	
σ_2^i	MIN. INSIDE PRINCIPAL STRESS, (AXIAL DIR.)	
θ_1^o	PRINCIPAL DIRECTION, OUTSIDE SURFACE	
θ_1^i	PRINCIPAL DIRECTION, INSIDE SURFACE	

CYLINDER 4C-1
(SKIN)

FIG. 8 CONT.

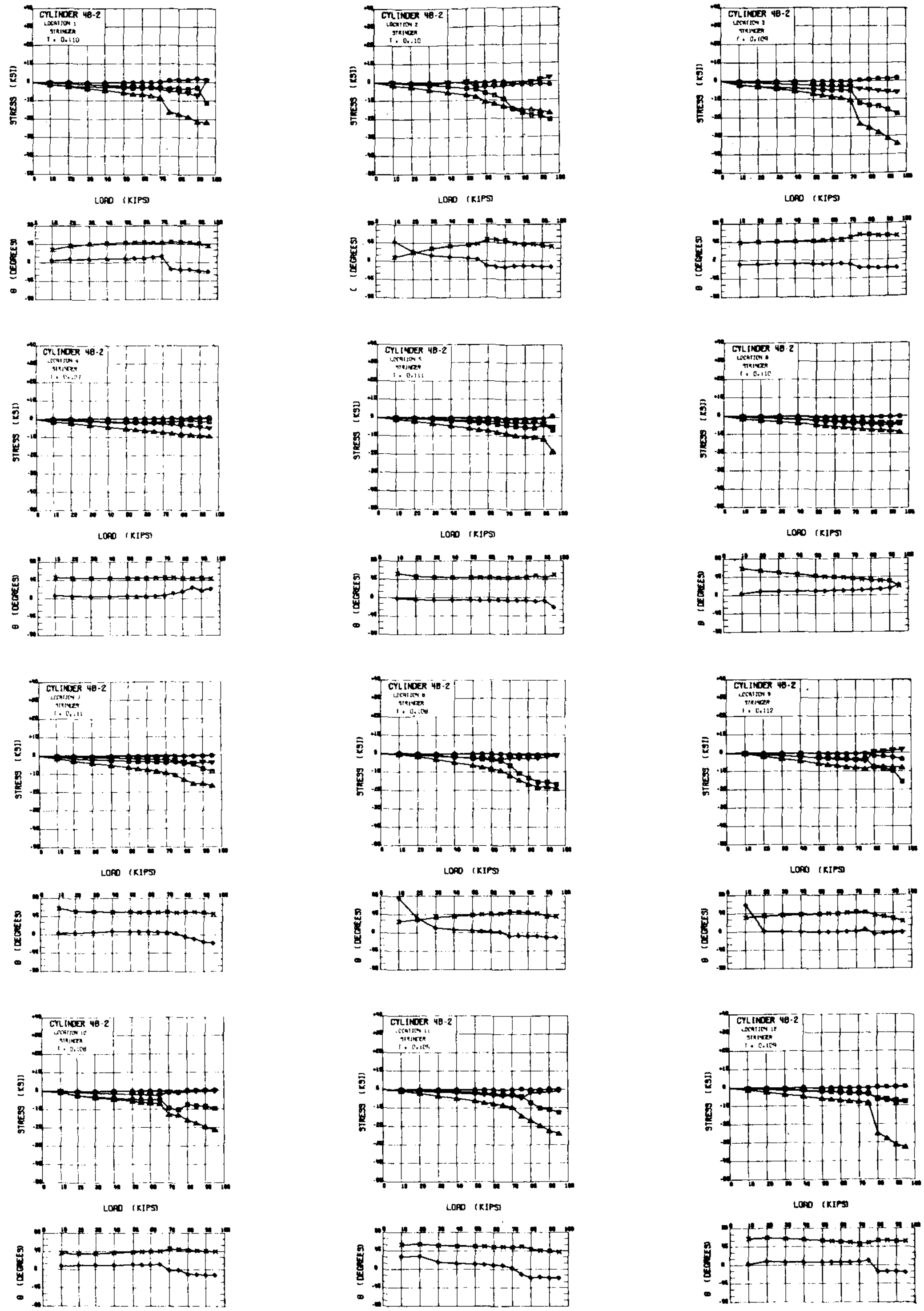

LEGEND		
ITEM	DESCRIPTION	SYMBOL
σ_1^o	MAX. OUTSIDE PRINCIPAL STRESS, (CIRCUM. DIR.)	-o-o-
σ_1^i	MAX. INSIDE PRINCIPAL STRESS, (CIRCUM. DIR.)	-▽-▽-
σ_2^o	MIN. OUTSIDE PRINCIPAL STRESS, (AXIAL DIR.)	-□-□-
σ_2^i	MIN. INSIDE PRINCIPAL STRESS, (AXIAL DIR.)	-△-△-
θ^o	PRINCIPAL DIRECTION, OUTSIDE SURFACE	-◇-◇-
θ^i	PRINCIPAL DIRECTION, INSIDE SURFACE	-x-x-

CYLINDER 4B-2
(STRINGER)

FIG. 8 CONT.

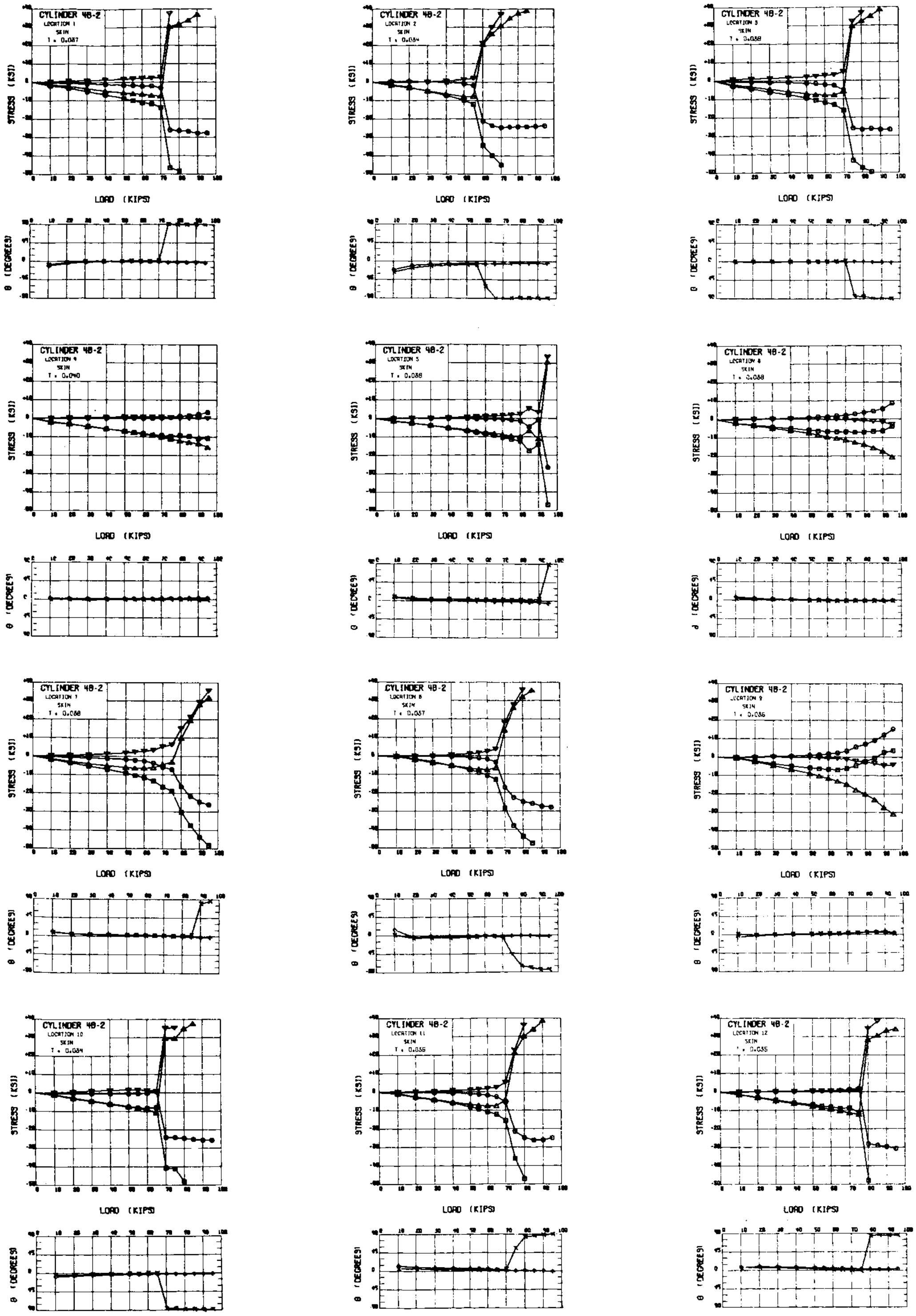

LEGEND		
ITEM	DESCRIPTION	SYMBOL
σ_1^o	MAX. OUTSIDE PRINCIPAL STRESS, (CIRCUM. DIR.)	-o-o-
σ_1^i	MAX. INSIDE PRINCIPAL STRESS, (CIRCUM. DIR.)	-▽-▽-
σ_2^o	MIN. OUTSIDE PRINCIPAL STRESS, (AXIAL DIR.)	-□-□-
σ_2^i	MIN. INSIDE PRINCIPAL STRESS, (AXIAL DIR.)	-△-△-
θ_1^o	PRINCIPAL DIRECTION, OUTSIDE SURFACE	-◇-◇-
θ_1^i	PRINCIPAL DIRECTION, INSIDE SURFACE	-×-×-

CYLINDER 4B-2
(SKIN)

FIG.8 CONT.

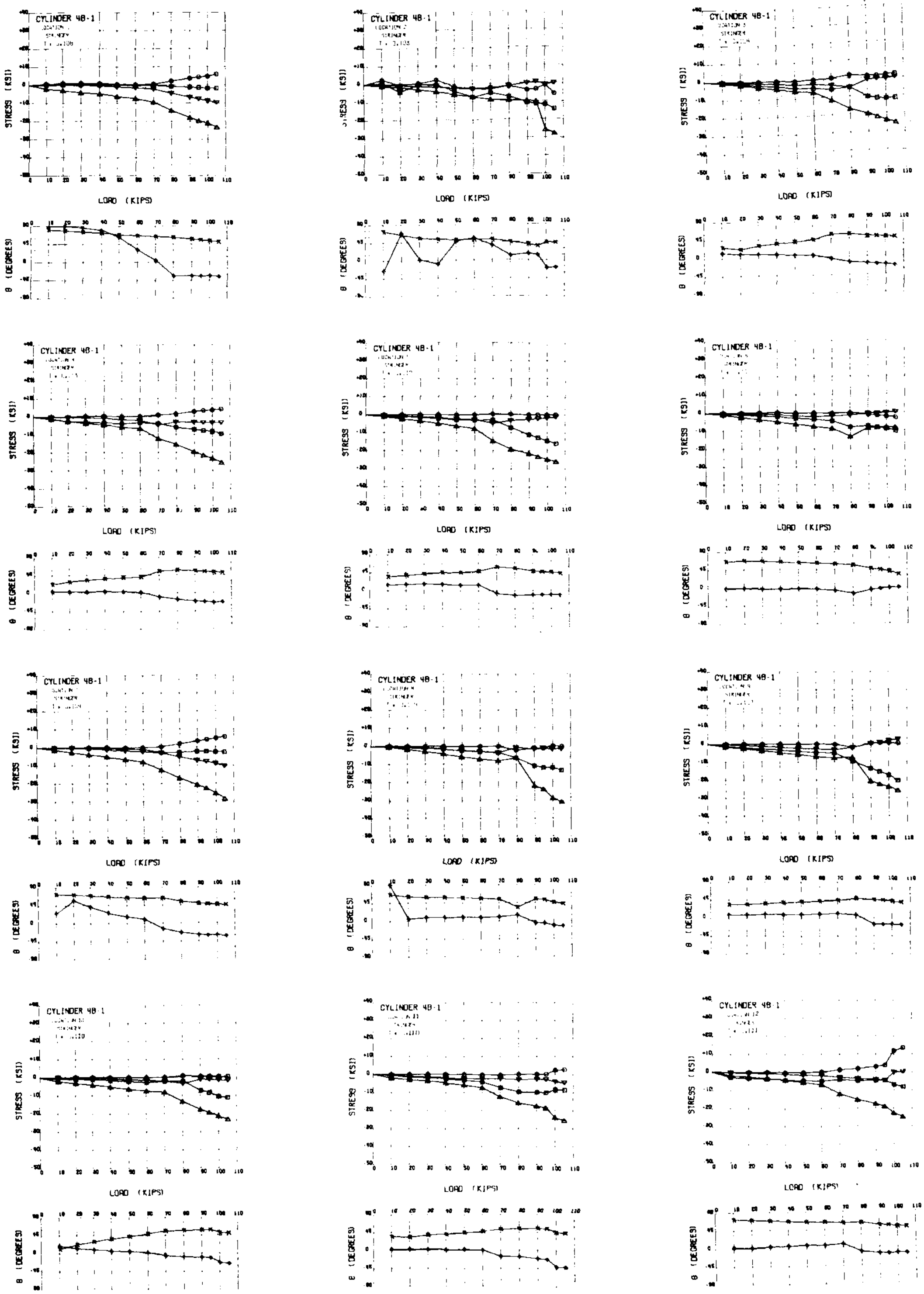

LEGEND

ITEM	DESCRIPTION	SYMBOL
σ_1^o	MAX OUTSIDE PRINCIPAL STRESS, (CIRCUM DIR)	-○-○-
σ_1^i	MAX INSIDE PRINCIPAL STRESS, (CIRCUM DIR)	-▽-▽-
σ_2^o	MIN OUTSIDE PRINCIPAL STRESS, (AXIAL DIR)	-□-□-
σ_2^i	MIN INSIDE PRINCIPAL STRESS, (AXIAL DIR)	-△-△-
θ_1^o	PRINCIPAL DIRECTION, OUTSIDE SURFACE	-◇-◇-
θ_1^i	PRINCIPAL DIRECTION, INSIDE SURFACE	-×-×-

CYLINDER 4B-1
(STRINGER)

FIG. 8 CONT.

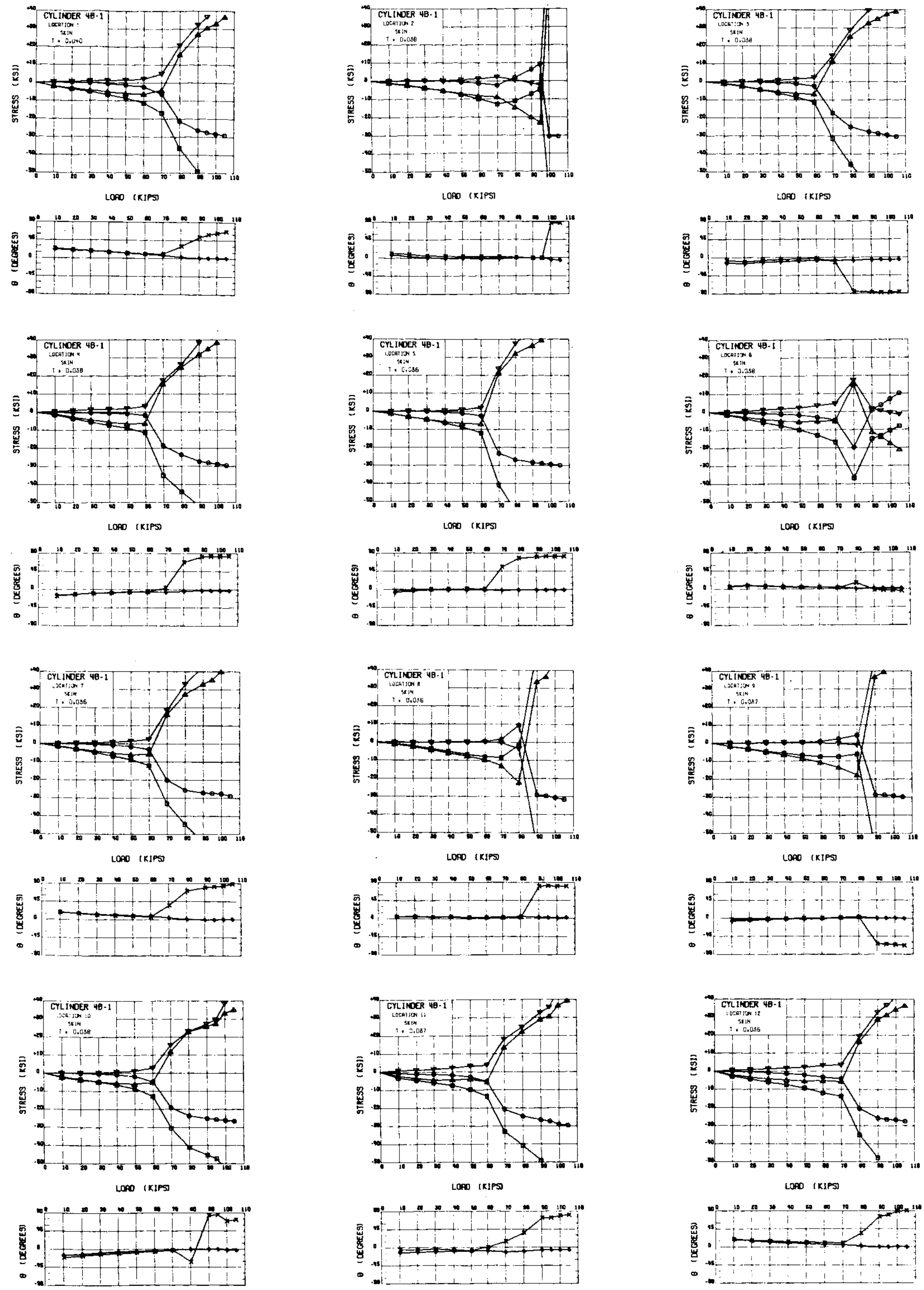

LEGEND		
ITEM	DESCRIPTION	SYMBOL
σ_1^o	MAX. OUTSIDE PRINCIPAL STRESS, (CIRCUM. DIR.)	
σ_1^i	MAX. INSIDE PRINCIPAL STRESS, (CIRCUM. DIR.)	
σ_2^o	MIN. OUTSIDE PRINCIPAL STRESS, (AXIAL DIR.)	
σ_2^i	MIN. INSIDE PRINCIPAL STRESS, (AXIAL DIR.)	
θ_1^o	PRINCIPAL DIRECTION, OUTSIDE SURFACE	
θ_1^i	PRINCIPAL DIRECTION, INSIDE SURFACE	

CYLINDER 4B-1
(SKIN)

FIG. 8 CONT.

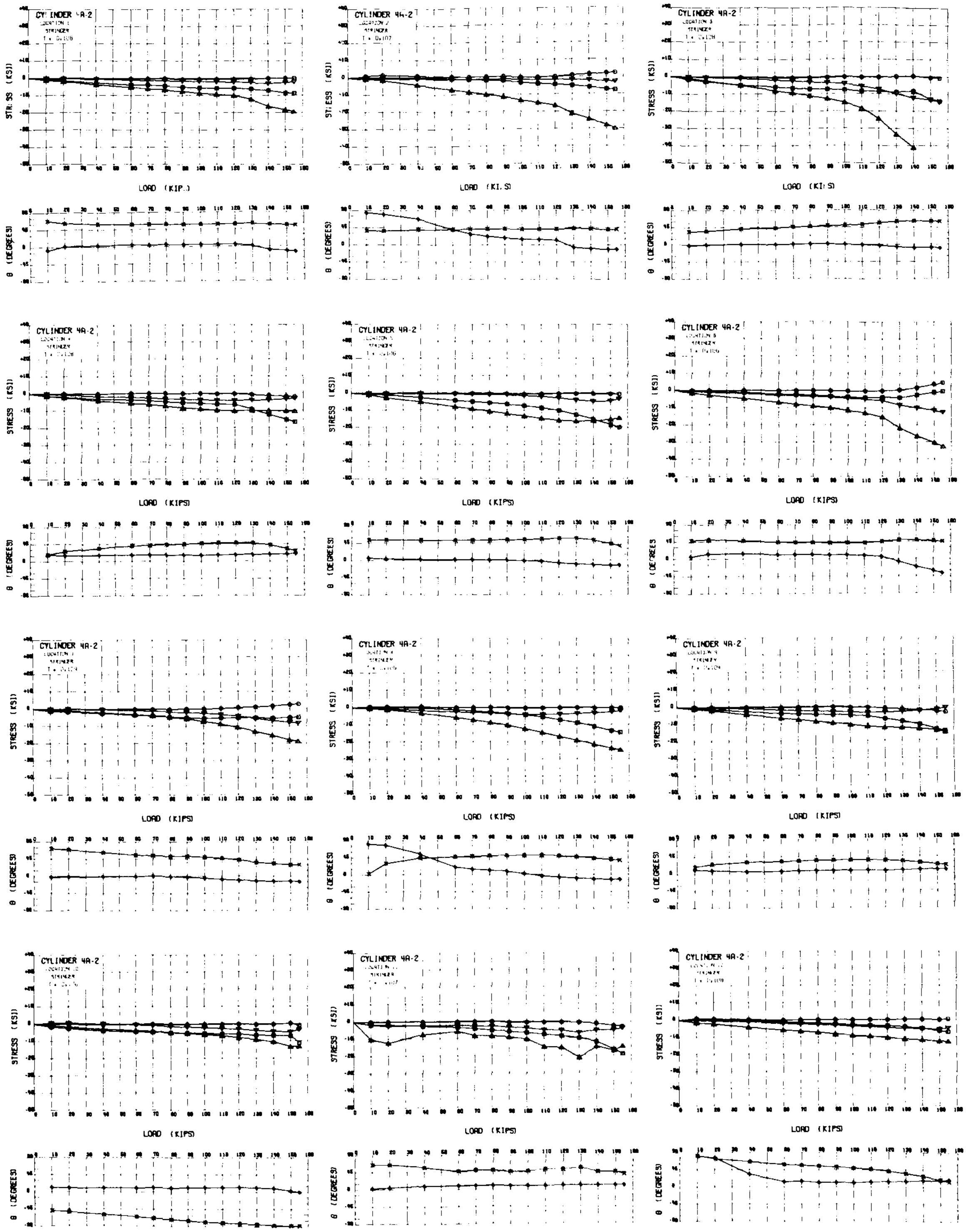

ITEM	LEGEND DESCRIPTION	SYMBOL
σ_1^o	MAX OUTSIDE PRINCIPAL STRESS, (CIRCUM DIR)	-o-o-
σ_1^i	MAX INSIDE PRINCIPAL STRESS, (CIRCUM DIR)	-▽-▽-
σ_2^o	MIN OUTSIDE PRINCIPAL STRESS, (AXIAL DIR)	-□-□-
σ_2^i	MIN INSIDE PRINCIPAL STRESS, (AXIAL DIR)	-△-△-
θ^o	PRINCIPAL DIRECTION, OUTSIDE SURFACE	-◇-◇-
θ^i	PRINCIPAL DIRECTION, INSIDE SURFACE	-x-x-

CYLINDER 4A-2
(STRINGER)

FIG. 8 CONT.

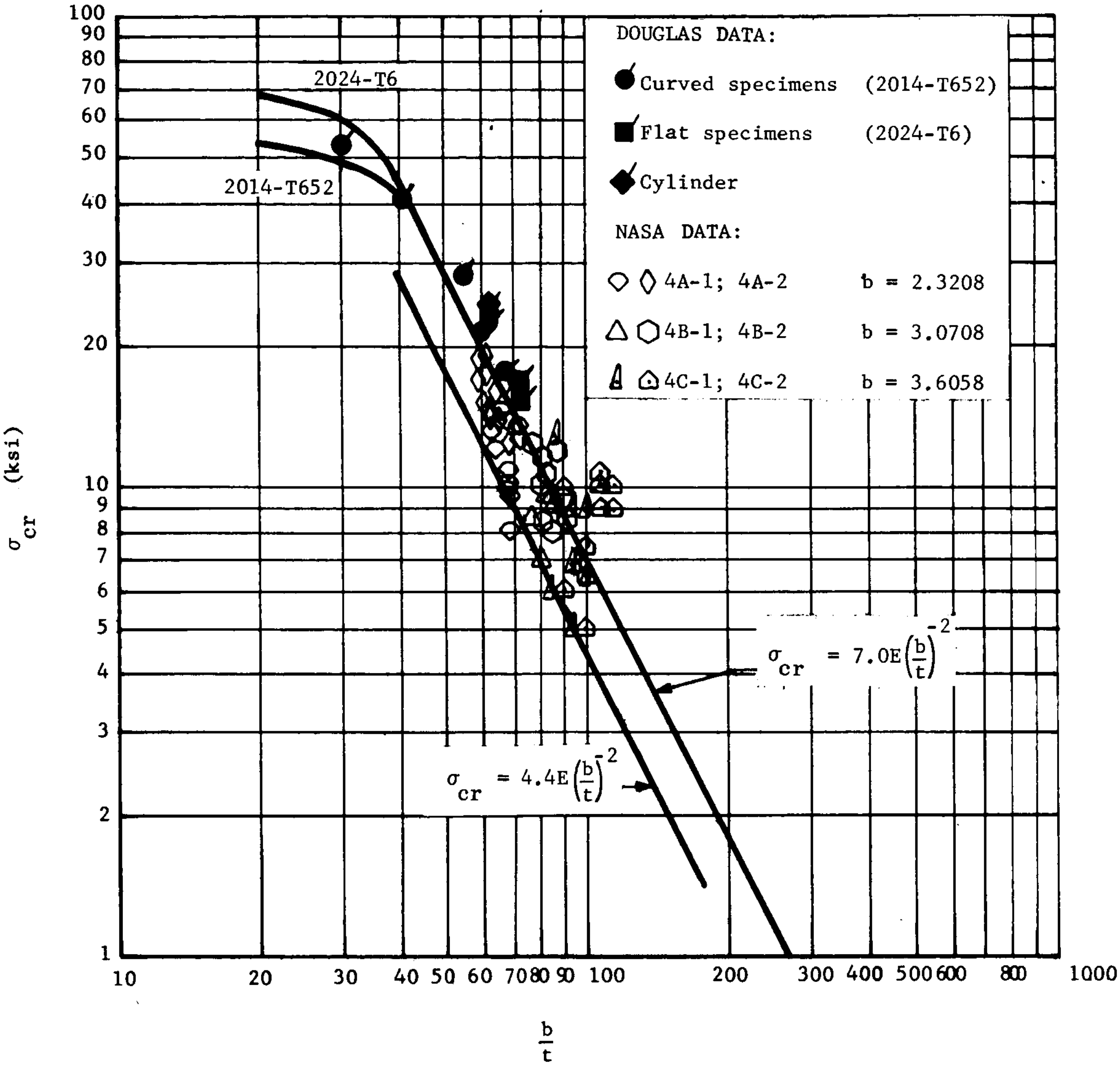

LOCAL BUCKLING RESULTS FOR GROUP 4 (45°) CYLINDERS

FIG. 13

NOMINAL CYLINDER GEOMETRY

TABLE I

CYLINDER NO.	b_f	b_s	b_x	b_y	H	L	n_s	n_{sx}	n_{sy}	n_x	n_y	R	R_c	R_f	t	t_f	t_h	t_s	t_x	t_y	L/R	R/t	t/H	t_h/t_f	NUMBER OF WELDS Longitudinal Direction	NUMBER OF WELDS Circumferential Direction
1A	*	*	*	*	0.040	58.250	*	*	*	*	*	26.180	*	*	0.0400	*	*	*	*	*	2.2	654	*	*	2	0
1B	*	*	*	*	0.094	58.250	*	*	*	*	*	26.190	*	*	0.0940	*	*	*	*	*	2.2	279	*	*	2	0
2A	*	*	1.250	2.427	0.250	56.106	*	*	*	44	68	26.773	0.2124	0.0354	0.0375	*	0.2125	*	0.1062	0.1062	2.1	714	0.15	6.0	4	1
2B-1	*	*	2.427	2.427	0.250	54.500	*	*	*	22	68	26.990	0.2124	0.0354	0.0375	*	0.2125	*	0.1062	0.1062	2.0	720	0.15	6.0	4	1
2B-2	*	*	2.427	2.427	0.250	54.500	*	*	*	22	68	26.517	0.2124	0.0354	0.0375	*	0.2125	*	0.1062	0.1062	2.1	707	0.15	6.0	4	1
2C	*	*	7.500	2.427	0.250	46.106	*	*	*	6	68	26.768	0.2124	0.0354	0.0375	*	0.2125	*	0.1062	0.1062	1.7	714	0.15	6.0	4	1
3A	*	*	1.250	2.427	0.250	55.000	*	*	*	44	68	26.182	0.2124	0.0354	0.0375	*	0.2125	*	0.1062	0.1062	2.1	698	0.15	6.0	4	0
3B-1	*	*	2.427	2.427	0.250	53.394	*	*	*	22	68	26.176	0.2124	0.0354	0.0375	*	0.2125	*	0.1062	0.1062	2.0	698	0.15	6.0	4	0
3B-2	*	*	2.427	2.427	0.250	53.394	*	*	*	22	68	26.191	0.2124	0.0354	0.0375	*	0.2125	*	0.1062	0.1062	2.0	698	0.15	6.0	4	0
3C	*	*	5.000	2.427	0.250	55.000	*	*	*	11	68	26.191	0.2124	0.0354	0.0375	*	0.2125	*	0.1062	0.1062	2.1	698	0.15	6.0	4	0
3D	*	*	7.500	2.427	0.250	52.500	*	*	*	7	68	26.201	0.2124	0.0354	0.0375	*	0.2125	*	0.1062	0.1062	2.0	698	0.15	6.0	4	0
4A-1	*	2.427	*	*	0.250	54.908	1424	96	128	*	*	26.131	0.2124	0.0354	0.0375	*	0.2125	0.1062	*	*	2.1	697	0.15	6.0	4	0
4A-2	*	2.427	*	*	0.250	54.908	1424	96	128	*	*	26.132	0.2124	0.0354	0.0375	*	0.2125	0.1062	*	*	2.1	697	0.15	6.0	4	0
4B-1	*	3.177	*	*	0.250	53.907	780	72	96	*	*	26.643	0.2124	0.0354	0.0375	*	0.2125	0.1062	*	*	2.0	710	0.15	6.0	4	0
4B-2	*	3.177	*	*	0.250	53.907	780	72	96	*	*	26.657	0.2124	0.0354	0.0375	*	0.2125	0.1062	*	*	2.0	711	0.15	6.0	4	0
4C-1	*	3.712	*	*	0.250	52.488	568	64	80	*	*	26.153	0.2124	0.0354	0.0375	*	0.2125	0.1062	*	*	2.0	697	0.15	6.0	4	0
4C-2	*	3.712	*	*	0.250	52.488	568	64	80	*	*	26.155	0.2124	0.0354	0.0375	*	0.2125	0.1062	*	*	2.0	697	0.15	6.0	4	0
5A-1	*	*	*	2.427	0.250	55.356	*	*	*	*	68	26.144	*	0.0354	0.0375	*	0.2125	*	*	0.1062	2.1	697	0.15	6.0	2	0
5A-2	*	*	*	2.427	0.250	55.356	*	*	*	*	68	26.167	*	0.0354	0.0375	*	0.2125	*	*	0.1062	2.1	698	0.15	6.0	2	0
5B-1	*	*	*	1.712	0.250	55.356	*	*	*	*	96	26.039	*	0.0354	0.0375	*	0.2125	*	*	0.1062	2.1	694	0.15	6.0	2	0
5B-2	*	*	*	1.712	0.250	55.356	*	*	*	*	96	26.039	*	0.0354	0.0375	*	0.2125	*	*	0.1062	2.1	694	0.15	6.0	2	0
5C-1	0.209	*	*	1.712	0.250	55.356	*	*	*	*	96	26.054	*	0.0354	0.0375	0.103	0.2125	*	*	0.1062	2.1	695	0.15	6.0	2	0
5C-2	0.209	*	*	1.712	0.250	55.356	*	*	*	*	96	26.054	*	0.0354	0.0375	0.103	0.2125	*	*	0.1062	2.1	.695	0.15	6.0	2	0

LEGEND: * = DOES NOT APPLY

TABLE II

CYLINDER DIMENSIONS IN GENERAL INSTABILITY REGION[a]

CYLINDER NUMBER	b_f	t	t_f	t_h	t_s	t_x	t_y	$\bar{t}$	Circumference
1A	*	0.040	*	*	*	*	*	0.040	164.494
1B	*	0.094	*	*	*	*	*	0.094	164.557
2A	*	0.037	*	0.213	*	0.105	0.104	0.0640	168.220
2B-1	*	0.038	*	0.212	*	0.111	0.107	0.0570	169.584
2B-2	*	0.038	*	0.212	*	0.108	0.107	0.0568	166.612
2C	*	0.031	*	0.219	*	0.103	0.104	0.0434	168.189
3A	*	0.037	*	0.213	*	0.101	0.100	0.0630	164.507
3B-1	*	0.037	*	0.213	*	0.109	0.103	0.0556	164.469
3B-2	*	0.035	*	0.215	*	0.110	0.104	0.0540	164.563
3C	*	0.036	*	0.214	*	0.106	0.105	0.0498	164.563
3D	*	0.039	*	0.211	*	0.106	0.106	0.0512	164.626
4A-1	*	0.034	*	0.216	0.108	*	*	0.0532	164.186
4A-2	*	0.038	*	0.212	0.106	*	*	0.0565	164.193
4B-1	*	0.037	*	0.213	0.106	*	*	0.0512	167.403
4B-2	*	0.037	*	0.213	0.108	*	*	0.0515	167.491
4C-1	*	0.038	*	0.212	0.106	*	*	0.0441	164.325
4C-2	*	0.036	*	0.214	0.108	*	*	0.0485	164.337
5A-1	*	0.038	*	0.212	*	*	0.106	0.0473	164.267
5A-2	*	0.037	*	0.213	*	*	0.106	0.0463	164.412
5B-1	*	0.038	*	0.212	*	*	0.107	0.0513	163.608
5B-2	*	0.038	*	0.212	*	*	0.104	0.0509	163.608
5C-1	0.208	0.039	0.102	0.109	*	*	0.100	0.0578	163.702
5C-2	0.207	0.038	0.102	0.110	*	*	0.099	0.0567	163.702

(a) Values listed are those which differ from nominal values shown in Table I.

* signifies "does not apply"

TABLE III

LOAD SUMMARY

Group	Cylinder Number	General Instability Load (kips)	Number[a] of Buckle Wavelengths x-Direction (Half-waves)	Number[a] of Buckle Wavelengths y-Direction (Full-waves)	First Load at which any Local[b] Buckling Occurs (kips)	Comments
1	1A	22.9	3	9	-	Local buckling observed near weld (location 6) at 17 kips, cylinder 1A.
	1B	143.5	4	8	-	
2	2A	171.5	3	8	-	The circumferential weld peculiar to these cylinders degraded their critical load capability
	2B-1	118.3	4	9	80	
	2B-2	131.5	4	9	80	
	2C	77.2	4	8	70	
3	3A	172.1	5	9	-	Premature failure occurred near top of cylinder 3A.
	3B-1	150.0	4	8	90	
	3B-2	154.7	4	9	90	
	3C	122.2	4	8	70	
	3D	103.9	4	9	90	
4	4A-1	154.0	4	8	60	Local buckling always occurred far below the general instability level (in most cases below 50% of P_{cr})
	4A-2	164.8	4	9	70	
	4B-1	110.0	4	6	51	
	4B-2	104.3	4	8	55	
	4C-1	97.3	4	7	40	
	4C-2	93.4	4	7	60	
5	5A-1	44.2	1	8	-	Local buckling was observed at location 12 at 21 kips, cylinder 5B-2.
	5A-2	41.9	1	8	-	
	5B-1	43.7	1	8	-	
	5B-2	42.0	1	8	-	
	5C-1	58.7	1	8	-	
	5C-2	70.0	1	8	-	

(a) The values indicate the integral number of half or full waves which could fit in the x and y directions if the cylinders buckled over their entire surface.

(b) Figures 12 and 13 give the local buckling data in great detail.

TABLE IV

GENERAL INSTABILITY PREDICTIONS, P_{cr} (kips)
FOR INTEGRALLY STIFFENED CYLINDERS

Group	Cylinder Number	P_{cr} Test Values	Predicted Values[a] P_{cr}							
			(1)	(3)	(4)	(5)	(6)	(8)	(12)	(13)
2*	2A	171.5	369	300	-	192	224	106	350	271
	2B-1	118.3	326	264	-	159	166	93.9	305	247
	2B-2	131.5	324	263	-	160	168	94.2	302	244
	2C	77.2	214	176	-	90.8	86	58.2	193	162
3	3A*	172.1	340	277	-	190	211	106	342	268
	3B-1	150.0	299	243	-	156	158	91.9	296	239
	3B-2	154.7	294	238	-	152	157	87.7	292	234
	3C	122.2	244	199	-	118	106	73.7	237	198
	3D	103.9	221	185	-	107	83.9	68.3	215	185
4	4A-1	154.0	-	-	-	-	-	141	-	245
	4A-2	164.8	-	-	-	-	-	145	-	255
	4B-1	110.0	-	-	-	-	-	122	-	221
	4B-2	104.3	-	-	-	-	-	128	-	223
	4C-1	97.3	-	-	-	-	-	113	-	208
	4C-2	93.4	-	-	-	-	-	113	-	205
5	5A-1	44.2	325	63.8	45.9	36.4	52.2	18.0	-	64.9
	5A-2	41.9	321	60.7	43.7	34.7	50.6	17.0	-	61.7
	5B-1	43.7	376	66.5	49.4	40.0	62.4	19.1	-	64.9
	5B-2	42.0	372	66.3	49.1	39.9	61.6	19.1	-	64.8
	5C-1	58.7	1,090	73.3	56.8	46.6	81.8	-	-	-
	5C-2	70.0	1,080	69.9	54.2	44.4	79.3	-	-	-

(a) References appear in rear of report. Assumptions in using methods are shown in Appendix A.

* See comments of Table III and Discussion

\- Indicates method was not in a form readily applicable to the cylinder goemetry.

APPENDIX

This section indicated the assumptions and engineering judgments made in using the methods listed in Table IV, and Figures 12 and 13. Because of the large number of cylinder geometries that were tested, all the methods were programmed for the high-speed digital computer. The methods are identified by reference number and author. Only method [12] attempts to include the effects of stiffener eccentricity on buckling strength.

A. GENERAL INSTABILITY METHODS

1. Becker and Gerard [1]. The value of the effective shear stiffness of the cylinder wall was assumed equal to $t + \frac{t_f b_f + t_y t_h}{b_y}$. The distributed area of the frame was chosen as $t + \frac{t_x t_h}{b_x}$, while the effective area of the stringer was $t + \frac{t_f b_f + t_y t_h}{b_y}$. The values for the torsional moments of inertia of the frame and of the stiffener were obtained from [2].

2. Dschou [3]. The method was employed with no deviations from the equations.

3. Peterson and Dow [4]. The radius was taken to the centroid of the stringer-skin combination. The coefficient of end fixity C was taken as 3.5. The values of γ were obtained from the equation $\gamma = 2.18432 - 0.49829 \log \frac{R}{\left(\frac{I_x t^2}{12\,\overline{t}}\right)^{\frac{1}{4}}}$.

4. Almroth [5]. The values used for the orthotropic extensional and flexural constants A_{ij} and D_{ij} were:

$$A_{11} = \frac{C_y}{E\,t}, \quad A_{12} = -\frac{\nu\, C_x C_y}{E\,t}, \quad A_{22} = \frac{C_x}{E\,t}, \quad A_{33} = \frac{2\,(1+\nu)}{E\,t}, \quad \text{where } C_y = \frac{t}{t + \frac{t_h t_y}{b_y}}$$

and $C_x = \dfrac{t}{t + \dfrac{t_h t_x}{b_x}}$. Also $D_{11} = E\,I_x$, $D_{12} = \nu\,E\,I_x$, $D_{22} = E\,I_y$, $D_{33} = \dfrac{EJ}{4(1+\nu)}$.

The values for P_{cr} in Table IV are the 90 percent probability values.

5. Anonymous [6]. This method, while it is the result of buckling tests of stiffened cylinders in bending conducted at GALCIT [7], is sometimes used to obtain axially compressive buckling predictions. The value of σ_{cr} used for the effective skin calculation was $\sigma_{cr} = \dfrac{K_c \pi^2 E}{12(1-\nu^2)} \left(\dfrac{t}{b_y}\right)^2$, with $K_c = 5.4$. Since the radius of gyration of the effective skin depended on the general instability stress (σ_c in the reference); an iterative procedure was employed to calculate σ_c and the effective skin.

6. Seide [8]. This method was directed toward the investigation of 45° integral waffle-stiffened cylinders under axial compression. By using [9] and [10], the method was extended to 0°-90° waffle stiffened cylinders and stringer-only stiffened cylinders. The resulting values of t^*/H determined from this method were then substituted in critical buckling coefficient equation $C = 0.606 - 0.546 \cdot (1 - e^{-\frac{1}{16}\sqrt{R/t^*}})$ of [11]. The values of P_{cr} shown in Table IV were obtained from $P_{cr} = 2\pi C E t^{*2}$. Originally Seide had suggested the use of the Kanemitsu-Nojima equation [18], or any bonafide semi-empirical coefficient obtained from monocoque results. Later, in [11] Seide, Weingarten and Morgan obtained the value for C which was used to obtain P_{cr} for the Group 4 cylinders. Figure 10 shows that good agreement is obtained between the test results of monocoque cylinders 1A and 1B, and C from [11]. Since one of the assumptions in [8] was the absence of local buckling, the predictions by [8] for the skew stiffened test cylinders are surprisingly good.

7. van der Neut [12]. The method outlined in the beginning of the paper was programmed for the 0°-90° waffle configurations. Each cylinder was checked for the minimum instability load using Class I, II, III, IV, and V solutions. The entire skin between stringers was chosen as effective.

8. Schneider [13]. This method was employed with no deviations. No semi-empirical "knock down" factor was applied to the results. Although the paper states that its results are applicable to skew stiffened and 0°-90° waffle stiffened cylinders, the method was also applied to the stringer-only configurations having stiffeners with rectangular cross sections (cylinders 5A-1, 2 and 5B-1, 2) see Table IV.

B. LOCAL INSTABILITY METHODS

1. Kanemitsu and Nojima [14]. The local buckling stress was taken as $\sigma_{cr} = E\left[9\left(\frac{t}{R}\right)^{1.6} + 0.16\left(\frac{t}{L}\right)^{1.3}\right] + \frac{K\pi^2 E}{12(1-\nu^2)}\left(\frac{t}{b}\right)^2$, where for all edges: simply supported $K = 4.0$, clamped $K = 6.98$.

2. Jackson and Hall [19]. The local buckling stress was taken as $\sigma_{cr} = \frac{K\pi^2 E}{12(1-\nu^2)}\left(\frac{t}{b}\right)^2$, where $K = 6.5$ for lower limit values, and $K = 7.3$ for mean values.

3. Redshaw [18]. The local buckling stress was taken as

$$\frac{\sigma_{cr}}{E} = \sqrt{\left(\frac{\sigma_{cr}}{E}\right)_c^2 + \frac{1}{4}\left(\frac{\sigma_{cr}}{E}\right)_f^2} + \frac{1}{2}\left(\frac{\sigma_{cr}}{E}\right)_f ,$$

where $\left(\frac{\sigma_{cr}}{E}\right)_c = \frac{1}{\sqrt{3(1-\nu^2)}}\ \frac{t}{R}$, and $\left(\frac{\sigma_{cr}}{E}\right)_f = \frac{K\pi^2}{12(1-\nu^2)}\left(\frac{t}{b}\right)^2$ with $K = 4.0$ for simply supported edges.

4. Modified Redshaw [18]. $\frac{\sigma_{cr}}{E}$ is the same as that for 3, except that $\left(\frac{\sigma_{cr}}{E}\right)_c = 9\left(\frac{t}{R}\right)^{1.6} + 0.16\left(\frac{t}{L}\right)^{1.3}$.

5. Wenzek [18]. The local buckling stress was taken as

$$\frac{\sigma_{cr}}{E} + \frac{1}{\sqrt{3(1-\nu^2)}}\ \frac{t}{R} + \frac{K\pi^2}{12(1-\nu^2)}\left(\frac{t}{b}\right)^2 ,$$

and $K = 4.0$ for simply supported edges.

6. <u>Schneider [13].</u> The local buckling stress had the form $\sigma_{cr} = K\,E\left(\frac{t}{b}\right)^2$. For 0°-90° waffle stiffenening the value of K was taken from the reference's curve of K versus Aspect Ratio; for 45° waffle stiffening the value K = 7.0 was used.

C. CONVERSION OF U.S. CUSTOMARY UNITS TO SI UNITS

The following information is quoted from Card's report [17]. The International System of Units (SI) was adopted by the Eleventh General Conference on Weights and Measures, Paris, October 1960, in Resolution No. 12. Conversion factors required for units used herein are:

Length:	Inches × 0.0254 = Meters (m)
Area:	Square Inches × 0.00064516 = Square meters (m^2)
Force:	kips × 448.2216 = Newtons (N)
Stress:	ksi × 6894.757 = Newtons per square meter (N/m^2)

Prefixes to indicate multiples of units are:

10^3	kilo	(k)
10^{-2}	centi	(c)
10^6	mega	(M)

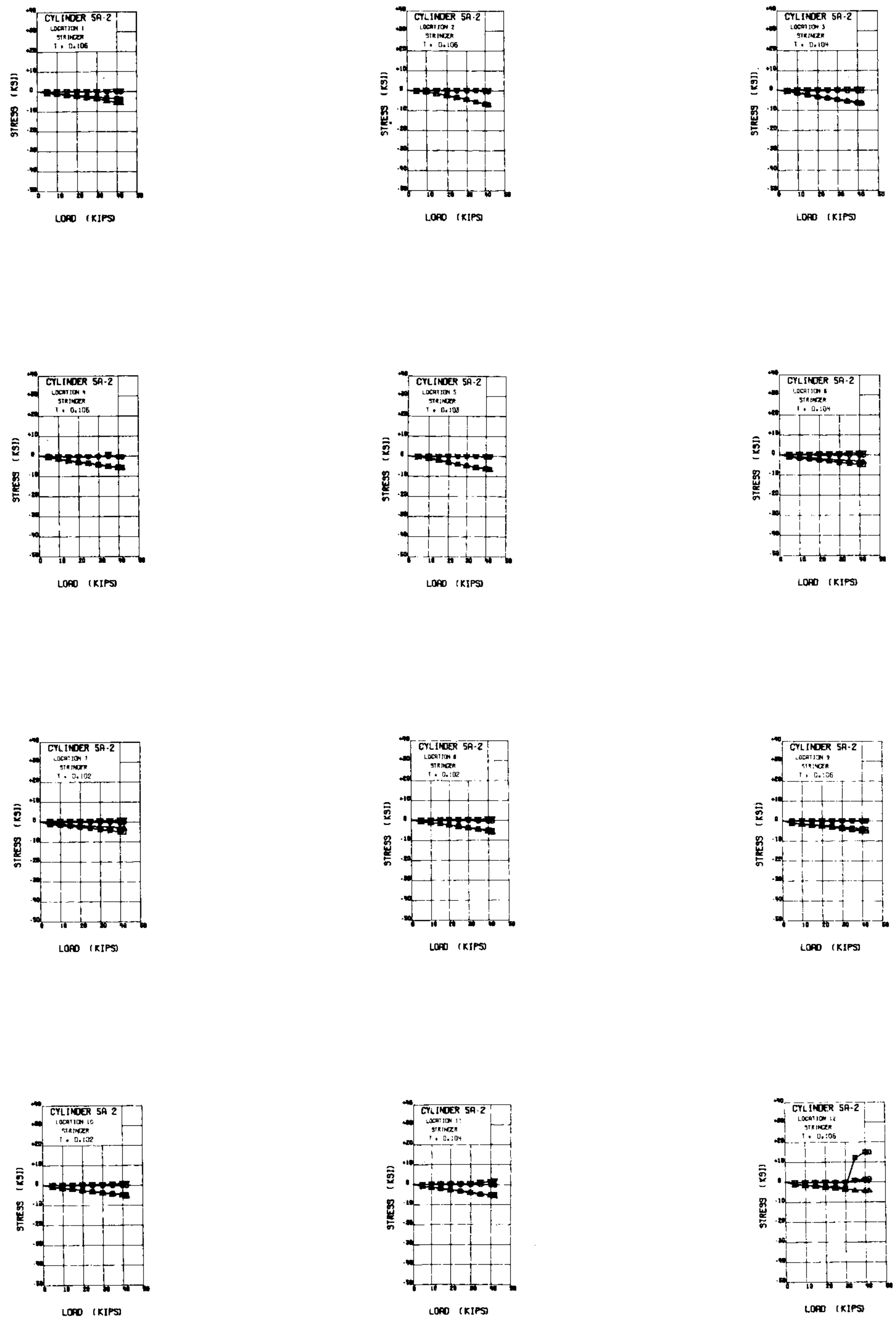

LEGEND		
ITEM	DESCRIPTION	SYMBOL
σ_1^{o}	MAX. OUTSIDE PRINCIPAL STRESS, (CIRCUM. DIR.)	-o-o-
σ_1^{i}	MAX. INSIDE PRINCIPAL STRESS, (CIRCUM. DIR.)	-▽-▽-
σ_2^{o}	MIN. OUTSIDE PRINCIPAL STRESS, (AXIAL DIR.)	-□-□-
σ_2^{i}	MIN. INSIDE PRINCIPAL STRESS, (AXIAL DIR.)	-△-△-
θ_1^{o}	PRINCIPAL DIRECTION, OUTSIDE SURFACE	-◇-◇-
θ_1^{i}	PRINCIPAL DIRECTION, INSIDE SURFACE	-×-×-

CYLINDER 5A-2
(STRINGER)

FIG. 8 CONT.

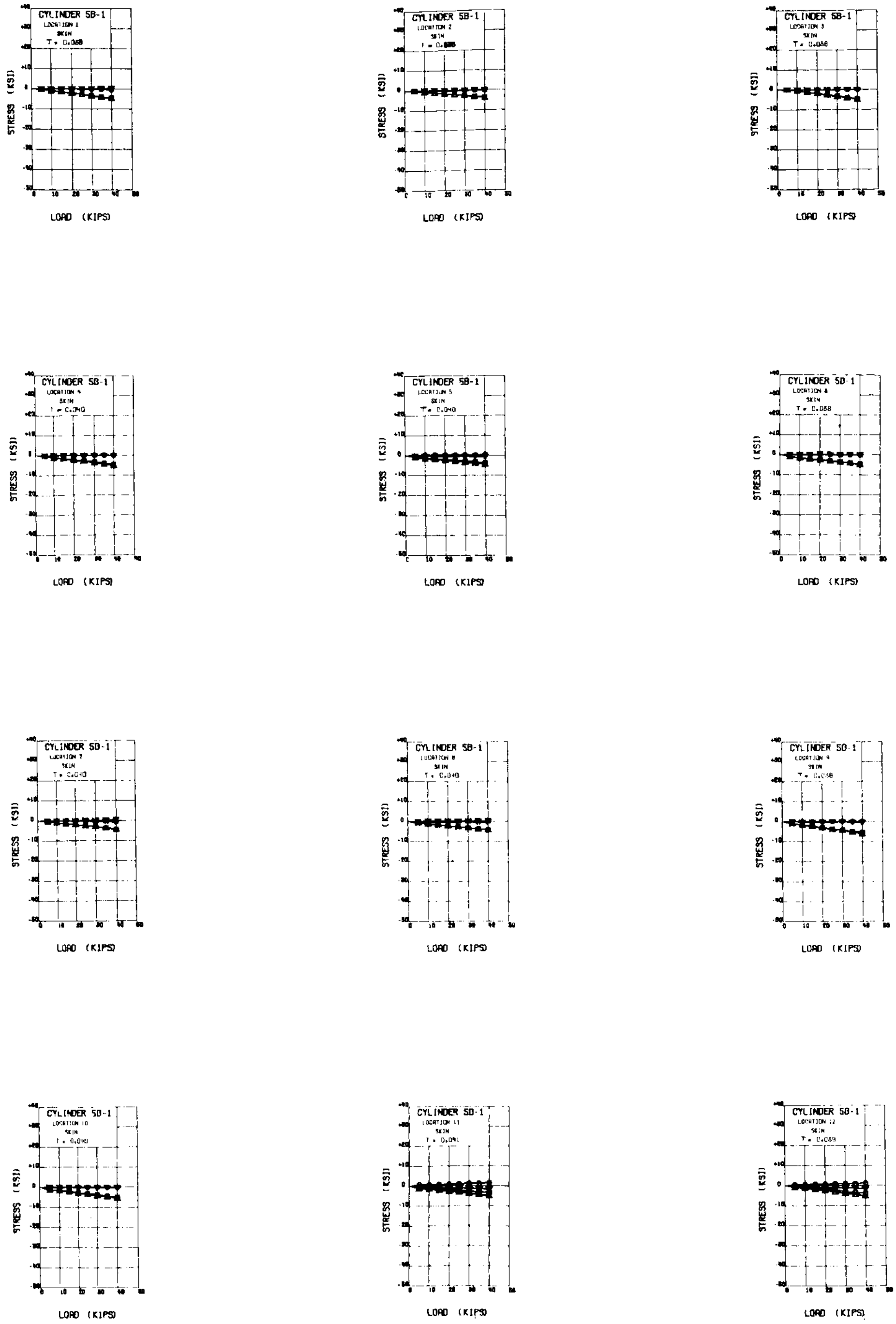

LEGEND		
ITEM	DESCRIPTION	SYMBOL
σ_1^{o}	MAX. OUTSIDE PRINCIPAL STRESS, (CIRCUM. DIR.)	
σ_1^{i}	MAX. INSIDE PRINCIPAL STRESS, (CIRCUM. DIR.)	
σ_2^{o}	MIN. OUTSIDE PRINCIPAL STRESS, (AXIAL DIR.)	
σ_2^{i}	MIN. INSIDE PRINCIPAL STRESS, (AXIAL DIR.)	
θ_1^{o}	PRINCIPAL DIRECTION, OUTSIDE SURFACE	
θ_1^{i}	PRINCIPAL DIRECTION, INSIDE SURFACE	

CYLINDER 5B-1
(SKIN)

FIG. 8 CONT.

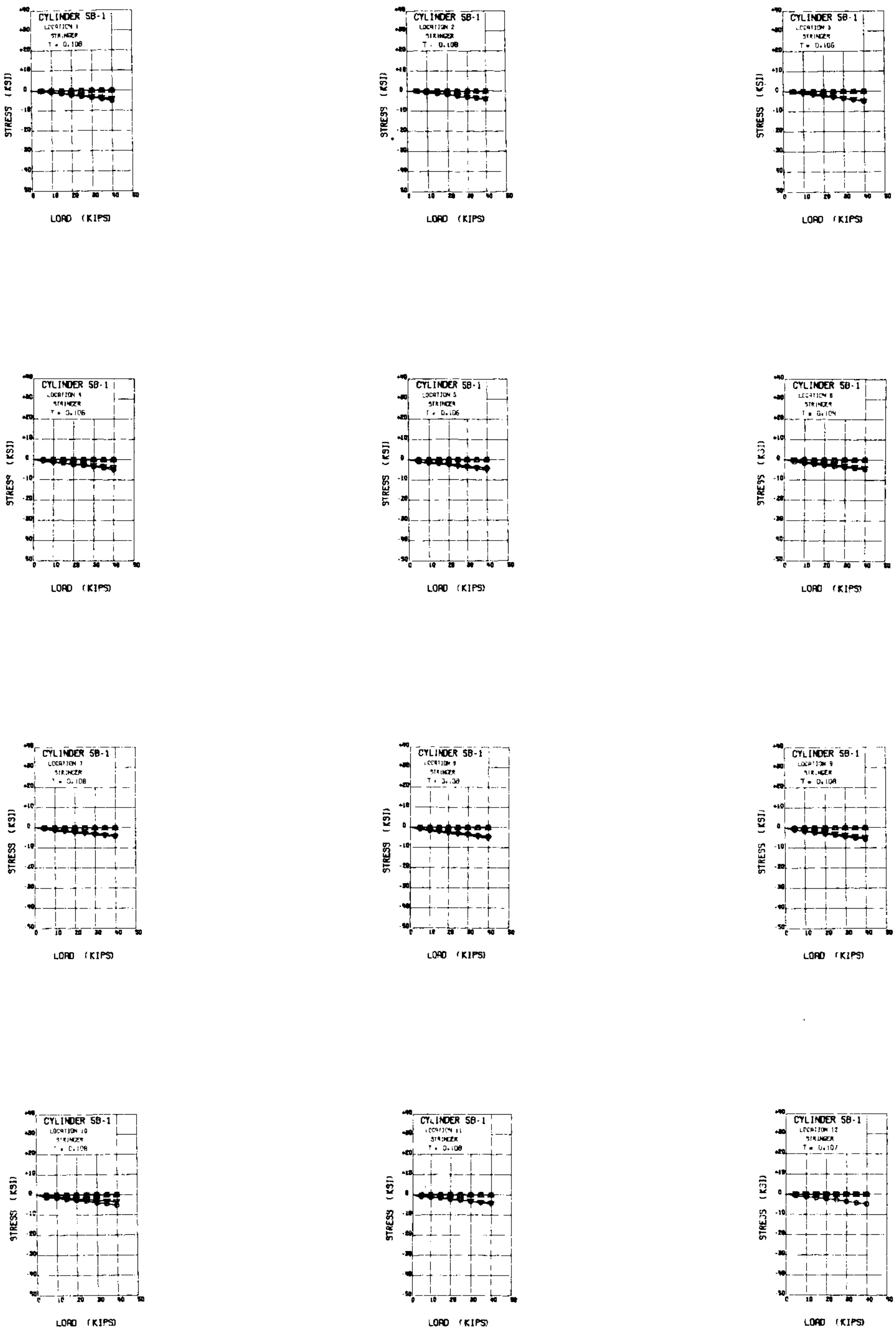

LEGEND		
ITEM	DESCRIPTION	SYMBOL
σ_1^o	MAX. OUTSIDE PRINCIPAL STRESS, (CIRCUM. DIR.)	
σ_1^i	MAX. INSIDE PRINCIPAL STRESS, (CIRCUM. DIR.)	
σ_2^o	MIN. OUTSIDE PRINCIPAL STRESS, (AXIAL DIR.)	
σ_2^i	MIN. INSIDE PRINCIPAL STRESS, (AXIAL DIR.)	
θ_1^o	PRINCIPAL DIRECTION, OUTSIDE SURFACE	
θ_1^i	PRINCIPAL DIRECTION, INSIDE SURFACE	

CYLINDER 5B-1
(STRINGER)

FIG. 8 CONT.

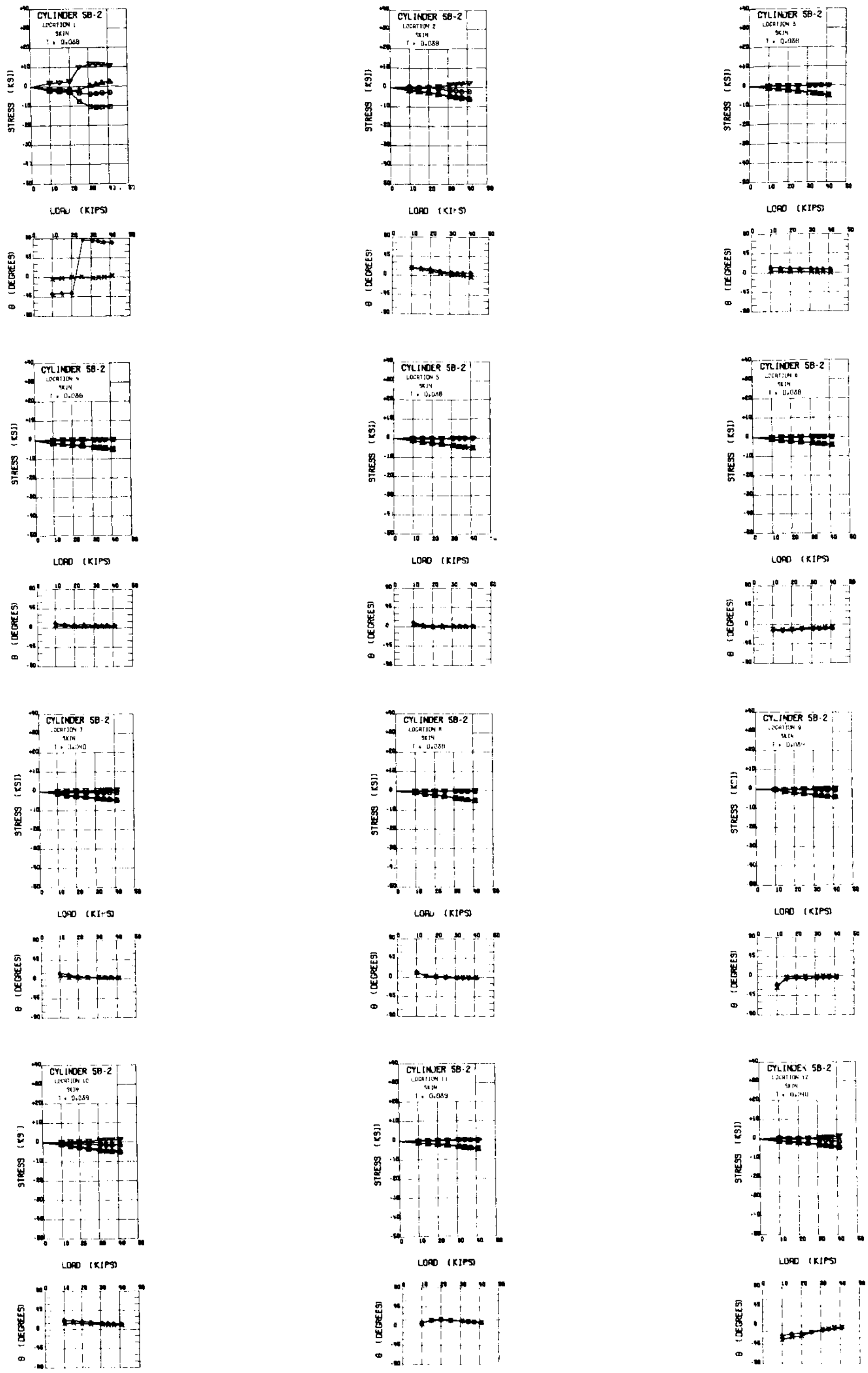

LEGEND		
ITEM	DESCRIPTION	SYMBOL
σ_1^o	MAX OUTSIDE PRINCIPAL STRESS, (CIRCUM. DIR.)	-o-o-
σ_1^i	MAX INSIDE PRINCIPAL STRESS, (CIRCUM. DIR.)	-▽-▽-
σ_2^o	MIN OUTSIDE PRINCIPAL STRESS, (AXIAL DIR)	-□-□-
σ_2^i	MIN INSIDE PRINCIPAL STRESS, (AXIAL DIR)	-△-△-
θ_1^o	PRINCIPAL DIRECTION, OUTSIDE SURFACE	-◇-◇-
θ_1^i	PRINCIPAL DIRECTION, INSIDE SURFACE	-×-×-

CYLINDER 5B-2
(SKIN)

FIG. 8 CONT.

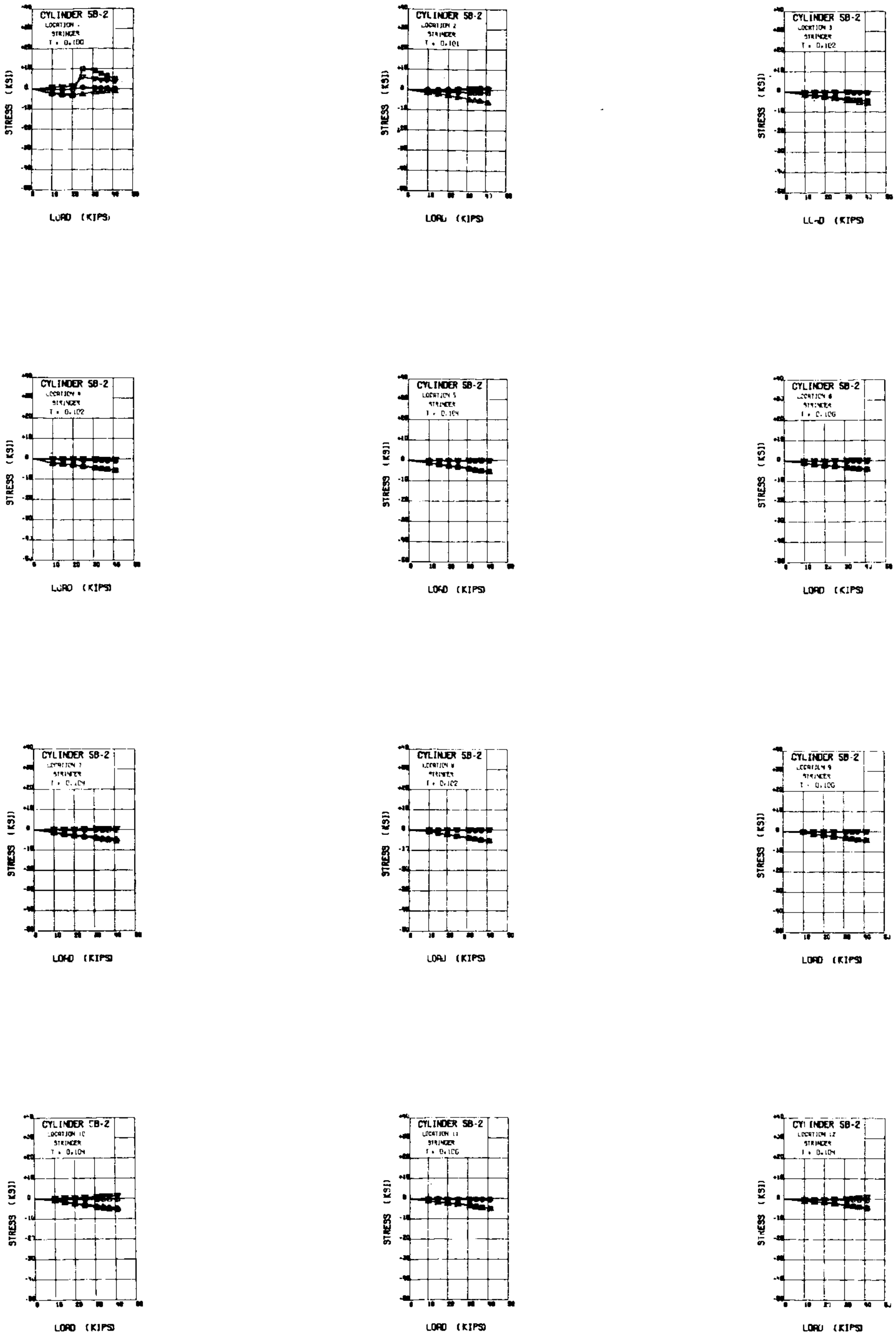

LEGEND		
ITEM	DESCRIPTION	SYMBOL
σ_1^o	MAX. OUTSIDE PRINCIPAL STRESS, (CIRCUM. DIR.)	
σ_1^i	MAX. INSIDE PRINCIPAL STRESS, (CIRCUM. DIR.)	
σ_2^o	MIN. OUTSIDE PRINCIPAL STRESS, (AXIAL DIR.)	
σ_2^i	MIN. INSIDE PRINCIPAL STRESS, (AXIAL DIR.)	
θ_1^o	PRINCIPAL DIRECTION, OUTSIDE SURFACE	
θ_1^i	PRINCIPAL DIRECTION, INSIDE SURFACE	

CYLINDER 5B-2
(STRINGER)

FIG. 8 CONT.

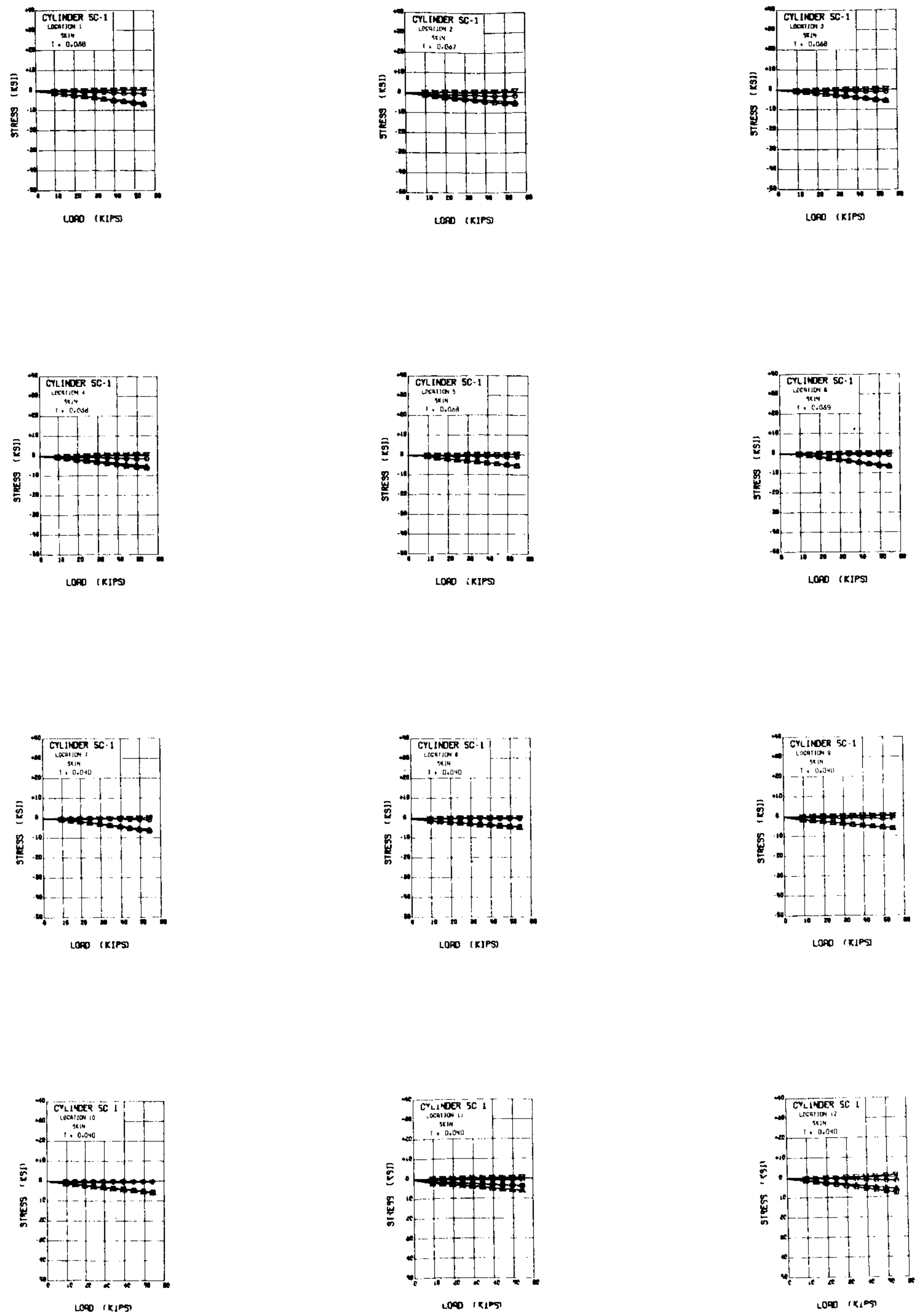

LEGEND		
ITEM	DESCRIPTION	SYMBOL
σ_1^o	MAX OUTSIDE PRINCIPAL STRESS, (CIRCUM DIR)	-○-○-
σ_1^i	MAX INSIDE PRINCIPAL STRESS, (CIRCUM DIR)	-▽-▽-
σ_2^o	MIN OUTSIDE PRINCIPAL STRESS, (AXIAL DIR)	-□-□-
σ_2^i	MIN INSIDE PRINCIPAL STRESS, (AXIAL DIR)	-△-△-
θ_1^o	PRINCIPAL DIRECTION, OUTSIDE SURFACE	-◇-◇-
θ_1^i	PRINCIPAL DIRECTION, INSIDE SURFACE	-×-×-

CYLINDER 5C-1
(SKIN)

FIG. 8 CONT.

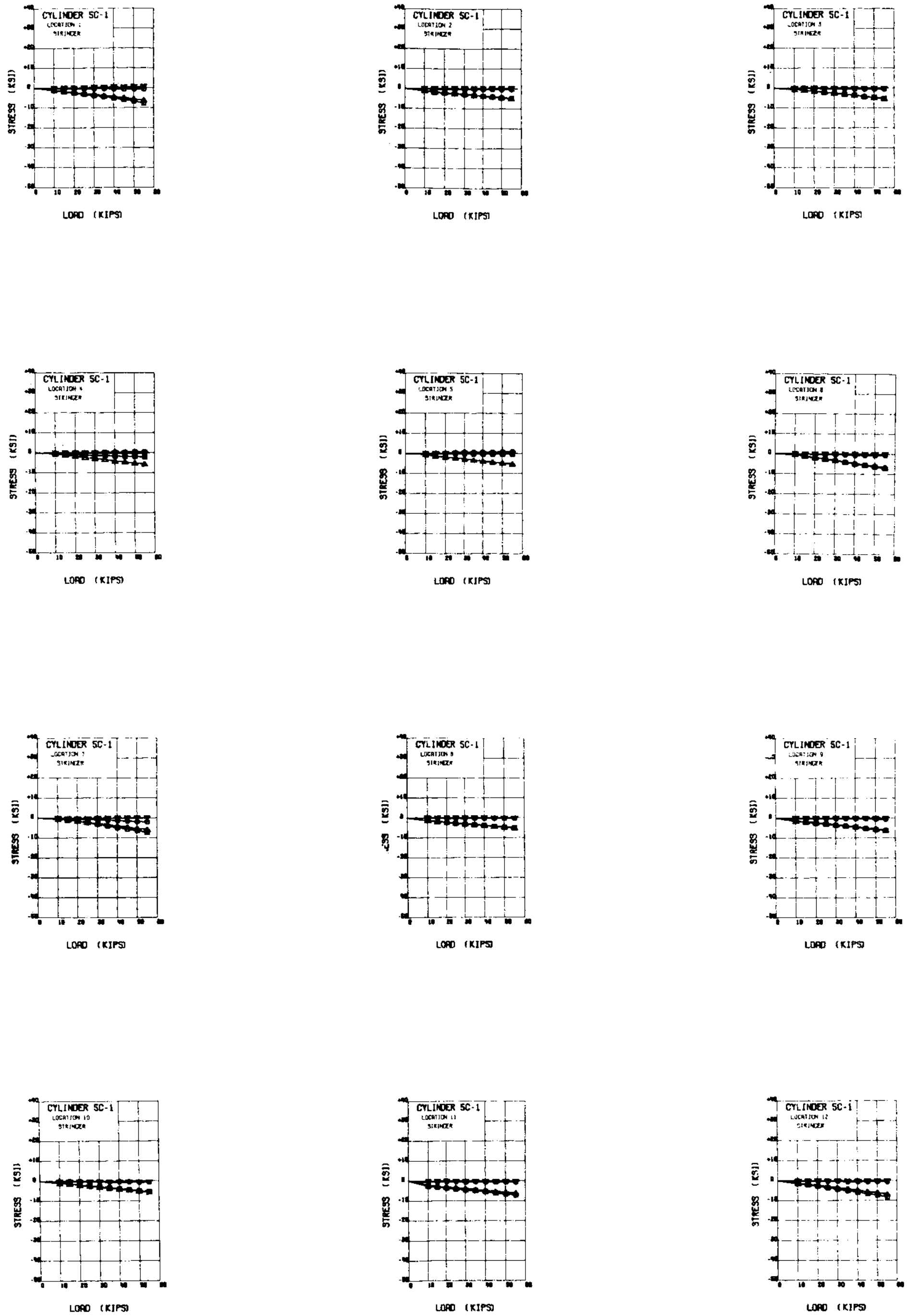

LEGEND		
ITEM	DESCRIPTION	SYMBOL
σ_1^o	MAX. OUTSIDE PRINCIPAL STRESS, (CIRCUM. DIR.)	-o-o-
σ_1^i	MAX. INSIDE PRINCIPAL STRESS, (CIRCUM. DIR.)	-▽-▽-
σ_2^o	MIN. OUTSIDE PRINCIPAL STRESS, (AXIAL DIR.)	-□-□-
σ_2^i	MIN. INSIDE PRINCIPAL STRESS, (AXIAL DIR.)	-△-△-
θ_1^o	PRINCIPAL DIRECTION, OUTSIDE SURFACE	-◇-◇-
θ_1^i	PRINCIPAL DIRECTION, INSIDE SURFACE	-x-x-

CYLINDER 5C-1
(STRINGER)

FIG. 8 CONT.

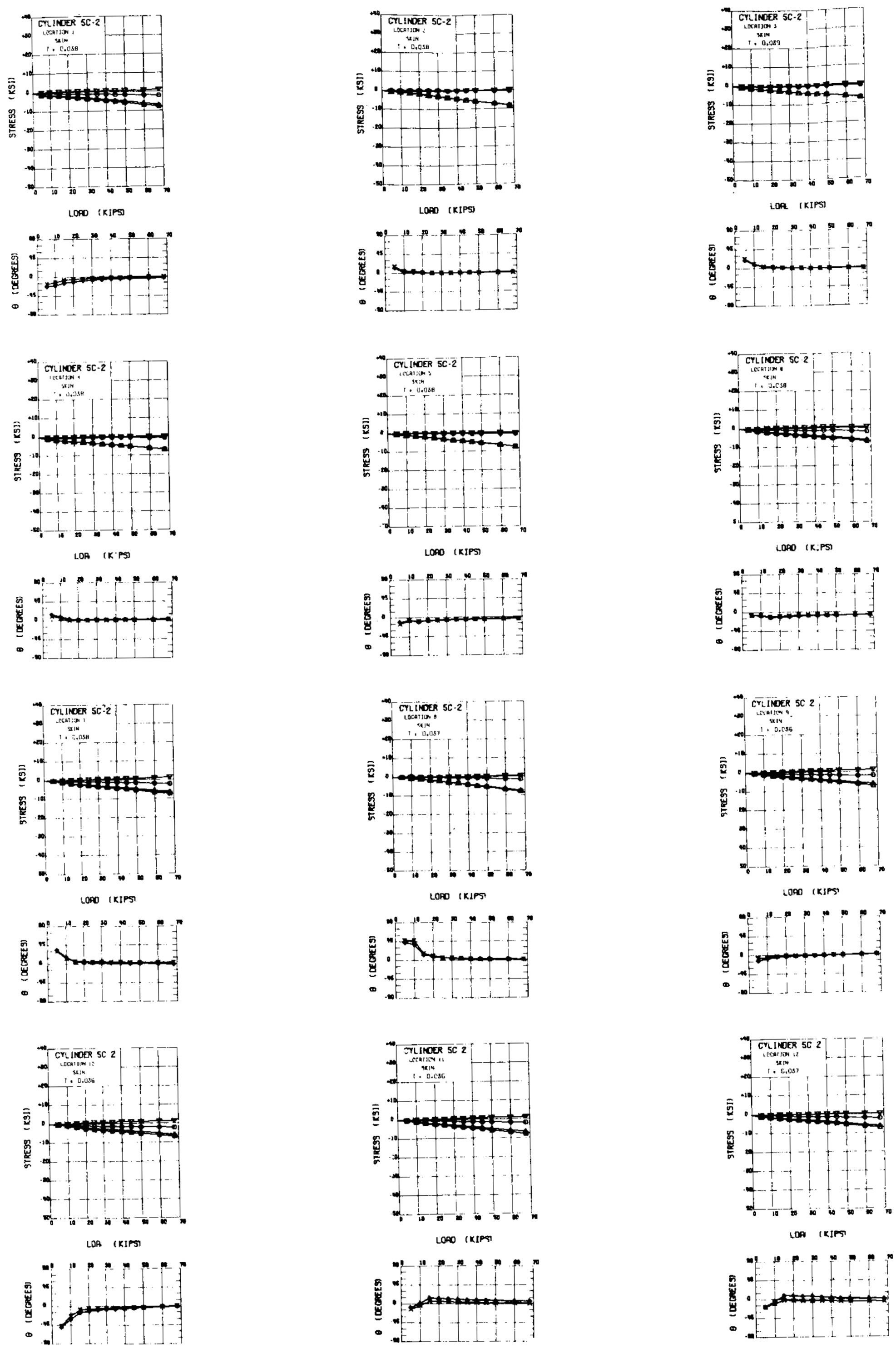

LEGEND		
ITEM	DESCRIPTION	SYMBOL
σ_1^o	MAX OUTSIDE PRINCIPAL STRESS, (CIRCUM. DIR.)	-o-o-
σ_1^i	MAX INSIDE PRINCIPAL STRESS, (CIRCUM. DIR.)	-▽-▽-
σ_2^o	MIN. OUTSIDE PRINCIPAL STRESS, (AXIAL DIR.)	-□-□-
σ_2^i	MIN. INSIDE PRINCIPAL STRESS, (AXIAL DIR.)	-△-△-
θ^o	PRINCIPAL DIRECTION, OUTSIDE SURFACE	-◆-◆-
θ^i	PRINCIPAL DIRECTION, INSIDE SURFACE	-×-×-

CYLINDER 5C-2
(SKIN)

FIG. 8 CONT.

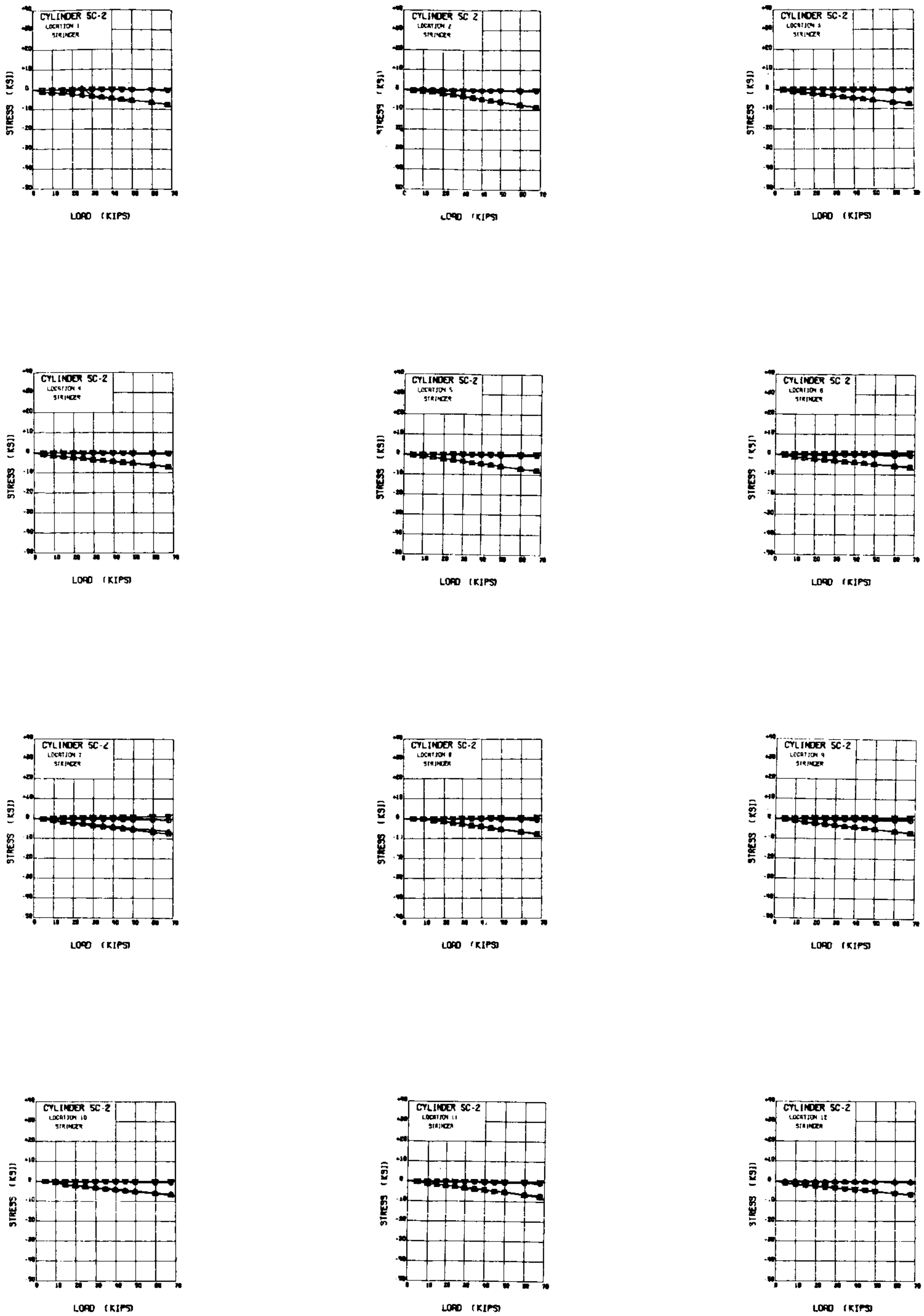

LEGEND		
ITEM	DESCRIPTION	SYMBOL
σ_1^o	MAX. OUTSIDE PRINCIPAL STRESS, (CIRCUM. DIR.)	-o-o-
σ_1^i	MAX. INSIDE PRINCIPAL STRESS, (CIRCUM. DIR.)	-▽-▽-
σ_2^o	MIN. OUTSIDE PRINCIPAL STRESS, (AXIAL DIR.)	-□-□-
σ_2^i	MIN. INSIDE PRINCIPAL STRESS, (AXIAL DIR.)	-△-△-
θ_1^o	PRINCIPAL DIRECTION, OUTSIDE SURFACE	-◇-◇-
θ_1^i	PRINCIPAL DIRECTION, INSIDE SURFACE	-x-x-

CYLINDER 5C-2
(STRINGER)

FIG. 8 CONCLUDED

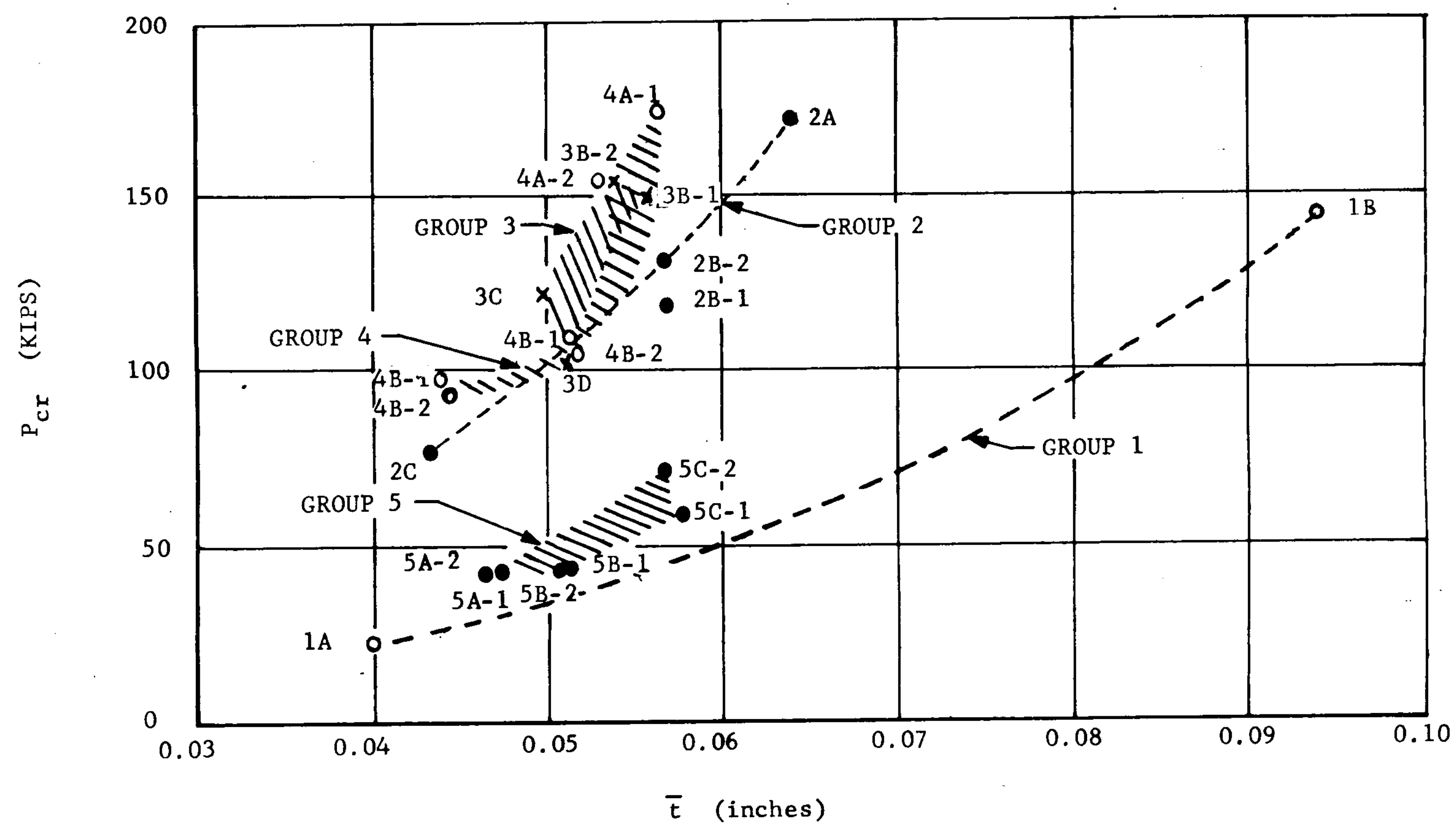

TEST RESULTS

FIG. 9

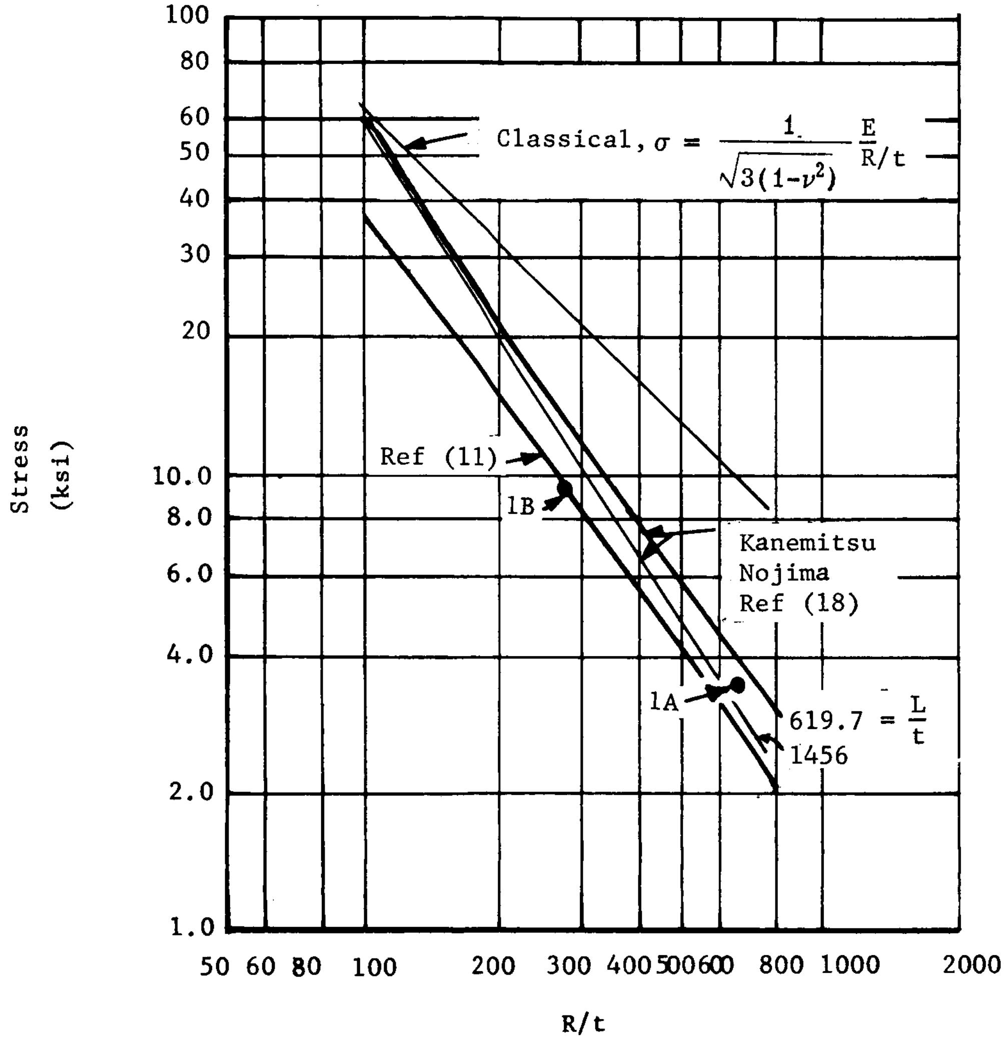

MONOCOQUE RESULTS

FIG. 10

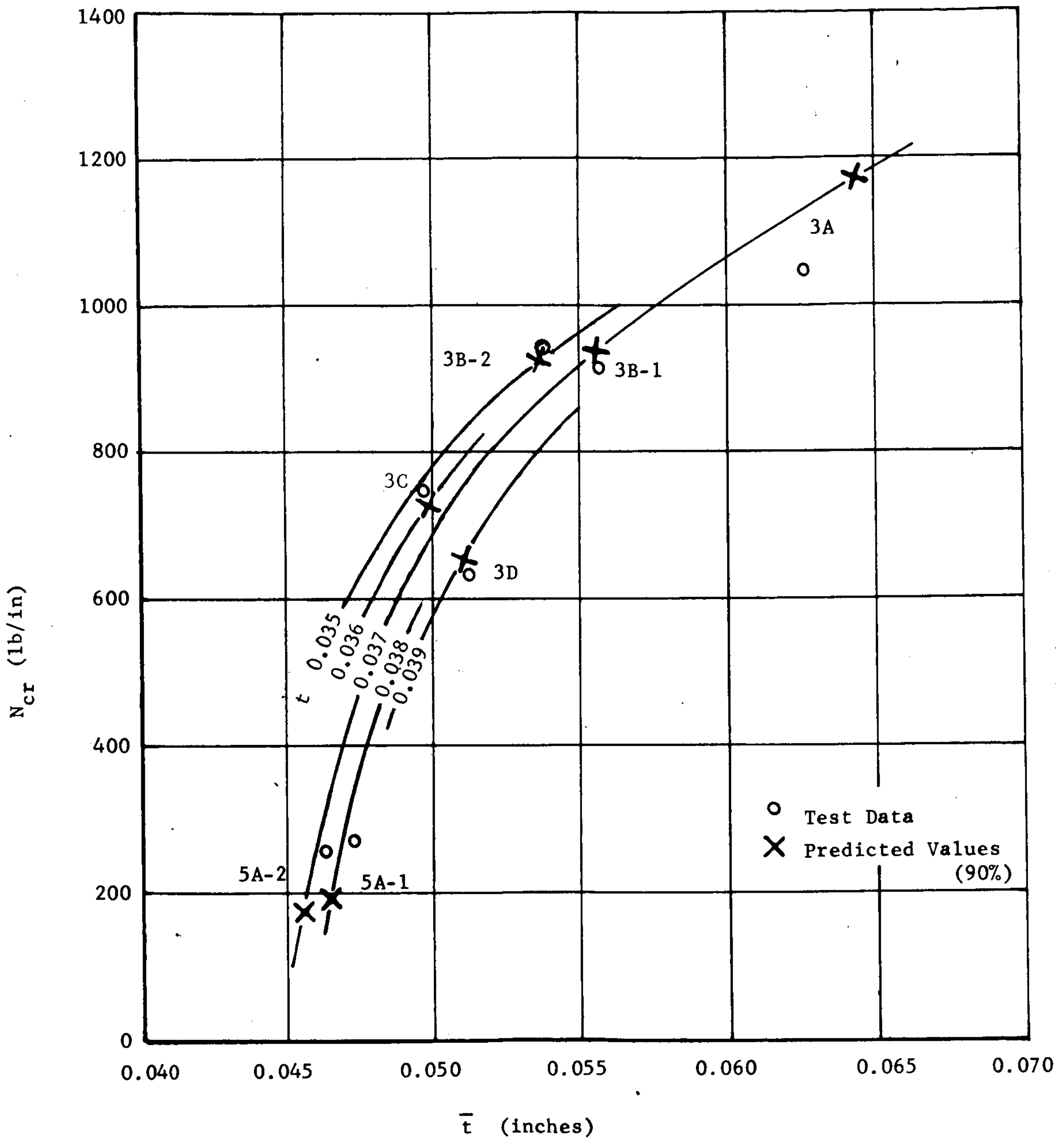

COMPARISON OF TEST DATA WITH METHOD OF REF. 5

FIG. 11

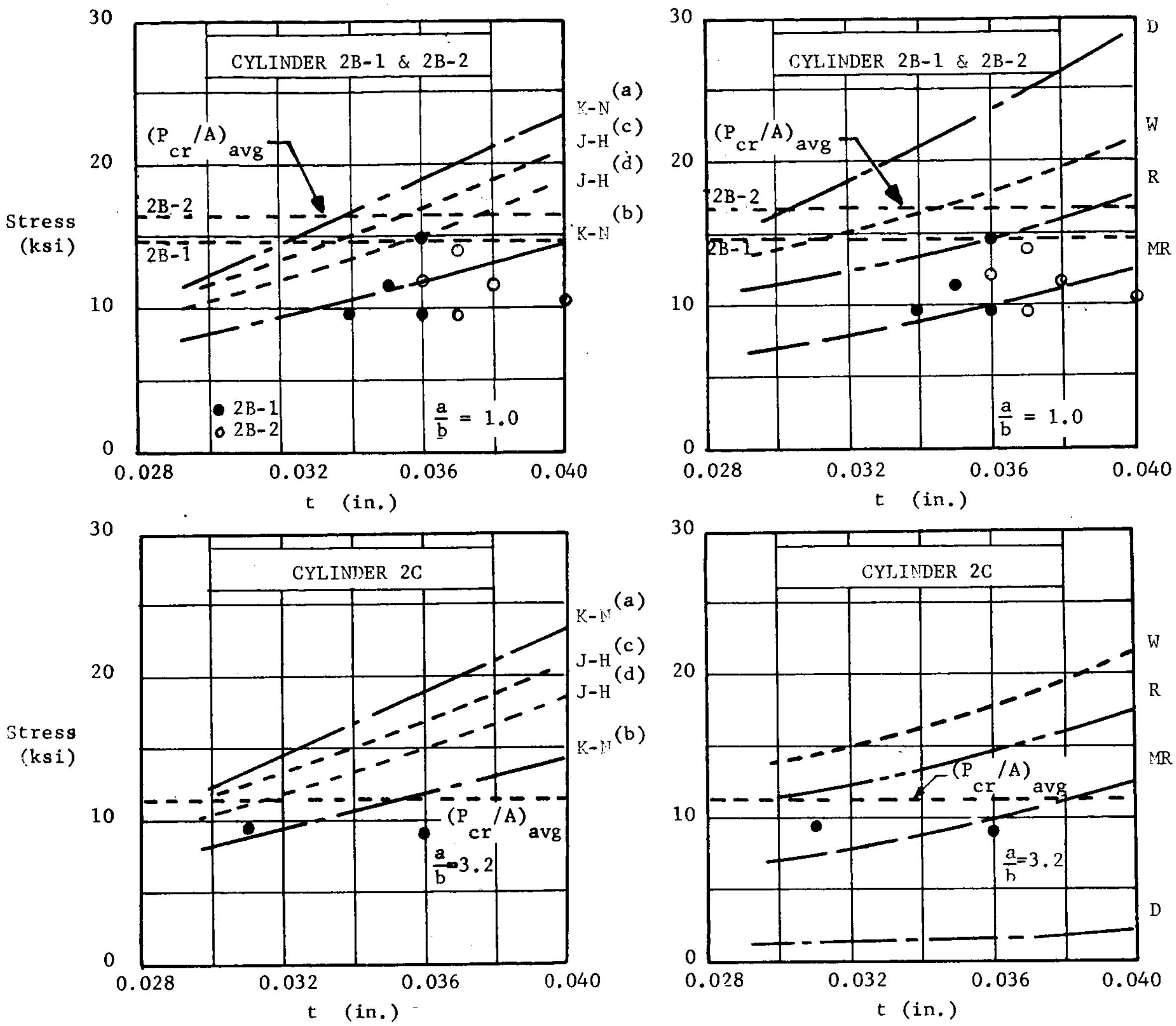

SYMBOL	METHOD	APPENDIX
K-N(a) K-N(b)	Kanemitsu-Nojima edges; clamped (a) simply supported (b)	B.1
J-H(c) J-H(d)	Jackson - Hall mean value (c) lower limit (d)	B.2
MR	Modified Redshaw	B.3a
R	Redshaw	B.3b
W	Wenzek	B.4
D	Douglas (Schneider)	B.5

LOCAL BUCKLING STRESSES FOR GROUP 2 (0-90°) CYLINDERS

FIG. 12a

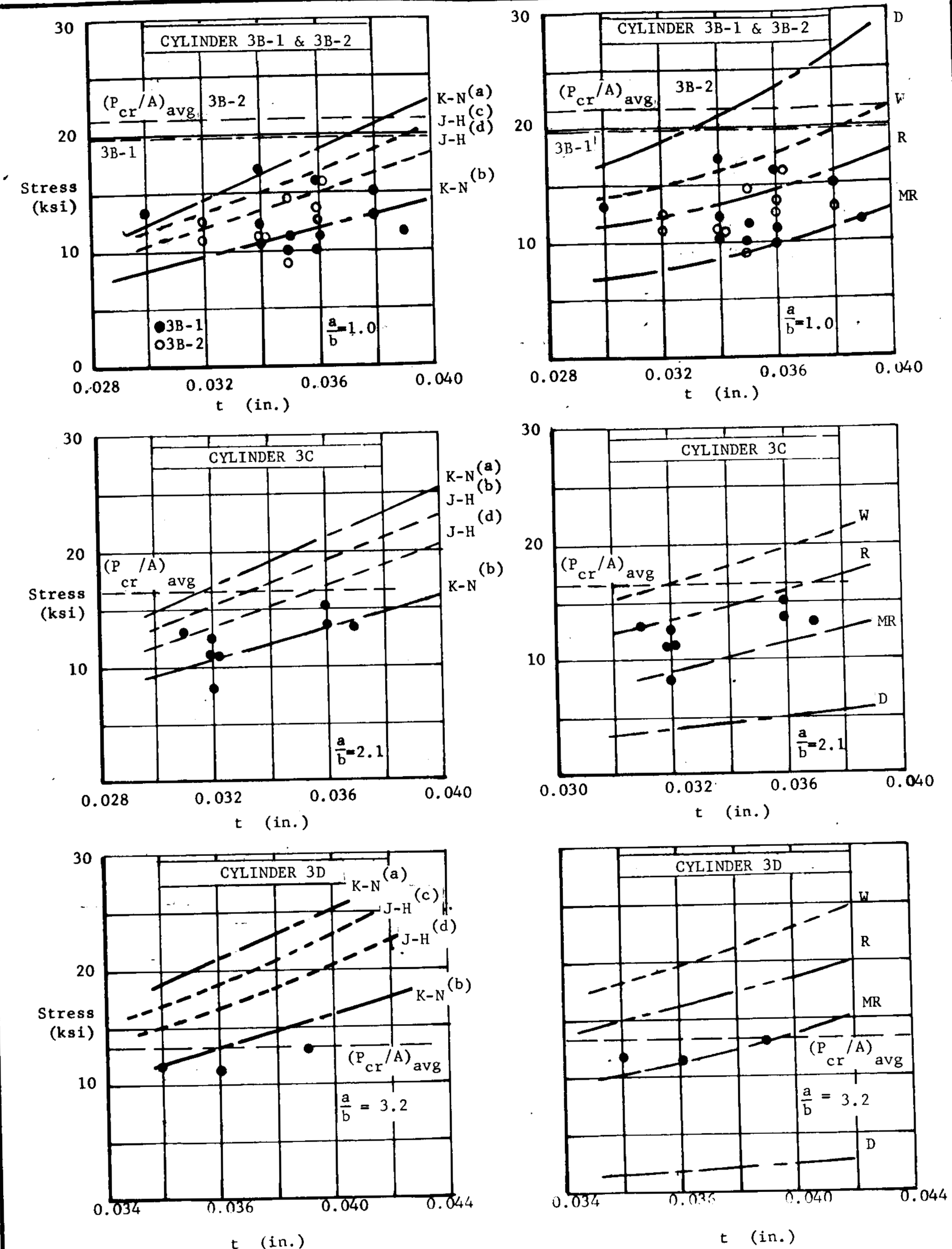

LOCAL BUCKLING STRESSES FOR GROUP 3 (0-90°) CYLINDERS

FIG. 12b

REFERENCES

1. Becker, H. and Gerard, G; "Elastic Stability of Orthotropic Shells." J. Aerospace Sci., Vol. 29, No. 5, May 1962.

2. Lyse, I. and Johnston, B. G.; "Structural Beams in Torsion." Trans ASCE, Vol 101, 1936, pp. 857-896.

3. Timoshenko, S. P.; "Theory of Elastic Stability." McGraw-Hill, New York, 1936, p. 473.

4. Peterson, J. P. and Dow, M. B.; "Compression Tests on Circular Cylinders Stiffened Longitudinally by Closely Spaced Z-Section Stringers." NASA Memo 2-12-59L, March 1959.

5. Almroth, B. O.; "Buckling of Orthotropic Cylinders under Axial Compression." Lockheed Missiles and Space Co. Report LMSC-6-90-63-65, June 1963.

6. Becker, H.; "Handbook of Structural Stability, Part VI - Strength of Stiffened Curved Plates and Shells." NACA TN 3786, 1958.

7. Anon.; "Some Investigations of the General Instability of Stiffened Metal Cylinders, V - Stiffened Metal Cylinders Subjected to Pure Bending." NACA TN 909, 1943.

8. Seide, P.; "The Effectiveness of Integral Waffle-like Stiffening for Long, Thin Circular Cylinders under Axial Compression, Part II - Mechanically Milled Sheet." Ramo-Wooldridge Corp., Guided Missile Research Division, Rep. No. GM-TR-38, 1956.

9. Dow, N. F., Libove, C. and Hubka, R. E.; "Formulas for the Elastic Constants of Plates with Integral Waffle-like Stiffening." NACA Rep. 1195, 1954.

10. Stein, M. and Meyers, J.; "A Small Deflection Theory for Curved Sandwich Plates." NACA Rep. 1008, 1951.

11. Seide, P., Weingarten V. I. and Morgan, E. J.; "The Development of Design Criteria for Elastic Stability of Thin Wall Structures." Space Technology Laboratories Rep. STL/TR-60-0000-19425, Dec. 1960, p. 24.

REFERENCES (Cont'd)

12. van der Neut, A.; "The General Instability of Stiffened Shells Under Axial Compression." Rep. S. 314, Nat. Aero. Res. Inst. (Amsterdam), Rep. and Trans., Vol XIII, 1947, pp. S 57- S 84.

13. Schneider, M. H.; "Structural Optimization of Waffle Cylinders Under Axial Compression and External Pressure." Douglas Aircraft Co., Rep. No. SM-42441, Oct. 1962.

14. Peery D. J.; "Aircraft Structures," McGraw Hill Book Co. Inc. N.Y., N.Y., 1950, p. 389.

15. Timoshenko, S. P.; "Theory of Plates and Shells," McGraw-Hill Book Co., Inc. New York, 1940, p. 393.

16. Horton, W. H. and Durham, S. C.; "The Effect of Restricting Buckle Depth in Circular Cylindrical Shells Repeatedly Compressed to the Buckling Limit." SUDAER No. 174, Nov. 1963.

17. Card, M. F.; "Preliminary Results of Compression Tests on Cylinders With Eccentric Longitudinal Stiffeners." NASA TM X-1004, 1964.

18. Sechler, E. E. and Dunn, L. G.; "Airplane Structural Analysis and Design." John Wiley & Sons, Inc. New York, 1942.

19. Jackson, K. B. and Hall, A. H.; "Curved Plates in Compression." National Research Council of Canada, AR-1, 1947.

NASA TM X - 53315 APPROVAL

COMPRESSION TESTS ON INTEGRALLY STIFFENED CYLINDERS

By Lester Katz

The information in this report has been reviewed for security classification. Review of any information concerning Department of Defense or Atomic Energy Commission programs has been made by the MSFC Security Classification Officer. This report, in its entirety, has been determined to be unclassified.

This document has also been reviewed and approved for technical accuracy.

P. FREDERICK
Chief, Strength Analysis Branch

G. A. KROLL
Chief, Structures Division

for F. B. CLINE
Director, Propulsion and Vehicle Engineering Laboratory

DISTRIBUTION

INTERNAL

I-SE
Dr. Mrazek

R-DIR
Mr. Weidner

R-AERO-DIR
Dr. Geissler

R-ME-DIR
Mr. Kuers

R-ME-X
Mr. Wuenscher

R-ME-IS
Mr. Montgomery (2)

R-P&VE-DIR
Mr. Cline
Mr. Hellebrand

R-P&VE-A
Mr. Goerner

R-P&VE-M
Dr. Lucas

R-P&VE-P
Mr. Paul

R-P&VE-RT
Mr. Hofues

R-P&VE-S
Mr. Kroll
Mr. Sterett
Dr. Glaser
Mr. Hunt
Mr. Verble

R-P&VE-SA
Mr. Blumrich (5)

R-P&VE-SE
Mr. Garrett

R-P&VE-SJ
Mr. Furman

R-P&VE-SL
Mr. Showers

R-P&VE-SS
Mr. Frederick (7)

R-P&VE-SSM
Mr. Katz (40)

R-P&VE-SV
Mr. Farrow

R-QUAL-DIR
Mr. Grau

R-RP-DIR
Dr. Stuhlinger

DISTRIBUTION (Concluded)

INTERNAL (Cont'd)

R-TEST-DIR
Mr. Heimburg

MS-IP
Mr. Ziak

MS-IL
Miss Robertson (8)

MS-H
Mr. Akens

CC-P
Mr. Wofford

MS-T (5)
I-RM-M
DIR
DEP-T

EXTERNAL

Scientific & Technical Information Facility (25)
Attn: NASA Representative
(S-AK/RKT)
P. O. Box 5700
Bethesda, Maryland 20014